AFFDL-TR-77-23

ADA046152

DESIGN AND ANALYSIS OF WINGLETS FOR MILITARY AIRCRAFT. PHASE II

K. K. ISHIMITSU
D. F. ZANTON

BOEING COMMERCIAL AIRPLANE COMPANY
P. O. BOX 3707
SEATTLE, WASHINGTON 98124

MAY 1977   131 p.
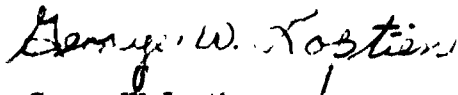
D D C
RECEIVED
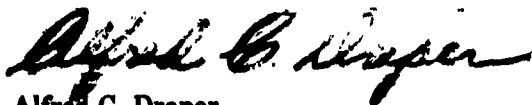NOV 1 1977
F.

D6-45090

A 029 345

390 145

NOTICES

When Government drawings, specifications, or other data are used for any purpose other than in connection with a definitely related Government procurement operation, the United States Government thereby incurs no responsibility nor any obligation whatsoever; and the fact that the Government may have formulated, furnished, or in any way supplied the said drawings, specifications, or other data is not to be regarded by implication or otherwise as in any manner licensing the holder or any other person or corporation, or conveying any rights or permission to manufacture, use, or sell any patented invention that may in any way be related thereto.

This report has been reviewed by the Office of Information (OI) and is releasable to the National Technical Information Service (NTIS). At NTIS, it will be available to the general public, including foreign nations.

This technical report has been reviewed and is approved for publication.

George W. Loptien
Project Engineer

Alfred C. Draper
Assistant for Research and Technology
Aeromechanics Division

Copies of this report should not be returned unless return is required by security considerations, contractual obligations, or notice on a specific document.

SECURITY CLASSIFICATION OF THIS PAGE *(When Data Entered)*

REPORT DOCUMENTATION PAGE		READ INSTRUCTIONS BEFORE COMPLETING FORM
1. REPORT NUMBER AFFDL-TR-77-23	2. GOVT ACCESSION NO.	3. RECIPIENT'S CATALOG NUMBER
4. TITLE *(and Subtitle)* DESIGN AND ANALYSIS OF WINGLETS FOR MILITARY AIRCRAFT: PHASE II		5. TYPE OF REPORT & PERIOD COVERED Final Report May 1976 to Nov 1976
		6. PERFORMING ORG. REPORT NUMBER D6-45090
7. AUTHOR(s) K. K. Ishimitsu, D. F. Zanton		8. CONTRACT OR GRANT NUMBER(s) F33615-75-C-3123
9. PERFORMING ORGANIZATION NAME AND ADDRESS Boeing Commercial Airplane Company P.O. Box 3707 Seattle, Washington 98124		10. PROGRAM ELEMENT, PROJECT, TASK AREA & WORK UNIT NUMBERS Program Element 62201F Project 1431, Task 143101 Work Unit 14310125
11. CONTROLLING OFFICE NAME AND ADDRESS Aeromechanics Division (FX) Air Force Flight Dynamics Laboratory Wright-Patterson AFB, Ohio 45433		12. REPORT DATE May 1977
		13. NUMBER OF PAGES
14. MONITORING AGENCY NAME & ADDRESS(*if different from Controlling Office*)		15. SECURITY CLASS. *(of this report)* Unclassified
		15a. DECLASSIFICATION/DOWNGRADING SCHEDULE

16. DISTRIBUTION STATEMENT *(of this Report)*

Approved for public release: Distribution Unlimited

17. DISTRIBUTION STATEMENT *(of the abstract entered in Block 20, if different from Report)*

18. SUPPLEMENTARY NOTES

19. KEY WORDS *(Continue on reverse side if necessary and identify by block number)*

KC-135, Winglets, Induced Drag, Drag Reduction, Fuel Savings, Wing-Root Bending Moment, Landing and Take-Off Configurations, Low-Speed Performance, Buffet, Mach Tuck, Drag Divergence, Longitudinal, Lateral Stability and Control, Retrofit.

20. ABSTRACT *(Continue on reverse side if necessary and identify by block number)*

A study of the design and analysis of winglets for military aircraft has been completed. This study is a continuation of the work reported in AFFDL-TR-76-6. The program consisted of investigating analytically the AFFDL/Boeing winglet on the take off and landing configuration of the KC-135A. Also investigated analytically were the effect of a wing leading-edge device on the performance of the AFFDL/Boeing winglets and the design of a compromise high-speed/low-speed winglet.

DD $_{1\ JAN\ 73}^{FORM}$ 1473   EDITION OF 1 NOV 65 IS OBSOLETE

20. Continued

Two wind tunnel tests were conducted by the NASA-Langley Research Center 8-foot transonic tunnel. A high-speed and low-speed test were conducted to determine the effect of the AFFDL/Boeing winglets on the KC-135A's aerodynamic performance and longitudinal and lateral-directional stability.

A preliminary plan for a KC-135A winglet retrofit program was developed and its cost estimated. Based on a 1979 program start, the retrofit costs would be recovered by the start of 1984.

FOREWORD

This is the final report on the design and analysis of winglets for military aircraft. This report has been assigned Boeing document number D6-45090 for internal use and covers work performed by the Boeing Commercial Airplane Company, Seattle, Washington, and Boeing Wichita Division, Wichita, Kansas. This work was accomplished under project 1431, Aerodynamic Synthesis and Flight Research, task 143101, Unified Flight Mechanics Technology, work unit 14310125, Design and Analysis of Winglets for Military Aircraft. Mr. George W. Loptien of the Air Force Flight Dynamics Laboratory/FXS provided the technical direction.

Mr. A. L. daCosta was the program Manager and K. K. Ishimitsu was the Technical Leader. Others supporting the effort were D. F. Zanton, R. O. Dodson, and R. A. Shepard.

The work was performed under contract F33615-75-C-3123.

iii

TABLE OF CONTENTS

LIST OF FIGURES

LIST OF FIGURES–(Continued)

LIST OF FIGURES–(Concluded)

LIST OF TABLES

LIST OF SYMBOLS

a.c.   aerodynamic center

b   wing span

B.S.   body station

C   section chord length

C_{avg} average chord of the wing alone

C_{MAC} mean aerodynamic chord

C_D drag coefficient

C_{D_i} induced drag coefficient

c.g.   center of gravity

C_{ℓ_β} rolling moment coefficient derivative, with respect to β

C_ℓ section lift coefficient

C_L lift coefficient

$C_{m_{.25\bar{c}}}$ pitching moment coefficient about the quarter chord of the MAC

C_{m_x} rolling moment of the right half of the configuration

C_N normal force coefficient

C_{n_β} yawing moment coefficient derivative, with respect to β

C_p pressure coefficient

C_y side force coefficient

C_{y_β}	side force coefficient derivative with respect to β
D	drag
G_w	gross weight
h	altitude
H	boundary layer shape factor, δ^*/θ
l	winglet length
L	lift
L/D	lift-to-drag ratio
M	Mach number
$m_{.25\bar{c}}$	pitching moment about quarter chord of MAC
n	load factor
P	pressure
q	dynamic pressure
S	wing area
S_{REF}	wing reference area
W	weight of airplane
WBL	wing buttock line
WRBM	wing-root bending moment
W.S.	wing station
$X_{a.c.}$	location of the aerodynamic center
α_w	wing angle of attack
β	sideslip angle
i	winglet incidence angle, toe-in direction is positive direction

δ^*	boundary layer displacement thickness
Δ	increment
θ	boundary layer momentum thickness
λ	taper ratio
Λ	winglet leading-edge sweep angle
η	nondimensional spanwise location
ψ	yaw angle
ϕ	winglet cant angle, angle of winglet plane from X-Z with positive direction being clockwise as viewed from rear of airplane of the right-hand side

SUMMARY

An investigation has been conducted to determine the performance benefits of winglets when applied to military aircraft. Analytical methods that have been proven extremely reliable for the design and analysis of winglets for the cruise condition were applied to the KC-135A takeoff and landing configurations. The results of two tests conducted at the NASA-Langley Research Center 8-ft transonic wind tunnel to evaluate the effects of winglets on the KC-135A aerodynamic performance and stability characteristics were analyzed and are reported here. These tests were conducted at M = 0.30 for the low-speed configuration and at M = 0.50 to 0.95 for the high-speed configuration. In addition to the performance analyses of winglets, a study was also conducted to determine preliminary cost figures for retrofitting the KC-135A fleet with winglets.

Analysis methods provided good estimates of the aerodynamic effects of winglets on KC-135 performance. At takeoff with a 30° flap setting, the winglets reduced drag of the KC-135A by 72 counts or about 4.7% of airplane drag. At landing with a 50° flap setting, the winglets reduced drag by 42 counts or about 2.5% of airplane drag at lift coefficients corresponding to the approach condition.

The effect of full-span wing leading-edge devices on the performance of winglets at high-lift conditions was investigated analytically and found to be small. Although there was a slight increase in the winglet leading-edge peak pressure and pressure gradients, the change was negligible. The leading-edge device, however, allows the airplane to fly at higher angles of attack and thus achieve higher lift coefficients. At these higher lift coefficients, the winglet will be subjected to higher loads, increased crossflow velocities, and higher leading-edge peak pressures, which may cause the boundary layer to separate. To avoid flow separation requires that a leading-edge device be incorporated in the winglet design. An alternative approach, pursued in this feasibility investigation, was to redesign the winglet with the objective of achieving good low-speed performance with minimal reduction of high-speed performance.

The high-speed wind tunnel test of the KC-135A with winglets showed a 7.2% reduction in airplane drag. The initial buffet boundary was increased by 1.6% to 5.2% through the Mach range from 0.5 to 0.8, and the drag divergence was increased by 0.4% to 0.8% through the C_L range from 0.2 to 0.7. The winglets caused an aft shift in the aerodynamic center of 1.5% to 2.5% of MAC from the basic KC-135A. This shift will result in an insignificant increase in the control force gradients for maneuver and speed changes. The tail-off Mach tuck characteristics did not change significantly with the winglets.

The winglets increased lateral stability, directional stability, and side force due to sideslip. These changes in the lateral-directional stability derivatives could have a significant effect on the unaugmented Dutch roll characteristics.

The low-speed wind tunnel test showed that winglets would reduce the drag of the KC-135A with 30° flaps by 4.1% and increase the lift-to-drag ratio (L/D) by 4.2% at the takeoff condition. With 50° flap deflection and at the approach condition, the drag was reduced by 2.5%. The trimmed $C_{L_{trim}}$ was increased by 0.2% with flaps deflected to 30° and by 1.1% with flaps deflected to 50° with the addition of winglets. The limited amount of pressure data indicated the winglet boundary layer to be attached at conditions representing takeoff, $C_L = 1.23$, and at C_L slightly lower than that for landing, $C_L = 1.21$. No large changes of the longitudinal handling characteristics were exhibited by the low-speed winglet data. The lateral-directional characteristics did change significantly with the addition of winglets. Areas of concern, which would require additional analysis, are the unaugmented Dutch roll damping, ground minimum control speeds, and crosswind takeoff and landing capability.

A study of retrofitting the KC-135A with winglets estimated the cost of $66,000 per unit, based on 1977 dollars. Based on a 1979 program start, the fuel savings benefit obtained by winglets would pay for the cost of this retrofit program by 1984.

With the data generated by the winglet study reported in AFFDL-TR-76-6, *Design and Analysis of Winglets for Military Aircraft,* and by this present study, major questions of concern, which could adversely impact this program, have been answered.

In summary, winglets reduce the fuel consumption of the KC-135A throughout its performance envelope. Initial buffet boundary is increased as well as the drag divergence boundary with winglets. Tail-off Mach tuck characteristics of the KC-135A with winglets appear to be as good as the basic airplane. Longitudinal characteristics are not changed greatly by the winglets. Lateral-directional characteristics exhibit significant changes, and most of these changes are favorable. A winglet retrofit program for the KC-135A would pay for itself in 5 years. By the year 1990, the KC-135A fleet with winglets would save about $200 million, and from 1990 to the year 2000, they would save 437 million gallons of fuel and $770 million.

The need for further investigations on this program would involve additional wind tunnel testing to assess the high-speed tail-on configuration with winglets and the nonlinear sideslip data, further analysis of handling characteristics including aeroelastic effects, and a flight demonstration program. The flight program would provide full-scale data on the effect of winglets on the KC-135A and full confidence to continue into the retrofit program.

SECTION I
INTRODUCTION

Analytic studies and a limited amount of wind tunnel data have confirmed that winglets will improve the cruise efficiency of transport-type military aircraft (refs. 1 and 2). This program and other in-house studies have established a high degree of confidence in these analytic methods for predicting gains in high-speed performance due to winglets.

An objective of the second phase of this program was to establish through the use of numercial methods and wind tunnel data a high degree of confidence in predicting the effect of winglets on high-lift configurations at low speeds. This methodology needed validation in order to achieve the proper compromises for the high-speed/low-speed winglet design with a reasonable guarantee of success.

Certain airplane characteristics, such as buffet, drag rise, longitudinal-lateral stability and control derivatives, low-speed CD_{trim}, etc., are best determined through analysis of wind tunnel data. The NASA-Langley Research Center 8-ft transonic wind tunnel facility tested a 0.035 scale model of the KC-135A with and without winglets at both high- and low-speed conditions. An analysis of these wind tunnel data is included in this study.

To determine the effect of winglets on the KC-135A fleet, a study was conducted to retrofit the KC-135A with winglets. A preliminary program plan was determined, and the cost and savings of the retrofit program for the KC-135A fleet were estimated.

SECTION II
LOW-SPEED AERODYNAMIC ANALYSIS OF AFFDL/BOEING
WINGLET ON THE KC-135A

An aerodynamic analysis of the KC-135A airplane incorporating the AFFDL/Boeing high-speed winglet designed under AFFDL contract F33615-75-C-3123 was undertaken for a landing and a takeoff configuration. The objectives of this analysis were twofold. The first objective was to verify the effectiveness of the analytic tools to predict wing and winglet surface pressure, loads, and changes in drag at low-speed flight conditions. Theoretical estimates obtained through computational methods were compared with data acquired in the NASA-Langley wind tunnel. A good correlation of theoretical and experimental data will give the designer confidence in redesigning an existing winglet geometry as well as designing and predicting the performance of all-new winglets. The second objective was to evaluate the performance of the winglet at low-speed, high-lift conditions and identify any potential aerodynamic problems that may exist. The analysis method used for this study is described in reference 3.

1

1. DESCRIPTION OF ANALYTIC MODEL

The high-lift conditions analyzed were 30° and 50° flap settings corresponding to the takeoff and landing conditions, respectively. These conditions were selected to match the available flap settings for an existing 0.035 scale wind tunnel model. Lift coefficients corresponding to conditions of most concern were estimated for each of the flap settings (see ref. 4), and care was taken to best represent the configuration at these C_L's.

The analytic modeling was accomplished in Boeing computer program TEA 230, a three-dimensional potential flow program, which accounts for thickness and compressibility effects. (See appendix for program description.) Appropriate flap geometry was used, which best modeled the distribution of circulation along the span of the wing and the overall lift level. Establishing the correct lift level on the wing and the corresponding circulation in the outboard region is important because the crossflow velocity at the wingtip is strongly related to these two parameters. If care is not taken in maintaining these features, abnormally high or low fin loadings may result, and the fin upper surface minimum pressure may be poorly estimated. Figures 1 and 2 show the basic geometry and the wing paneling devised for the 30° flap model. The winglet is shown positioned at the tip of the wing.

The winglet designed under AFFDL contract F33615-75-C-3123 was intended to be canted outboard 20°. Through an error in the design and manufacturing of the wind tunnel model, this cant was reduced to 6°. These winglets were identified as Z_1 and Z_2. Z_1 is the winglet with a 20° cant angle, and Z_2 has a 6° cant. A more detailed explanation is given in section V. Since one of the objectives of this study was to validate the effectiveness of the analytical tools in estimating winglet parameters, it was decided that the winglet model used in TEA 230 should also be canted by 6° to correspond to the wind tunnel model. The length of the winglet remained 13.5% semispan. This geometry is shown in figure 3.

2. TAKEOFF CONFIGURATION

The estimated takeoff C_L at 30° flaps is 1.23. Buffet occurs at a C_L of 1.37. With a landing configuration at 30° flaps, touchdown occurs at $C_L = 1.05$. The critical condition, with respect to the performance of a winglet, occurs at higher C_L's since the higher circulation outboard results in an increase in crossflow velocity at the wingtip, which in turn places the winglet at a higher effective angle of attack. At this condition, separation is more likely to occur. For this reason, the takeoff condition, $C_L = 1.23$, was the most critical with respect to the winglet pressure distribution.

Surface pressures on the AFFDL/Boeing winglet Z_2 at both the landing and takeoff C_L's are presented in figure 4. The peak pressure at the takeoff C_L of 1.22 is substantially higher, as expected, than at the landing C_L of 1.05. Thus, flow separation will likely occur at the takeoff condition. Surface pressure distributions for 30° flaps, at the takeoff condition, are presented in figure 5. The highest peak pressure, $C_p = -10$, occurs at 35% of the winglet span in the area where the winglet strake intersects the leading edge of the basic winglet trapezoid. The winglet pressures indicate that the winglet is subjected

2

to higher local angles of attack due to the large crossflow velocities near the wingtip. The influence of the winglet on the wing surface pressures extends over a large portion of the outboard wing. Obviously these induced effects at the wing-winglet intersection increase with increasing wing lift coefficient. Examination of the wing surface pressures shows that: (1) the winglet does not have an adverse effect on the chordwise pressure distribution; (2) the wing peak pressures at the leading edge are reduced because of a reduction in wing angle of attack; (3) the pressure gradient in the chordwise direction is decreased because of an increase in velocity aft of the wing leading edge; and (4) pressure gradients in the spanwise direction are also reduced, which may be helpful in delaying separation at the wingtip.

The span loading for the KC-135A with winglet Z_2 is shown in figure 6 at the takeoff C_L of 1.22. The presence of the winglet allows the outboard wing to carry a greater load. Therefore, to fly at the same lift coefficient, the KC-135A with winglets can fly at a lower wing angle of attack than the basic KC-135A. For the same lift coefficient, the loading inboard of 82% of the wing span is reduced, while outboard of this span station the load increases, as shown in figure 7. The predicted reduction in drag, for the 30° flap setting, is compared with experimental data in figure 8. The results obtained by two analytical methods are presented. The lower curve uses the induced drag based on a Trefftz plane analysis. Span loads calculated in TEA 230 are analyzed in Boeing computer program TEA 242. (See appendix for program description.) The inherent conditions implied in a far-field analysis are not satisfied by a wing with deflected flaps or at high lift coefficients. Trefftz plane induced drag calculations assume a linearized model in which the downwash is fairly uniform across the span and is much smaller in magnitude than the freestream velocity. Obviously, this is not the case with a flapped configuration. The second method for calculating the induced drag, a near-field solution, is accomplished through the use of Boeing computer program TEA 372. (See app. A for program description.) TEA 372 is a vortex lattice program, capable of optimizing arbitrary geometries with respect to induced drag as well as analyzing a given configuration. Care must be taken in modeling the wing and winglet trailing vortices. In order to best simulate the actual flow conditions, the trailing vortices should coincide with streamlines. This was accomplished on the KC-135A by using an iterative process. The magnitude of the induced drag was not accurately predicted by either method; however, the trends were well predicted. Neither method accounts for induced drag changes that result from changes in span loading due to viscous effects, but these are typically small for lift coefficients below buffet. The "tapering off" of the experimental drag reduction at higher C_L's can probably be attributed to the beginning of flow separation on the winglet.

Figure 9a shows the theoretically predicted pitching moment curves for the baseline configuration and for the KC-135A with winglet Z_2. The increased loading at the wingtip causes a corresponding increase in nose-down pitching moment. This increment is shown in figure 9b. The change in angle of attack at a given configuration C_L is shown in figure 9c. Changes in wing bending moment nondimensionalized by the wing semispan and half of the total lift are shown in figure 10a. This nondimensional bending moment increment decreases slightly with increasing wing C_L because of shifts

3

in the load distribution along the span. Figure 10b shows the bending moment change as a percentage increment from the baseline KC-135A. The bending moment increases about 3% at the wing root and from 17% to 19% at 60% semispan for the C_L's of interest. In assessing structural weight due to winglets, it is necessary to consider not only the wing-root bending moment but also the bending moment distribution along the span.

3. LANDING CONFIGURATION

The AFFDL/Boeing winglet Z_2 was also analyzed on the KC-135A in a landing configuration with 50° flaps. At this flap setting, normal touchdown occurs at a C_L of 1.21 and buffet occurs at a C_L of 1.49.

Figure 11 compares the TEA 230 theoretical pressures with experimental data. Two stations on the winglet, $\eta = 0.25$ and $\eta = 0.75$, are depicted at a C_L of approximately 1.10. Agreement between the theoretical and experimental pressures is seen to be quite good. The shape of the pressure distribution is well defined although the theoretical level is a little high. The probable reason for this is the occurrence of flow separation which is just beginning to take place at the winglet trailing edge. Separation would tend to decrease the upper surface velocities and increase the lower surface velocities as the experimental data indicate. Theoretically predicted pressures obtained by a potential flow solution will not account for these viscous flow effects. However, the potential flow solution provides valuable data for tailoring the winglet chordwise geometry in order to obtain the desirable pressure distribution.

Winglet surface pressures measured experimentally were obtained only at the 50° landing flap setting. Figure 12 shows the chordwise pressure distributions for several stations on the outboard wing and winglet Z_2 at a C_L of 1.20. These pressures are similar to those shown for the takeoff configuration at 30° flaps except that pressure peaks and levels are slightly lower. Lower pressure levels were expected because at the 50° flaps landing condition the wing is at approximately 3° lower angle of attack than the 30° flaps takeoff condition previously discussed. Because of the reduced angle of attack, the outboard wing and the winglet carry proportionately less load. Figures 13 and 14 show the span load distribution and section C_ℓ's, respectively, at an airplane C_L of 1.20. Comparison of these data with data shown in figures 6 and 7 for the 30° flap configuration indicates that the load carried by the outboard wing is less for the landing configuration than for the takeoff configuration.

The reduction in airplane drag at 50° flaps due to winglet Z_2 is shown in figure 15. Again, both methods of calculating the induced drag, as discussed in section II.2, are shown. The theoretical drag estimation predicts reasonably well the experimental results at this flight condition. This good agreement is aided by the fact that there is apparently very little flow separation on the winglet for the C_L's shown. The lack of flow separation on the fin through this range of C_L's was expected since at the same angle of attack the lift increases from 0.95 to 1.20 when the flap deflection is increased from 30° to 50°. As shown in figure 8 for 30° flaps and at a C_L of 0.95, the predicted reduction in induced drag agrees with experimental results, indicating that flow

separation on the winglet has not yet occurred. The large reduction in drag predicted theoretically at a C_L of 1.3 and 50^0 flaps (fig. 15) is in part due to a decrease in parasite drag resulting from the reduction in wing angle of attack. A reduction of wing parasite drag of the order of magnitude predicted theoretically at high C_L's was not obtained experimentally.

Figure 16a shows the pitching moment variation with C_L at 50^0 flaps for the baseline configuration and for the KC-135A with winglet Z_2. The estimated change in pitching moment is shown in figure 16b. At a given C_L, the pitching moment change at 50^0 flaps is not as large as the pitching moment change at the 30^0 flap setting. The change in wing angle of attack with winglet Z_2 (shown in fig. 16c for the landing flaps configuration) is also smaller in magnitude at 50^0 flaps and a given C_L than at 30^0 flaps and the same C_L. The estimated change in wing bending moment is shown in figure 17a for a range of C_L's. The corresponding percent change is shown in figure 17b. Compared with the baseline configuration, the wing bending moment at 50^0 flaps increased about 3% at the wing root and from 17% to 20% at 60% semispan with winglet Z_2. This is approximately the same increase in wing bending moment as was found at the 30^0 flap setting.

4. POTENTIAL PROBLEM AREAS

The concept of a winglet is aimed at improving the cruise performance of transport-type aircraft. However, to achieve this objective, it is necessary to ensure that the winglet does not have a detrimental effect on the low-speed flight characteristics. The theoretical and experimental analyses of the KC-135A show the winglets can apparently operate effectively in the low-speed flight regime and, in fact, improve the low-speed performance. The reduction in drag is important when considering takeoff field length and rate of climb. Potential problem areas exist, which must also be considered.

Some of the problems identified at low-speed conditions are similar to those encountered at high speed. An increase in bending moment along the span of the wing due to the winglet must be analyzed to assess the structural weight penalty. A substantial increase in nose-down pitching moment because of the increased loading at the wingtip must be trimmed, causing a possible increase in trim drag, or it could restrict the aft c.g. limit. Changes in the low-speed lateral and longitudinal stability characteristics must be assessed, particularly the outboard aileron effectiveness. Many of these problem areas will be considered in detail later in this report.

A final problem area is, of course, flow separation at the low-speed flight conditions. As was mentioned previously in section II.2, the winglet appears to have a favorable effect on the wing pressure distribution. The increase in span loading at the wingtip allows the airplane to fly at a lower angle of attack. The reduction in angle of attack will reduce leading-edge peak pressures. Also, near the wingtip, the winglet increases the flow velocity on the upper surface of the wing aft of the leading edge and decreases the velocity on the lower surface. The increase in upper surface velocity tends to reduce the adverse pressure gradient that promoted separation.

5

Flow separation on the wing may occur if there is a well-developed separation on the winglet. It would appear, based on a theoretical analysis of the chordwise pressure distribution and on wind tunnel data, that flow separation on the winglet should not be a problem in the normal flight regime of the KC-135A. There is some flow separation on the winglet at wind tunnel Reynolds numbers and at very high C_L's, but the flow separation is not well developed and did not deteriorate the wing performance. Also, the results of the wind tunnel test of the full-span model are probably conservative, because of the lower Reynolds number and wingtip deflections of this model as compared to either the semispan model or the full-size KC-135. (The semispan model was tailored to have the same relative wing deflections as the full-size airplane.) However, any flow separation on the winglet substantially increases pressure drag and thus may eliminate altogether any performance gains that may be achieved through a reduction in induced drag. It is therefore necessary to improve the low-speed performance of the winglet without seriously compromising the high-speed performance. This problem will be considered in depth in section IV of this report.

SECTION III
EFFECT OF A LEADING-EDGE DEVICE ON AFFDL/BOEING WINGLET

The effect of wing leading-edge devices on the performance of the KC-135A with winglets at low-speed, high-lift conditions was investigated analytically. Although most military transport aircraft in service today do not have full leading-edge devices, future military aircraft may incorporate these devices.

1. DESCRIPTION OF ANALYTIC MODEL

The effect of a wing leading-edge device on winglet performance was determined by examining its effect on wing span loading and winglet surface pressures. Analysis was performed at the takeoff flap setting of 30° because the winglet surface pressures were determined to be more critical with respect to flow separation at this condition than for the 50° landing flap condition. (See secs. I.2 and II.3.) Winglet Z_2, designed under AFFDL contract F33615-75-C-3123, was used in the analysis. It was positioned at the wingtip and canted outboard 6° in order to maintain consistency with the previous analysis.

The leading-edge device selected for the analysis was a scaled-down 747-type Krueger. It covered the leading edge of the wing from the inboard nacelle to the wingtip (see fig. 18). A nominal location was selected for positioning the device with respect to the wing leading edge. No attempt was made, however, to optimize this position.

2. ANALYTIC RESULTS

Figure 19 compares the outboard wing and winglet surface pressures with and without a leading-edge device. The wing pressures show the reduction in upper surface velocities expected through the use of a leading-edge device. On the winglet, there is little change in the pressure distribution between the two cases. The velocity levels are only slightly increased near the root of the winglet. Away from the wing, the winglet pressures are essentially the same with or without a leading-edge device on the wing.

The span loading is shown in figure 20 for the wing with and without a leading-edge device. Although the load distribution changes considerably with the addition of the leading-edge device the outboard span load is basically unaltered. The similarity of the winglet pressure distributions with and without the wing leading-edge device can be explained by the effect on the outboard span loading. In order to generate the same outboard wing load, the circulation in both cases must be essentially the same. This circulation, even though distributed differently in the chordwise direction along the wing, will induce a very similar flow field away from its immediate vicinity. The winglet therefore experiences approximately the same crossflow whether there is a leading-edge device on the wing or not. Only very close to the wing is the difference in chordwise load distribution reflected on the winglet pressures.

Minimum pressures are shown for the outboard wing in figure 21 and for the winglet in figure 22. In both cases the KC-135A with a wing leading-edge device and the baseline KC-135A configuration are depicted. As would be expected, the wing minimum pressures reflect a significant reduction in upper surface velocity with the use of a leading-edge device. Peak pressures on the winglet show a slight increase with the use of a leading-edge device. This increase in peak pressures is most noticeable near the fin root and at high C_L's. Away from the wing, the effect of the leading-edge device becomes insignificant.

3. CONCLUSIONS

A leading-edge device on the KC-135A has very little effect on the performance of a winglet at the C_L's that were analyzed. Although there is a slight increase in leading-edge peak pressure and the pressure gradients become more adverse, the magnitude of these increments is so small that it is insignificant. However, since the wing leading-edge device allows the airplane to fly at higher lift coefficients, the winglet will consequently be subjected to higher loads, increased crossflow velocity, and higher leading-edge peak pressures, which may cause flow separation to occur on the winglet. At these C_L's, it may be necessary to redesign the winglet in an attempt to improve its low-speed performance. The required redesign process is discussed in section IV.

SECTION IV
COMPROMISE HIGH-SPEED/LOW-SPEED WINGLET DESIGN

A winglet is designed to reduce airplane induced drag at the cruise condition. The design must be carefully tailored so that this reduction in induced drag is not offset by increases in skin friction drag, pressure drag, and interference drag. The high-speed winglet design must then be analyzed throughout the flight regime to ascertain that aircraft performance in this flight regime is not impaired. It should be noted that improvement in low-speed performance through the use of a winglet was not a primary requirement in this investigation; however, it was required that low-speed performance should not be impaired by the winglet which had been designed strictly from high-speed considerations.

Current transport aircraft operate through a wide range of lift coefficients; therefore, the winglet airfoil section characteristics such as camber, thickness, and leading-edge radius must be carefully selected in order to achieve appropriate chordwise pressures throughout the flight envelope. Further, the winglet design must be accomplished in the curvilinear flow field at the wingtip, which significantly changes characteristics with changes in aircraft C_L.

For many aircraft it may not be possible to design a fixed geometry winglet that performs well at cruise and does not deteriorate performance at low speed. For the KC-135A, which does not have the C_{Lmax} capability of many current aircraft, a fixed geometry fin is feasible. The winglet Z_2 designed under AFFDL contract F33615-75-C-3123 has demonstrated analytically (sec. II) and experimentally (sec. VI) that it can perform effectively in the low-speed flight regime. Slight modification of the winglet geometry may further improve its low-speed performance without incurring a reduction in cruise performance.

The following paragraphs discuss the procedure by which a winglet was designed for the 30° flap takeoff condition on the KC-135A.

1. DESIGN OF A WINGLET FOR LOW-SPEED FLIGHT CONDITION

Winglet Z_3 was designed for the 30° flap takeoff condition. This flight condition was found to be the most critical with respect to winglet surface pressure distribution. The purpose of designing a winglet based entirely on low-speed considerations was to evaluate the characteristics of the winglet airfoil sections when immersed in the curvilinear flow field generated at the wingtip. Based on this knowledge, the airfoil section properties of winglet Z_2 could be perturbed slightly to improve its low-speed performance.

The vortex lattice computer program TEA 372 was used to determine the camber shape and twist distribution of the new winglet for a specified chordwise loading and minimum induced drag. The planform shape of the low-speed winglet Z_3 was the same as the planform of winglet Z_2 designed previously. Winglet Z_3 was canted outboard 6°.

To achieve the minimum induced drag at the 30° flap takeoff condition, it is necessary for the new winglet design to carry a significantly greater load than the load carried by winglet Z_2 at this same flight condition. Winglet Z_3 airfoil sections are therefore more cambered than the sections of winglet Z_2. At high-speed flight conditions, this increased camber could be detrimental to the winglet performance.

Chordwise pressures for the outboard wing and winglet Z_3 at the takeoff condition are shown in figure 23. The pressure distributions for the lower portion of the winglet are quite reasonable except in the leading-edge region. The high leading-edge peak pressure and the excessive aft camber in the winglet airfoil result from coarse paneling in areas on the airfoil having high curvature. Figures 24 and 25 show the span loading and the section C_ℓ's, respectively, for the takeoff condition.

The reduction in induced drag at takeoff with winglet Z_3 is shown in figure 26. For comparison, results for winglet Z_2 are also shown. Winglet Z_3 designed for the takeoff flap condition at a C_L of 1.2, produces about a 10% greater reduction in induced drag than winglet Z_2 designed for the cruise condition. The increase in bending moment along the wing semispan with winglet Z_3 is shown in figure 27a. The corresponding percent increase in bending moment is shown in figure 27b. By comparing these results to those previously shown for winglet Z_2 (fig. 10a and 10b), the larger increase in wing bending moment with winglet Z_3 is evident. For example, at 60% wing semispan, winglet Z_2 increases the bending moment by about 17%, while winglet Z_3 increases the bending moment by 21.5%. The additional savings in induced drag at this flight condition with winglet Z_3 compared to winglet Z_2 does not compensate for the increase in wing bending moment incurred.

Pressure distributions obtained with the potential flow program TEA 230, at Mach 0.7, with winglet Z_3 are shown in figure 28. Obviously, the pressure distribution on the winglet is unacceptable. These data illustrate the fact that an increase in camber, required by low-speed considerations, is not compatible with the required camber characteristics for the cruise condition. Therefore, the best design will evolve from the consideration of the low- and high-speed requirements. Figure 29 shows the span load distribution at this flight condition.

From the data generated in the design of winglet Z_3, several conclusions are drawn. First, a large increase in camber on the winglet airfoil sections to improve low-speed performance will excessively penalize cruise performance. Second, increasing the load carried by the winglet to minimize induced drag at low speed is not advantageous for the overall design for the following reasons. For the same winglet planform, increasing the load will result in flow separation on the winglet, and possibly the wing, at lower airplane C_L's. If, on the other hand, the winglet planform area is increased proportionately to the increase in loading, skin friction drag will increase, and the increase in wing bending moment along the wing will result in higher structural weight. Finally, it appears that a drooped leading edge will improve the performance of winglet Z_2. As was noted previously, winglet Z_2 performs acceptably well in the low-speed flight regime. Increasing the leading-edge droop would reduce the adverse

9

pressure gradients in the leading-edge area and delay flow separation on the winglet, provided the cruise performance is not adversely affected by the occurrence of excessive lower surface peak pressures. Based on these considerations, winglet Z_2 leading camber was modified in order to improve the low-speed performance.

2. DESIGN OF A COMPROMISE HIGH-SPEED/LOW-SPEED WINGLET

To determine the droop required on winglet Z_2 to reduce the low-speed peak pressures, a number of airfoil sections were analyzed two-dimensionally at section C_{ℓ}'s corresponding to the takeoff condition. The amount of droop and the slope of the airfoil camber line at the leading edge were varied until a reasonable pressure distribution was obtained. When this new section was analyzed two-dimensionally at a typical cruise condition, the leading edge exhibited a high-pressure peak on the lower surface. To ensure acceptable high-speed winglet performance, it was necessary to reduce the lower surface pressure peak by selecting a lesser droop. This iterative process was continued until a design evolved that showed a significant reduction in peak pressures at the low-speed condition while maintaining the desired pressure characteristics at high speed.

This new airfoil section was applied to the outboard 60% of the span of the winglet. Other sections with similar increased leading-edge camber were applied to the remainder of the winglet. This compromise winglet design, which had the same planform and cant as Z_2, was identified as winglet Z_4. The compromise winglet was analyzed at both the cruise and the 30° flap conditions. Figure 30 compares the surface pressures of winglet Z_4 to the baseline winglet Z_2 at the takeoff condition. Clearly, there is very little change in the pressure distribution. The peak pressure level is essentially unchanged, but the adverse pressure gradients have become slightly more severe because of the earlier recovery from the pressure peak. The winglet pressures at cruise conditions are shown in figure 31. The pressure distribution on winglet Z_4 is slightly smoother than the pressure distribution on winglet Z_2; however, the absolute peaks and levels are essentially unchanged.

From these three-dimensional pressures, it was deduced that the increase in leading-edge camber was too conservative. Because of the curvature of the flow field at the winglet leading edge, it appears that an airfoil section with considerably increased leading-edge camber would be able to function effectively at both the high- and the low-speed flight conditions. A final winglet was designed to test this hypothesis.

3. FINAL COMPROMISE WINGLET DESIGN

Winglet Z_5, the second compromise winglet, was designed by substantially increasing the camber ahead of the 20% chord of the winglet airfoil. This droop amounted to an increase in camberline slope of 31° at the airfoil leading edge. Aft of about 25% chord, the winglet Z_2 airfoil section was retained. In order to improve the pressure distribution on the lower surface at the cruise condition, the airfoil's leading-edge radius was doubled, and the upper and lower surfaces were smoothed. To maintain consistency in the analysis, the planform and cant angle of winglet Z_2 was also retained for winglet

10

Z_5. Figure 32 shows the winglet geometry and compares the present airfoil section with a corresponding section on winglet Z_2. The increase in leading-edge radius and camber is quite evident.

Winglet Z_5 was analyzed in the three-dimensional potential flow program TEA 230 for the 30° flap takeoff configuration and for the cruise configuration. Figure 33 shows the comparisons of surface pressures of winglet Z_5 to those of winglet Z_2 at a C_L of 1.0 and with 30° flaps. The large reduction in the winglet leading-edge peak pressures is apparent in this figure. The span loading of the KC-135A with winglet Z_5 with 30° flaps is shown in figure 34. The induced drag reduction with winglet Z_5 is shown in figure 35. At the low-speed flight condition, the theoretical reduction in induced drag is about the same for winglets Z_2 and Z_5. However, because of the improvement in chordwise pressures on winglet Z_5, separation should be delayed and a "tapering off" of the drag reduction that was seen in the experimental data shown in figure 8 should be delayed to higher wing C_L's.

The pitching moment curves with 30° flaps for the basic KC-135A and for the KC-135A with winglet Z_5 are shown in figure 36a. The change in pitching moment is shown in figure 36b. Essentially the same pitching moment change occurs with either winglet Z_2 or winglet Z_5. The change in wing angle of attack is shown in figure 36c for the 30° flap configuration. A slightly larger reduction in angle of attack occurs with winglet Z_2 than with winglet Z_5. It is doubtful if this difference in angle-of-attack change could be measured in the wind tunnel. Viscous effects tend to reduce the lift curve slope from the slope predicted by potential flow theory. The change in wing bending moment with 30° flaps is shown in figure 37a, and the percent change in wing bending moment is shown in figure 37b. These increments in bending moment for winglet Z_5 are essentially the same as those shown for winglet Z_2 in figure 10.

Surface pressures for the high-speed configuration at Mach 0.7 are shown in figure 38. As was anticipated, there is a significant pressure peak on the lower surface of the winglet at this flight condition. However, this peak is not as large as on the two-dimensional airfoil section having the same amount of leading-edge camber as the airfoils of winglet Z_5. The lower surface peak pressure on the winglet increased in magnitude as the distance from the surface of the wing increased. The same amount of droop was used for all sections on the winglet, although it was realized that the crossflow velocity varies inversely with the distance from the wing and that the amount of droop added to the airfoil should also change in a similar manner. A two-dimensional viscous analysis of the chordwise pressure distribution was completed for winglet Z_5 at the cruise condition. At flight Reynolds numbers, the lower surface pressure peak could be expected to cause an early transition from laminar to turbulent bounday layer; however, separation is not expected to occur. At higher than cruise C_L's, the lower surface peak pressure is reduced. Figure 39 shows the span loading at the cruise condition. The reduction of induced drag at cruise is presented in figure 40. Winglet Z_5 produces almost as great an induced drag reduction as winglet Z_2 at the cruise C_L.

11

A boundary-layer analysis for several of the winglet designs was made with a two-dimensional boundary-layer program, TEA 200. (See app. A for program description.) The results obtained by strip theory, which couples the three-dimensional surface pressures obtained from TEA 230 with the two-dimensional boundary-layer program TEA 200, are shown in figure 41. All results were computed for flight Reynolds numbers. Figure 41a shows the growth of the boundary layer on the wing and winglet. The winglet displacement thickness growth was reduced on winglet Z_5, as might be expected from the pressure distribution. Estimated skin friction drag coefficient is shown in figure 41b, and the boundary-layer shape factor is shown in figure 41c. The accuracy of these viscous results is questionable in view of the three-dimensionality of the flow field near the wingtip, but the results should be valid and useful in establishing trends and in comparing one winglet design with another.

4. POSSIBLE DESIGN IMPROVEMENTS

The difficulties in determining a winglet design that properly balances the desired pressure distribution characteristics at cruise and at takeoff and landing conditions are apparent from the design process described in section IV.3. However, based upon the analysis of winglet Z_5, there is reasonable confidence that an increase in leading-edge camber to improve the low-speed performance of a winglet will not be detrimental to its high-speed performance. The curvilinear nature of the flow field at the wingtip may permit a substantial amount of leading-edge droop on the winglet, which would be entirely unacceptable in another type of application. It would be necessary to validate this experimentally before a firm conclusion may be drawn.

As previously stated, the design of winglet Z_5 could be improved by reducing the leading-edge camber. Furthermore, the droop should vary along the span of the winglet from greatest at the root to least at the tip to take into account variations in crossflow along the vertical plane. Both of these changes would help reduce the lower surface pressure peak at the high-speed cruise condition while realizing a reduction in upper surface peak pressure at low speed. The overall performance of the winglet could also be improved by reducing the load it carried at the cruise condition. By designing at a slightly less than optimum winglet loading, approximately the same reduction in induced drag could be obtained at cruise. The reduced loading should slightly delay separation on the winglet at the low-speed flight conditions. By combining the effect of leading-edge camber and decreased winglet loading at cruise, the low-speed performance of winglet Z_2 on the KC-135A at high C_L's should be improved with minimal impact on the winglet high-speed performance.

SECTION V
ANALYSIS OF HIGH-SPEED WIND TUNNEL DATA OF
AFFDL/BOEING WINGLETS

As stated in section I, certain aerodynamic data are best obtained by analyzing wind tunnel data. For the high-speed conditions. Mach tuck, buffet, drag rise, span loading, trim drag, and longitudinal and lateral stability and control data are identified as the desired aerodynamic data. These data were obtained from wind tunnel tests conducted at the NASA-Langley Research Center 8-ft transonic wind tunnel facility. This facility is a pressure tunnel with a 7.1-ft. square test section and a Mach number range from 0 to 1.3.

1. WIND TUNNEL MODEL DESCRIPTION

A 0.035 scale wing of the KC-135A with four nacelles and struts and a body from a NASA high-aspect-ratio wing model was used for the high-speed winglet wind tunnel test. A three-view drawing of this model is shown in figure 42. The model is an aft sting-mounted type and did not have provisions to attach either the vertical or horizontal stabilizers. The original KC-135A model designated as FR-174I had a center body structure that placed the center of the NASA internal strain gage balance a considerable distance aft of the quarter chord of the wing MAC, which would cause the balance pitching moment limit to be exceeded at very low values of wing lift. This situation was alleviated by replacing the FR-174I center body structure with the NASA high-aspect-ratio wing center body structure. This center body placed the balance center just aft of the quarter chord of the wing MAC. This center body had no structure aft of the balance, hence the vertical and horizontal stabilizers could not be attached. The NASA center body was slightly larger than the FR-174I model body skins could enclose; therefore, the NASA body skins were also used. Although the NASA body was slightly larger than the 0.035 scale KC-135A body and circular in cross section instead of oval, the conclusions were that the incremental changes in the aerodynamic parameters caused by the winglets were very good and that these increments could be applied to the KC-135A.

The AFFDL/Boeing-designed winglet is shown in figure 3. A discrepancy between the winglet defined in figure 3 and reference 1 should be noted. The cant angle is shown as 6° in figure 43 and 20° in reference 1. Because of an inadvertent error by the model designer through subtracting the 7° wing dihedral angle instel 1 of adding, the winglet model drawings showed the included angle between the wing plane and winglet plane to be 14° too small. Hence, when the winglet was mounted on the wing, the cant angle was 6° instead of the desired 20° cant angle. Although the specified cant angle of 20° was not built on the winglet model, the penalty of having 6° of cant is 1.8 drag counts or 0.7% of airplane drag, and the advantage is 1.4% less WRBM increase.

13

2. HIGH-SPEED WIND TUNNEL DATA

All the high-speed wind tunnel data obtained on the KC-135A with and without the AFFDL/Boeing-designed winglets were obtained without either the vertical or horizontal stabilizers on the model. The Reynolds number per foot was varied from 3.8 to 5.2 x 10^6 at Mach numbers from 0.5 to 0.95. The angle of attack varied from -2° to +7°, and the sideslip angle from -5° to +5°.

Six component force data and wing and winglet static pressure data were recorded. The balance data were reduced to force and moment coefficients about the stability axis placed on the boundary centerline at the quarter chord of the MAC. These data are shown for the basic KC-135A in figures 43 and 44 and for the KC-135A with winglets in figures 45 and 46.

The pressure data were reduced to pressure coefficients C_p and integrated section normal force coefficient C_N. The integrated normal force data are shown in terms of span loads in figures 47 through 51 for the basic KC-135A and in figures 52 through 57 for the KC-135A with winglets. Samples of the chordwise pressure distributions are shown in figures 58 through 60 for the basic KC-135A and in figures 61 though 65 for the KC-135A with winglets.

Strain gage data were also recorded to measure the wing-root bending moment. These data were compared with data from a NASA-LRC half-model test of a KC-135A with and without winglets (ref. 2) and with data from theoretical calculations in reference 1. The wing-root bending moment increase caused by winglets was about twice the increment determined by references 1 and 2. Because of this difference and the inability to check the strain gage data, these wing-root bending moment data were not presented in this report.

3. EFFECT OF WINGLETS ON KC-135A HIGH-SPEED AERODYNAMICS

The effects of the AFFDL/Boeing winglets on the KC-135A are summarized in figure 66 in terms of percent reduction in airplane drag and the corresponding increase in WRBM. The WRBM data were obtained from a NASA-LRC half-model test of the KC-135A. The stiffness of this half (semispan) model wing was tailored so that the model wing had the same relative deflections as the full-size KC-135. The full-span model had a stiffer wing which did not deflect very much; therefore, the WRBM data of the half model is probably more reliable than the full-span model. At approximately the cruise condition, $M = 0.78$ and $C_L = 0.426$, the winglets produced a 6.2% reduction in airplane drag with about a 3% increase in WRBM. The increment in drag produced by the winglets was not corrected for scale effects and the percent change in airplane drag was calculated by dividing the drag change by the full scale airplane drag as published in the KC-135 substantiation document, reference 4. If the KC-135A with winglets is reoptimized for the long-range cruise, then the average $C_{L cruise}$ changes from 0.426 to 0.447 and the cruise Mach number changes from 0.77 to 0.774. (See ref. 1.) For this long-range cruise case, the winglets increase the $M(L/D)_{cruise}$ by 7.2%, based on the high-speed wind tunnel data.

The initial buffet and drag divergence boundary of the KC-135A are expanded by the incorporation of winglets, as shown in figure 67. The lift coefficient for initial buffet $C_{L_{initial\ buffet}}$ was increased by 1.6% to 5.2% through the Mach range of 0.5 to 0.8. (See fig. 68.) The drag divergence Mach number M_{DD} was increased by 0.4% to 0.8% through the C_L range of 0.2 to 0.7.

At approximately cruise Mach number, M = 0.78, the winglet pressure data show that the inboard winglet and the outboard wing start to separate somewhere between $\alpha = 3^0$ to 5^0 or at $C_L = 0.6$ to 0.8. This corresponds closely to the initial buffet boundry as determined by the force data. The outboard winglet did not exhibit any separation up through $\alpha = 5^0$ or $C_L = 0.8$. On the basis of these data it is concluded that the flow on the AFFDL/Boeing winglets is not separated within the high-speed initial buffet and drag divergence boundaries.

4. EFFECT OF WINGLETS ON KC-135A HIGH-SPEED STABILITY

The effects of the AFFDL/Boeing winglets on the high-speed aerodynamic stability and control characteristics of the KC-135A are shown in figures 69 and 70. Since all the data taken during this test were with horizontal and vertical stabilizers off, the effects of the winglets on the total configuration can only be estimated.

The change in the aerodynamic center location caused by the winglets is shown in figure 69. The winglets show an aft shift in the tail-off aerodynamic center of approximately 2% to 3% of MAC from the basic KC-135A. Analysis of the low-speed flaps-up data indicates that the increments shown in figure 69 could be reduced by about 0.5% MAC for the tail-on configuration. Figure 70 shows that, for an altitude of 23,000 ft, the tail-off Mach tuck characteristics or static longitudinal stability characteristics at overspeed conditions of the KC-135A are not significantly changed by the addition of winglets. Although only tail-off data are available, the addition of winglets to the complete KC-135A configuration will probably cause an aft shift of the rigid aerodynamic center of 1.5% to 2.5% MAC. This shift will result in an insignificant incease in the control force gradients for maneuvers and speed changes.

Figure 71 shows the effect of the winglets on the vertical and horizontal tail-off lateral-directional derivatives. These data were derived from pitch runs at a constant sideslip angle of $\psi = 5^0$. The tail-off directional stability C_{n_β} is increased relative to that of the basic KC-135A by approximately 13%. Static lateral stability C_{l_β} for the winglet configurations is increased by approximately 23%. The side force due to sideslip derivative, C_{y_β} for the AFFDL/Boeing winglet is 14% to 19% higher than that of the basic KC-135A. These changes in the lateral-directional stability derivatives could have a significant effect on the unaugmented Dutch roll characteristics.

SECTION VI
ANALYSIS OF LOW-SPEED WIND TUNNEL DATA

For the low-speed conditions the airplane usually has trailing-edge flaps deflected and, even at low angles of attack, the flows on the flaps are separated. This is a difficult flow condition to analyze and, hence, makes estimations of airplanes' aerodynamic characteristics very difficult. The low-speed winglet aerodynamic characteristics that were identified for evaluation through the analysis of wind tunnel data are as follows: (1) airplane C_{Lmax}, (2) aileron-winglet interference, (3) trimmed drag polars, and (4) longitudinal and lateral stability and control.

The low-speed test of the AFFDL/Boeing winglets on a KC-135A was conducted in the same tunnel as the high-speed test – the NASA-Langley Research Center 8-ft transonic wind tunnel, which is described in section V.

1. WIND TUNNEL MODEL DESCRIPTION

An existing 0.035 scale KC-135A model designated as FR-174I was used for this test. This model is an aft sting-mounted type, as shown in figure 72. It has four flow-through nacelles that are strut mounted and a variable incidence horizontal stabilizer with settings of 0°, -4°, and -10°. Two flap deflections were used during this test, 30° and 50°, and a typical cross section of each of these flaps is shown in figure 73. The outboard aileron has a chord of 0.875 in. and extends from model wing station 25.14 to 33.26. These ailerons have brackets to set 0°, $\pm10^\circ$, and $\pm20^\circ$ deflections. Table 1 lists the model's geometric characteristics.

The winglets used for the low-speed test were the AFFDL/Boeing-designed winglets (ref. 1). The winglets are described in section V.1. and are shown in figure 3.

2. LOW-SPEED WIND TUNNEL DATA

The low-speed winglet wind tunnel data were obtained at Mach 0.30 and at a Reynolds number per foot of 3.7×10^6. The angle of attack was varied from -6° to $+14^\circ$ and the sideslip angle from -5° to $+5^\circ$.

Six component force data and winglet static pressure data were recorded. The force data for the KC-135A with 30° and 50° flaps are shown in figures 74 and 75. The winglet pressure data, which unfortunately were obtained only at 50° flap deflection, are shown in figures 76 and 77.

3. EFFECT OF WINGLETS ON KC-135A LOW-SPEED AERODYNAMICS

The trimmed drag polars for the basic KC-135A and for the KC-135A with winglets are shown in figure 78 for trailing-edge flap deflections of 30° and 50°. The trimmed lift curves at C_{Lmax} are shown in figure 79. These data are wind tunnel results trimmed to a c.g. located at 0.25 MAC.

Table 1. — KC-135A Model Geometry

	Full-size airplane	Wind tunnel model
WING		
Planform area, ft^2	2433	2.980
Span, ft	130.83	4.579
Aspect ratio	7.035	Same
Taper ratio	0.33	Same
Dihedral angel, deg	7	Same
Incidence angel, deg	2	Same
Aerodynamic twist, deg	0	Same
Sweep angle, degrees c/4 line	35	Same
Chords:		
Root, in.	337.8	11.82
Tip, in.	112.0	3.92
MAC, in.	241.88	8.47
Airfoil section		
Root	BAC 310*	Same
Tip	BAC 313*	Same
HORIZONTAL TAIL		
Planform area, ft^2	500.0	0.613
Span, ft	39.67	1.389
Aspect ratio	3.2	Same
Taper ratio	0.447	Same
Dihedral angle, deg	7	Same
Incidence angle, deg	+0.5 to -14	Same
Aerodynamic twist, deg	0	Same
Sweep angle, degrees c/4 line	35	Same
Chords:		
Root, in.	208	7.28
Tip, in.	95.05	3.33
MAC, in.	157.8	5.52
Airfoil section		
Root	BAC 319*	Same
Tip	BAC 317*	Same
VERTICAL TAIL		
Planform area, ft^2	337.0	.413
Span, ft	24.7	.865
Aspect ratio	1.80	Same
Taper ratio,	0.36	Same
Incidence angle, deg	0	0
Aerodynamic twist, deg	0	Same
Sweep angle, degrees c/4 line	31	Same
Chords:		
Root, in.	242.0	8.47
Tip, in.	86 92	3 04
MAC, in.	174.6	6.11
Airfoil section		
Root	BAC 277*	Same
Tip	BAC 279*	Same

*Boeing Airplane Company Series

17

At the 30° flap deflection and at the takeoff C_L of 1.23, winglets reduced the drag coefficient by 4.1% and improved the L/D by 4.2%, as shown in figures 80 and 81. With the flaps deflected to 50° and at an approach C_L of 1.05, the drag was reduced by 2.5% and the L/D increased by 2.5%. The trimmed $C_{L_{max}}$ was increased by 0.2% with the flaps deflected at 30° and by 1.1% at 50° with winglets added to the configuration. (See fig. 79.)

An analysis of the winglet pressure data, figure 82, indicates the flow on the inboard section of the winglet separates at an airplane C_L of 1.3 and on the outboard section of the winglet at an airplane C_L of 1.4. These C_L's are 92% and 99% of $C_{L_{max}}$, respectively. This is an indication that the AFFDL/Boeing winglets are essentially free of separation up to 92% of $C_{L_{max}}$ for the KC-135A with landing flaps, $\delta_F = 50°$. Also, separation on the winglet does not extend to 75% of the winglet span until 99% of $C_{L_{max}}$ is reached.

4. EFFECT OF WINGLETS ON KC-135A LOW-SPEED STABILITY

The effects of winglets on the low-speed longitudinal and lateral-directional stability characteristics of the KC-135A are shown in figures 83 through 86. In addition, the impact of winglets on the outboard aileron effectiveness is presented in figure 87 for the flaps-down configuration.

The incremental change in the aerodynamic center location caused by the AFFDL/Boeing winglet is shown in figure 83. The data indicate that both configurations exhibit an aft aerodynamic center shift of approximately 1.5% MAC relative to that of the baseline KC-135A. The effect of this aft movement of the aerodynamic center will be an insignificant increase in control force gradients in maneuvers and speed changes compared to those of the KC-135A.

Figure 84 shows tail-off pitching moment data for the basic KC-135A and the KC-135A with the NASA upper winglet at takeoff and landing flaps of 30° and 50°, respectively. Wind tunnel data obtained with the NASA upper winglet had to be used since no low-speed tail-off data were acquired with the AFFDL/Boeing winglet design. These data show an increment in pitching moment coefficient of approximately 0.025 at normal takeoff and landing C_L's. This nose-down increment will require approximately 0.8 unit of additional nose-up trim (or 0.8 degrees of stabilizer travel) but will not affect the forward center of gravity limit for landing.

Figures 85 and 86 show the effect of winglets on the static lateral-directional stability derived from pitch runs at a constant sideslip angle of $\beta = 5°$. Figure 85 shows the effect of the AFFDL/Boeing winglets on the lateral-directional stability parameters (C_{n_β}, C_{ℓ_β}, and C_{y_β}) for the KC-135A with 30° flaps. The winglets increased C_{n_β} over the basic KC-135A by about 15% at low C_L's. This increase is reduced to approximately 3% at the high C_L's; C_{y_β} is increased by about 14% at low C_L's and about 10% at high C_L's. The lateral stability C_{ℓ_β} is increased by approximately 22% at low C_L's and 14% at high C_L's.

18

Figure 86 presents the effects of the AFFDL/Boeing winglets on the lateral-directional stability parameters for the KC-135A with 50° flaps. The winglets show an increase of 6% to 9% in directional stability C_{n_β} over the base KC-135A in the C_L range shown. The increase in C_{y_β} is 10% to 13% in the C_L range tested. The lateral stability C_{ℓ_β} shows an increase of approximately 11%.

Figure 87 shows the effect of the AFFDL/Boeing winglets on the KC-135A outboard aileron effectiveness at 30° and 50° flaps. The winglets show an increase in outboard aileron effectiveness of about 7% at 30° flaps and 5% at 50° flaps.

These changes in lateral-directional stability and control parameters can be expected to modify some low-speed handling characteristics. Since the rudder effectiveness is not expected to change, the increase in directional stability and the large increase in lateral stability compared to that of the lateral control power would cause a reduction in the crosswind landing capability. Unaugmented Dutch roll characteristics, both the frequency and the damping, will be changed; however, the Dutch roll characteristics with the yaw damper on are expected to remain acceptable. Additional discussion of cross wind landing and Dutch roll characteristics will require additional analysis beyond the scope of this report. Since the air minimum control speed maneuver in the KC-135A is conducted at approximately zero sideslip, engine-out control in flight is expected to be unchanged.

SECTION VII
KC-135A WINGLET RETROFIT PROGRAM

The winglet retrofit program on the KC-135A aircraft will consist of a winglet size trade study, detail design, fabrication and installation of the first kit, qualification ground and flight tests of the first kit, and a production program for the rest of the fleet. A preliminary program schedule is presented in figure 88, and a preliminary price estimate is shown in table 2. For a more detailed discussion of these estimates, see reference 5.

Table 2. — KC-135A Winglet Retrofit Program Price

	1977 dollars (millions)
	Total
Winglet size trade study	0.2
Handbook revisions	0.24
Retrofit (kit and installation) nonrecurring	6.0
Retrofit (kit and installation) recurring	36.12
Total	42.56
Average unit price	0.066

● 642 aircraft

● Installation concurrent with PDM

Planning prices and schedules for the winglet retrofit on the KC-135A and KC-135Q fleet (642 airplanes) are based on a 68-month program flow time, assuming the winglet kits are installed during regular program depot maintenance (PDM) at a rate of approximately 160 per year. The preliminary program schedule is shown in figure 88. A winglet size trade study was included to optimize winglet size within allowable structural load and flutter limits. This is estimated to be a 3-1/2-month effort and is recommended to be completed coincident with the winglet flight demonstration program (ref. 6). Fabrication, installation, and qualification testing of the first unit were estimated to be complete after 19 months or 16 months aft the completion of the flight demonstration program. The price of the winglet retrofit is shown in table 2. Based on 1977 dollars, the total price is $42,560,000 at $66,000 per unit.

The net savings due to retrofitting the KC-135 fleet are very significant and are summarized in figure 89. The assumptions used for the estimate are noted on the figure. The 642 airplanes consisted of all the KC-135A and KC-135Q airplanes, and the 8% inflation rate was applied to the cost of both the modification and fuel. The fuel savings noted were based on 7% of the fuel used by the KC-135 fleet in 1975. As can be seen, the greatest expenditure will occur in 1981 at $25 to $30 million. By the start of 1984, the winglets will have paid for themselves, and a net saving will be realized from then on.

SECTION VIII
CONCLUSIONS

Drag polars and surface pressures were calculated for the takeoff and landing configurations of the KC-135A with and without AFFDL/Boeing winglets. The change in the drag of the KC-135A caused by the winglets compared well with experimental data up to where the wingtip exhibits signs of boundary-layer separation. The winglet surface pressures also compared well. Based on this evaluation of the winglet aerodynamic analysis method, the method can be used to predict the performance change of the low-speed configuration of transport-type aircraft with winglets up to where boundary-layer separation occurs on the wingtip and winglet.

A leading-edge device on the KC-135A wing has very little effect on the performance of the AFFDL/Boeing winglet at the C_L's that were analyzed (C_L up to 1.3). The point of concern when wing leading-edge devices are added is that the wing can then operate to higher lift coefficients and consequently subject the winglets to higher crossflow angles. If the performance benefits of winglets are desired for the low-speed conditions, then the winglets must be essentially free of separation during the critical operating range. Therefore, for configurations where wing leading-edge devices are added, the winglet performance must be compatible with the outboard wing. The design of such a winglet may require the use of leading-edge devices for the winglet or possibly a compromise design that has higher winglet C_L capability.

A compromise high-speed/low-speed winglet was designed. This winglet, which was designated Z_5, provides approximately the same high-speed performance but higher low-speed performance.

The high-speed wind tunnel test of the KC-135A with the AFFDL/Boeing winglets showed a 6.2% reduction in drag at a cruise C_L of 0.426. The initial buffet boundary was increased by 1.6% to 5.2% through the Mach range 0.5 to 0.8, and the drag divergence boundary was increased by 0.4% to 0.8% through the C_L range 0.2 to 0.7. These winglets appear to have attached flow up to the initial buffet boundary. These winglets caused an aft shift in the aerodynamic center of 1.5% to 2.5% of MAC. This shift will result in an insignificant increase in the control force gradients for maneuver and speed changes. The tail-off Mach tuck or static longitudinal overspeed characteristics of the KC-135A did not change significantly with these winglets. These winglets increased the tail-off directional stability C_{n_β} by approximately 13%. The static lateral stability C_{ℓ_β} increased by 23% and the side force due to sideslip derivative C_{y_β} increased by 14% to 19%. These changes in the lateral-directional stability derivatives could have a significant effect on the unaugmented Dutch roll characteristics, and this should be investigated.

The low-speed wind tunnel test showed that the AFFDL/Boeing winglets reduced the drag of the KC-135A with 30° flaps by 4.1% and increased the L/D by 4.2% at the takeoff condition. With 50° flaps and at the approach condition, the AFFDL/Boeing winglets reduced the drag by 2.5%. The trimmed $C_{L_{max}}$ was increased by 0.2% with

21

the 30° flap configuration and 1.1% with the 50° flap configuration. The 30° and 50° flap configurations with winglets exhibited an aft aerodynamic center (a.c.) shift of approximately 1.5% of MAC. This shift in a.c. will result in a very small increase in the control force gradients for maneuver and speed changes. The KC-135A with NASA upper winglet tail-on and tail-off data indicates that approximately 0.8° of additional nose-up trim will be required with winglets, but the forward center of gravity limit for landing will not be affected. The directional stability $C_{n\beta}$ of the KC-135A with 30° flaps increased by about 3% to 15% with the AFFDL/Boeing winglets. With 50° flaps, $C_{n\beta}$ increased by 6% to 9%. The static lateral stability $C_{\ell\beta}$ increased by 10% to 14% for flaps 30° and about 11% for flaps 50°. The side force derivative $C_{y\beta}$ increased by 14% to 22% for flaps 30° and 10% to 13% for flaps 50°. These large changes in the lateral-directional stability derivatives indicate that additional analysis beyond the scope of this study should be conducted.

The preliminary study to retrofit the KC-135A with the AFFDL/Boeing winglets estimated a per unit cost of $66,000 based on 1977 dollars. If a 1979 program start is assumed, the winglet fuel savings would pay for this retrofit program cost by the beginning of 1984. From 1984 to the turn of the century, the KC-135 fleet would save 700 million gallons of fuel and $970 million.
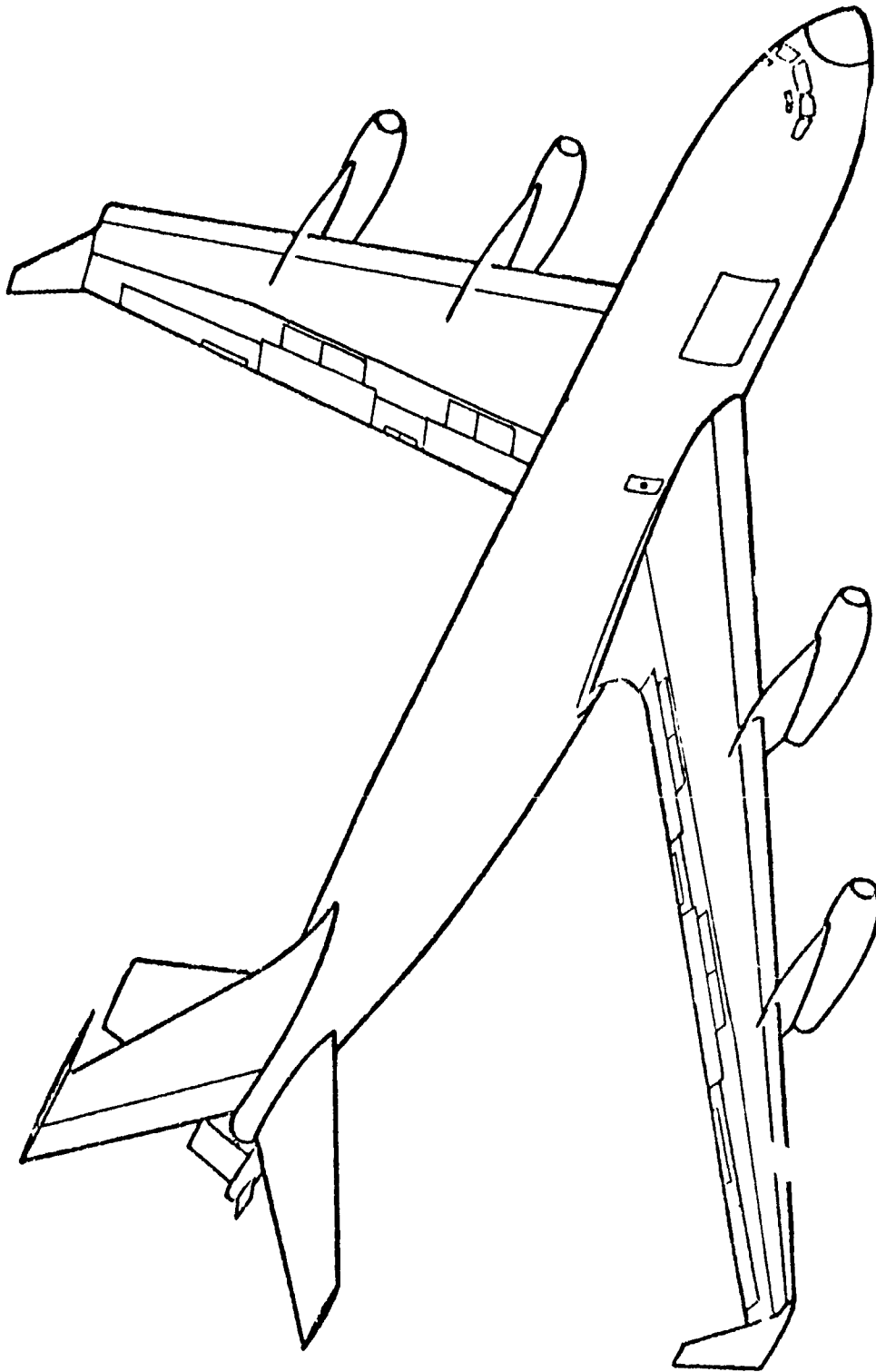
Figure 1. — Application of Winglets on the KC-135A
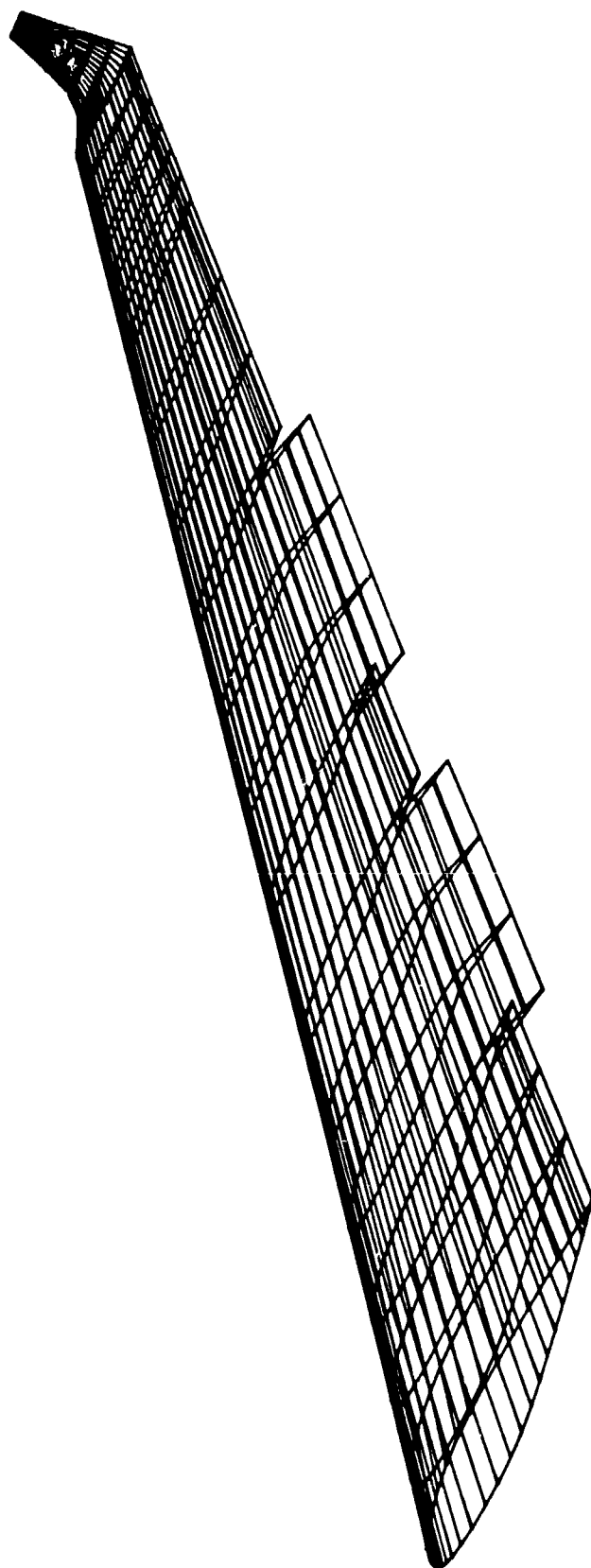
a. Source Singularities

Figure 2. — TEA 230 Modeling of KC-135A Wing and Winglet

24
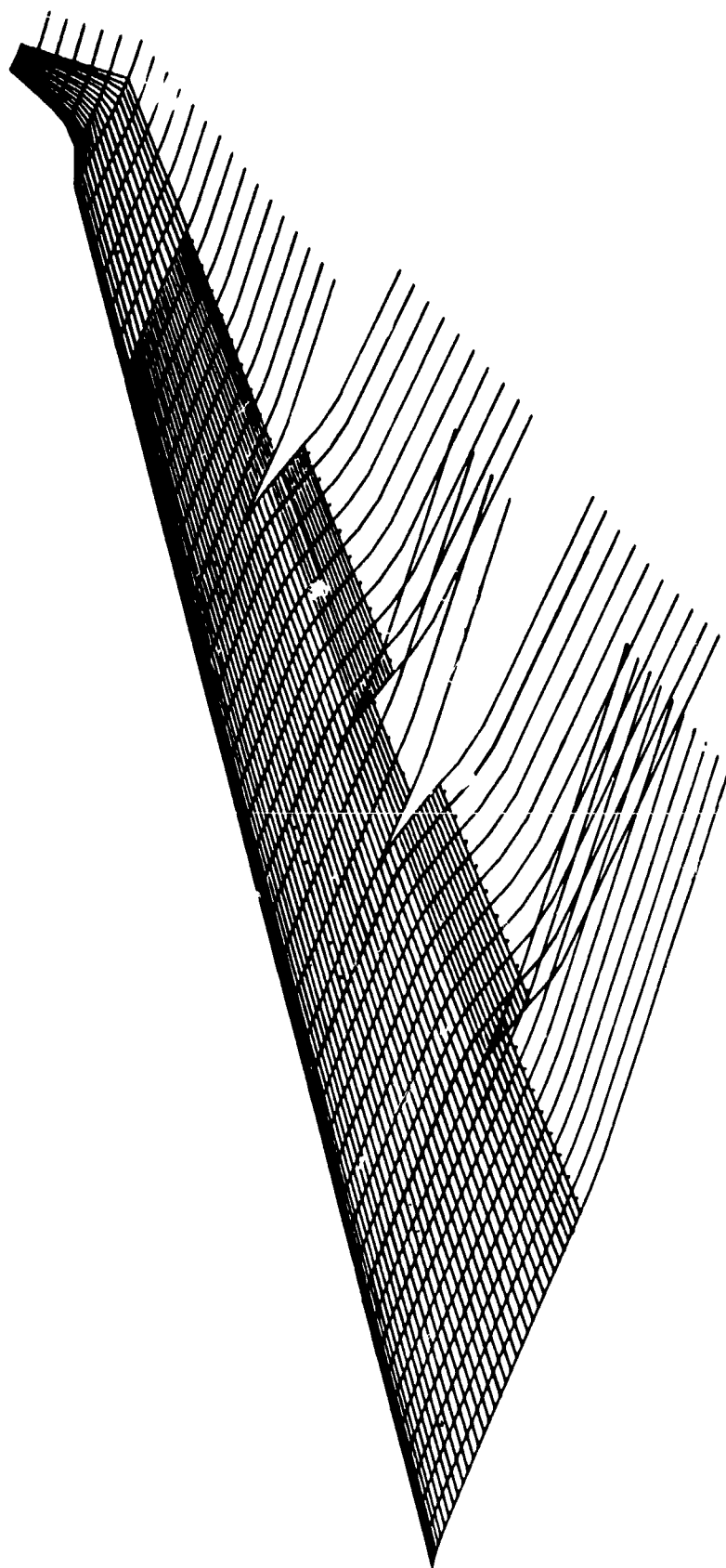
b. Vortex Singularities

Figure 2.—(Concluded)

Winglet Z_2

Typical Section, A-A

Rear View

0.135 b/2

6°

Top View

Side View

A

A
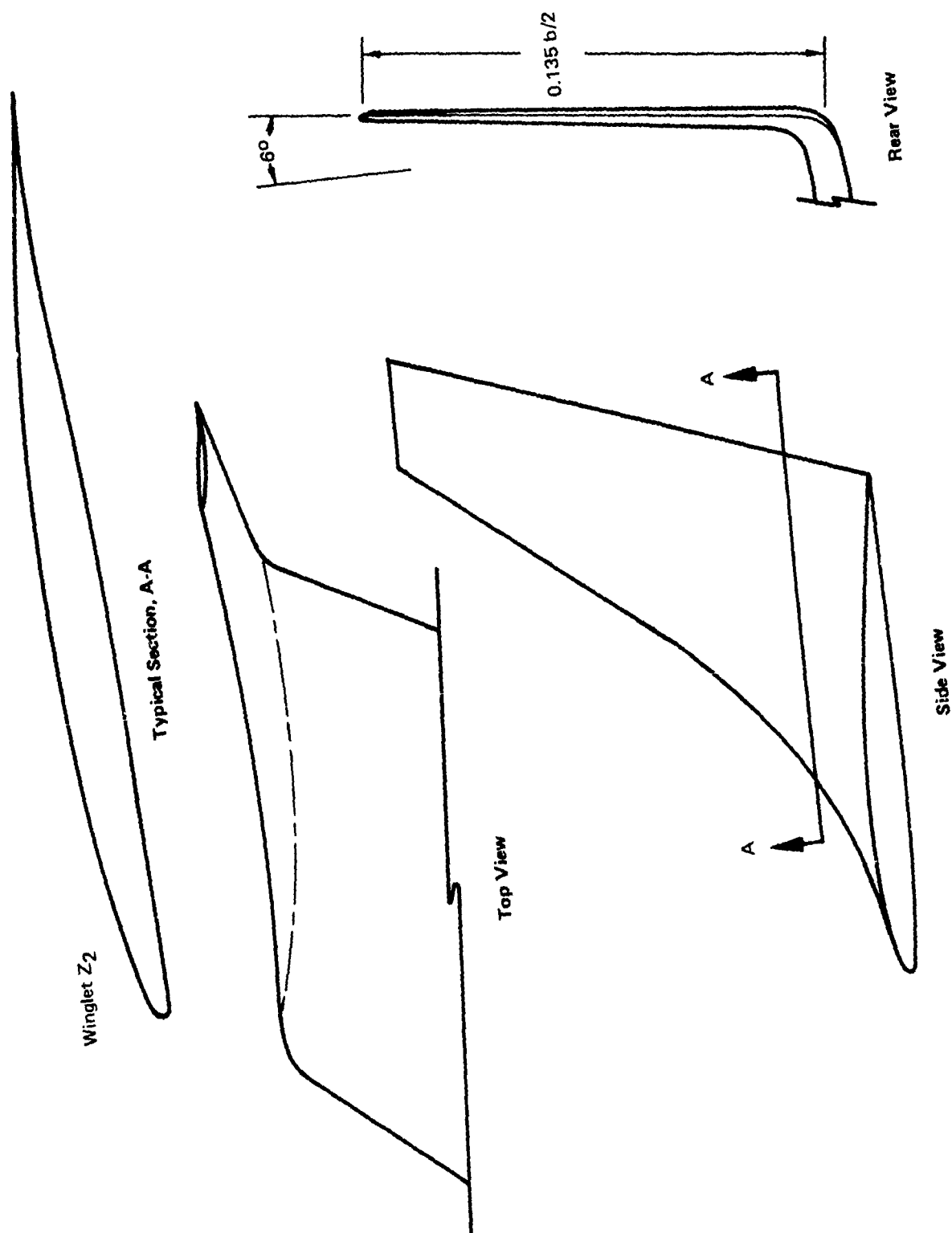
Figure 3. — KC-135 Winglet Geometry

26
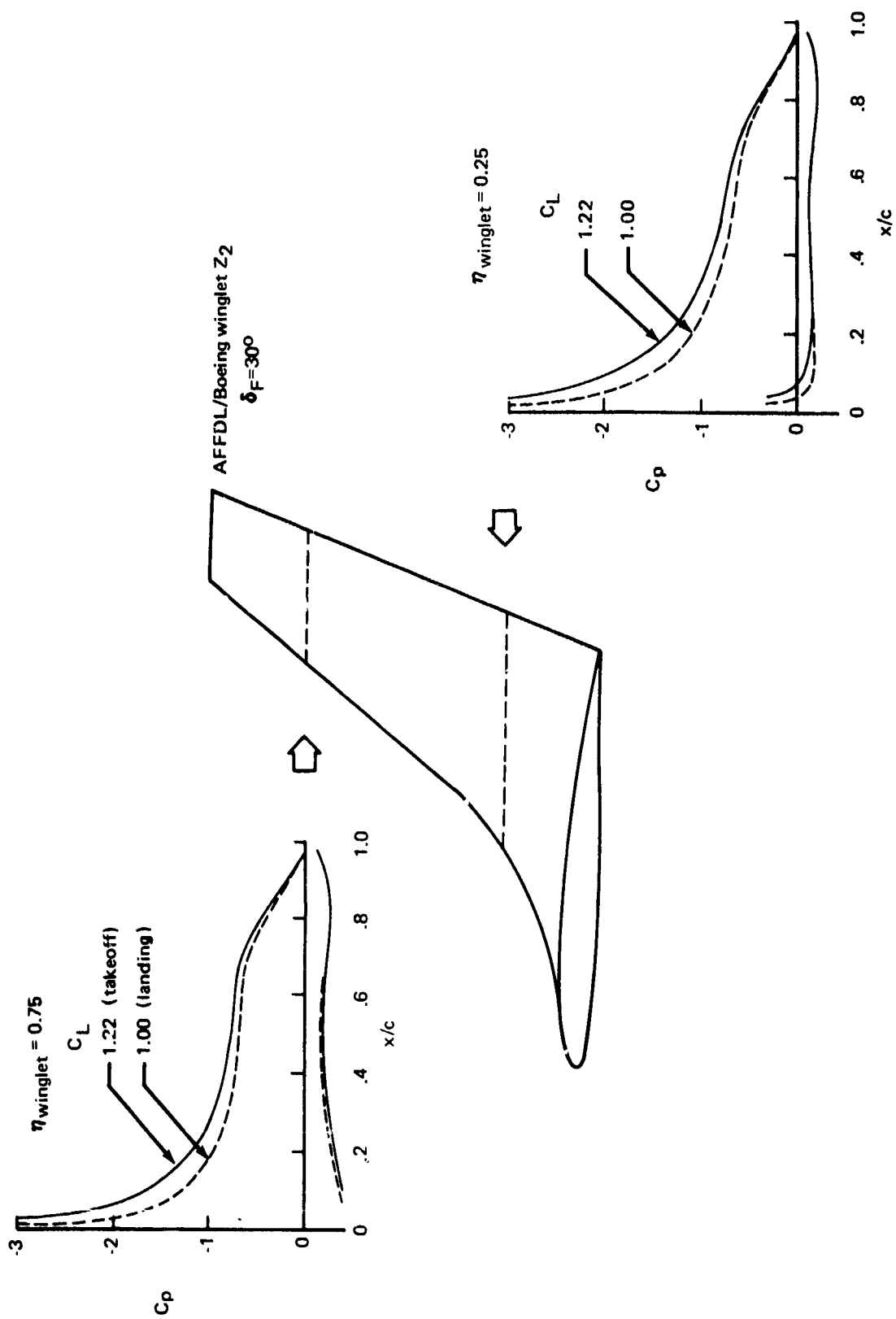
Figure 4. — Comparison of Winglet Pressures at Takeoff and Landing C_L's With Flaps $30°$

$C_L = 1.22$
$\delta_F = 30^\circ$
$M = 0.30$

$\eta_{winglet} = 0.750$

$\eta_{winglet} = 0.417$

$\eta_{winglet} = 0.250$

$\eta_{winglet} = 0.083$

$\eta_{wing} = 0.990$

$\eta_{wing} = 0.946$

Winglet Z_2

Basic KC-135A
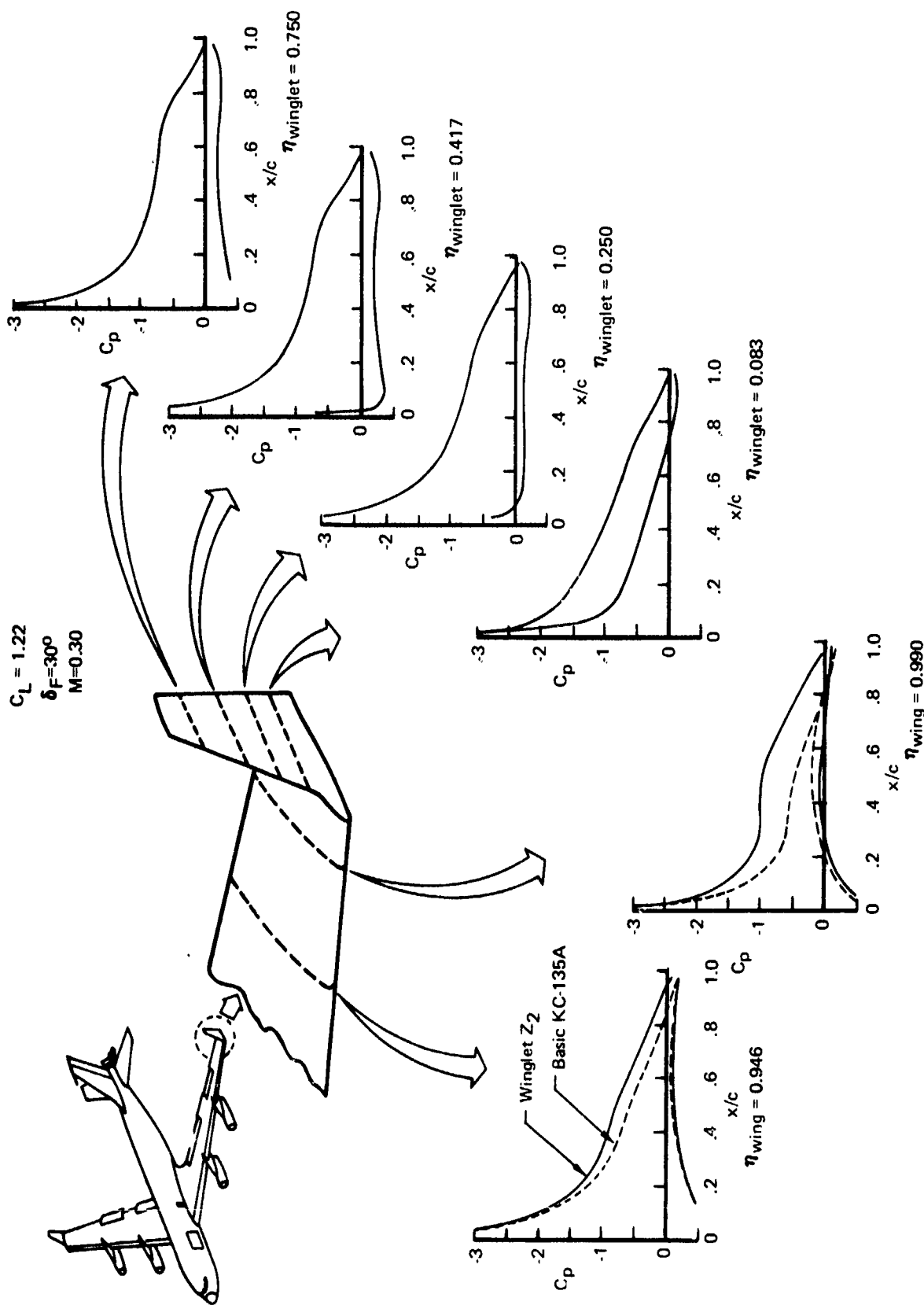
Figure 5. — Surface Pressures on Wing and Winglet at Takeoff

28

Figure 6. — Span Loading at Takeoff

$C_L = 1.22$

$\delta_F = 30^\circ$

$M = 0.30$

29
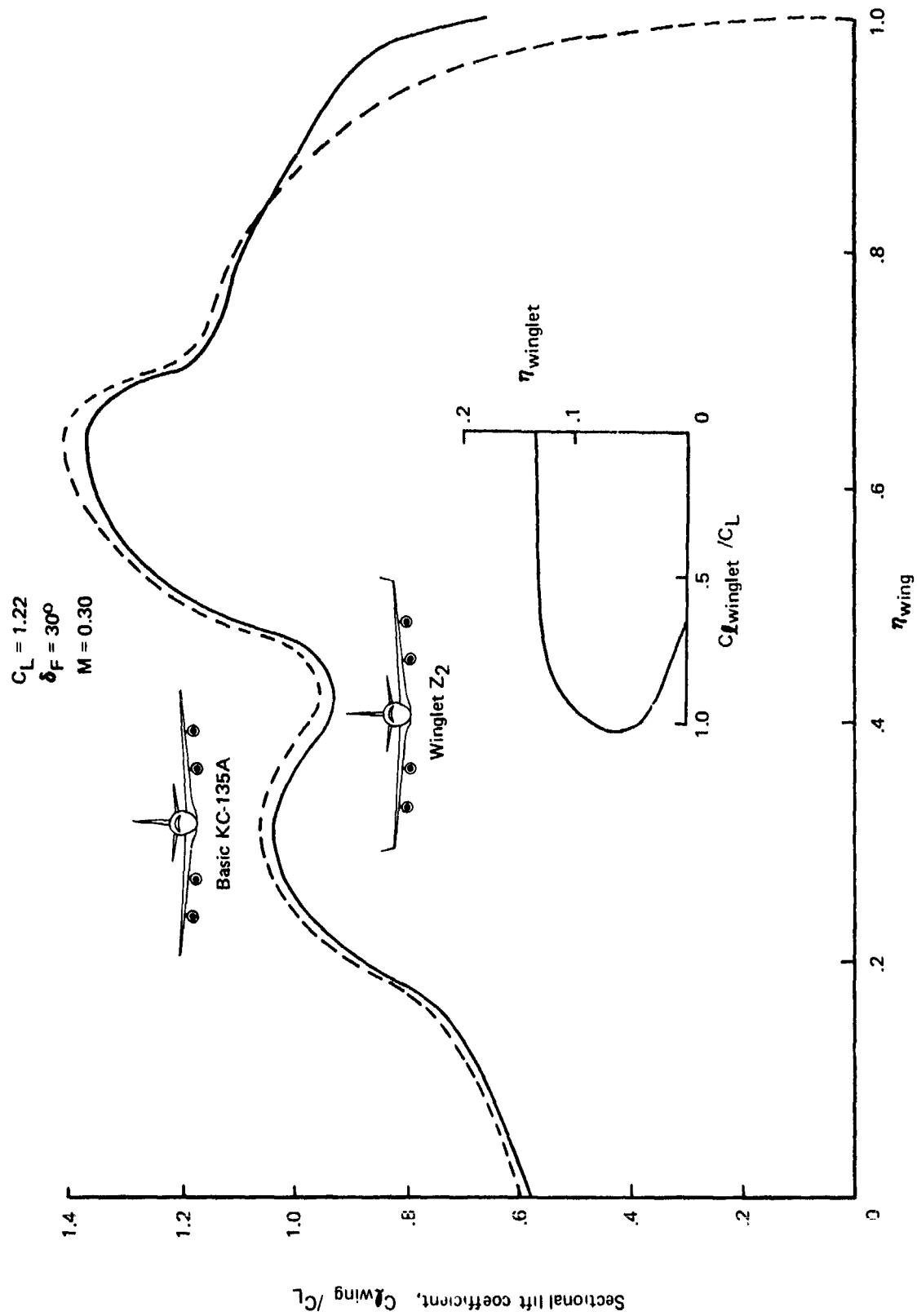
Figure 7. – Takeoff Wing and Winglet Section C_ℓ's

30

Winglet Z_2

$\delta_F = 30^\circ$

M = 0.30
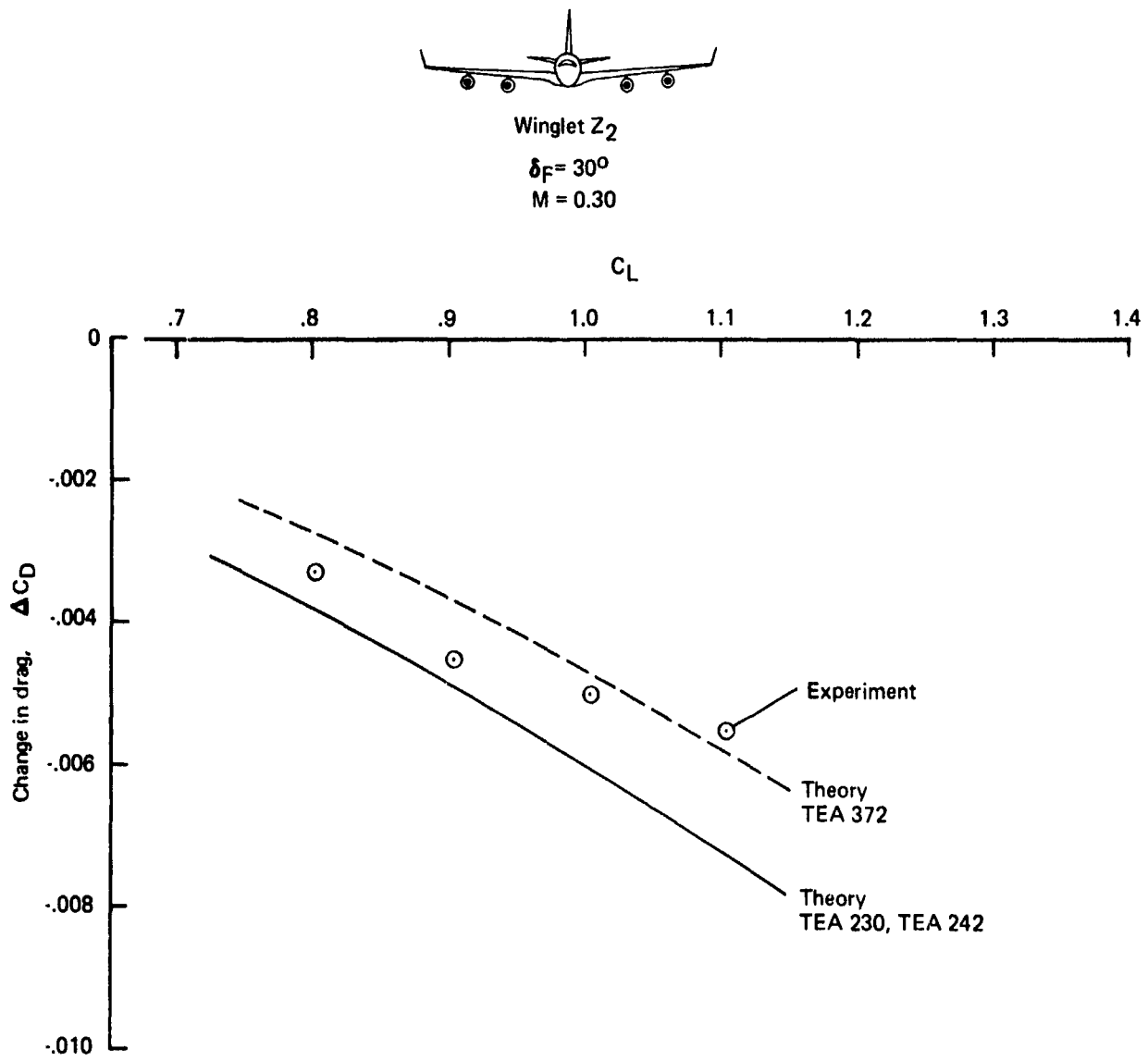
Figure 8. — Flaps 30° Reduction in Drag With High-Speed AFFDL/Boeing Winglets
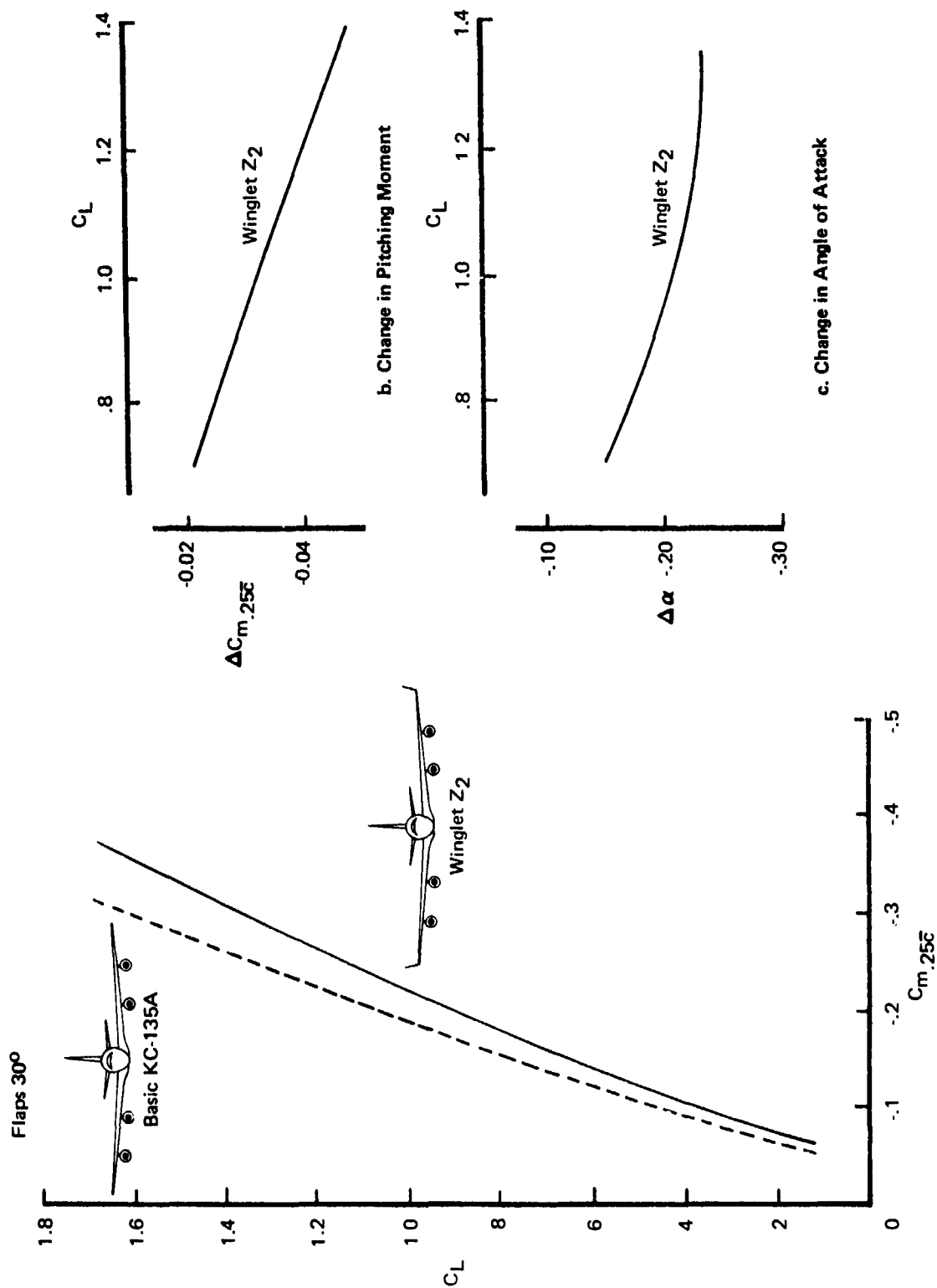
Figure 9. — Effect of AFFDL/Boeing Winglets on KC-135A Aerodynamics With Flaps 30°
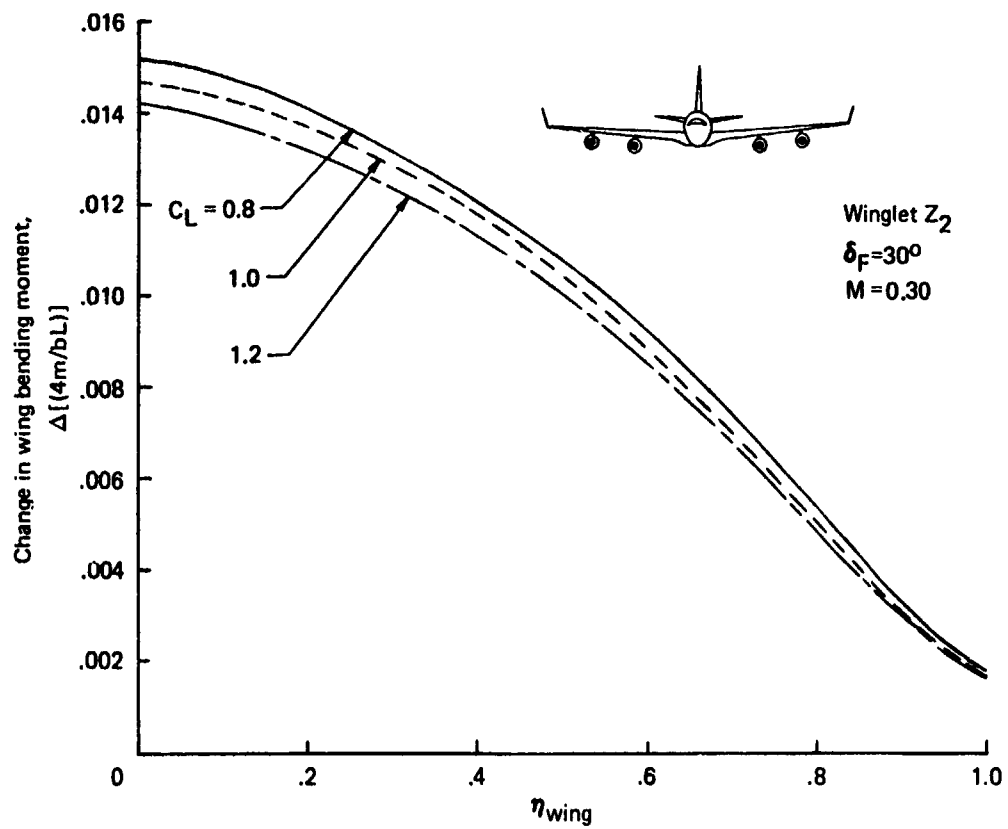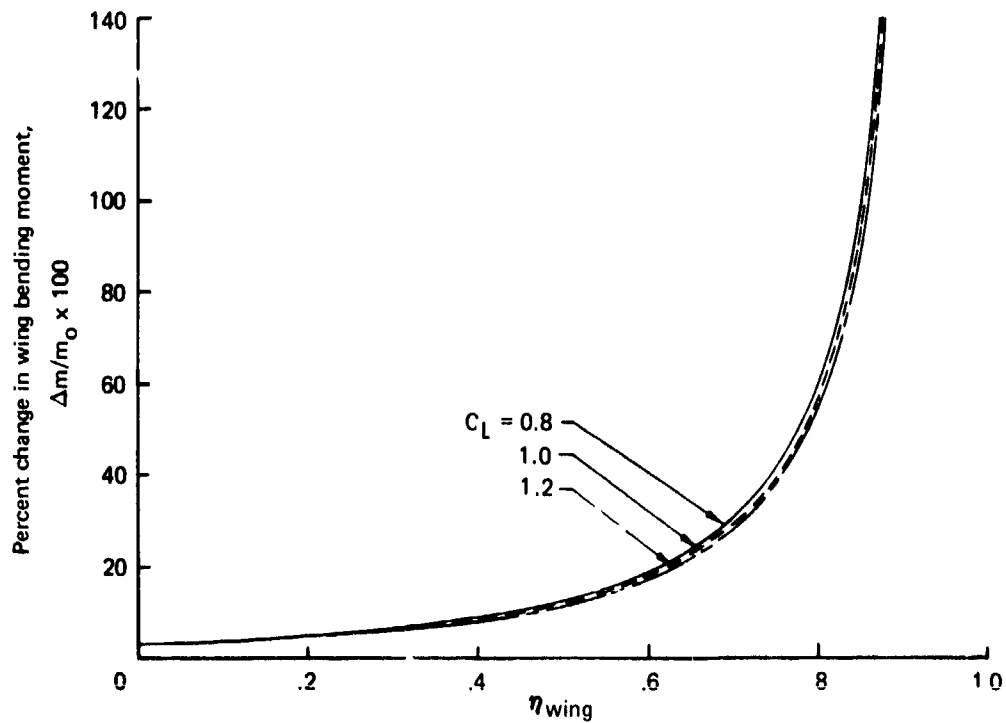
Figure 10. — Effect of AFFDL/Boeing Winglets on KC-135A Wing Bending Moment With Flaps 30°

33
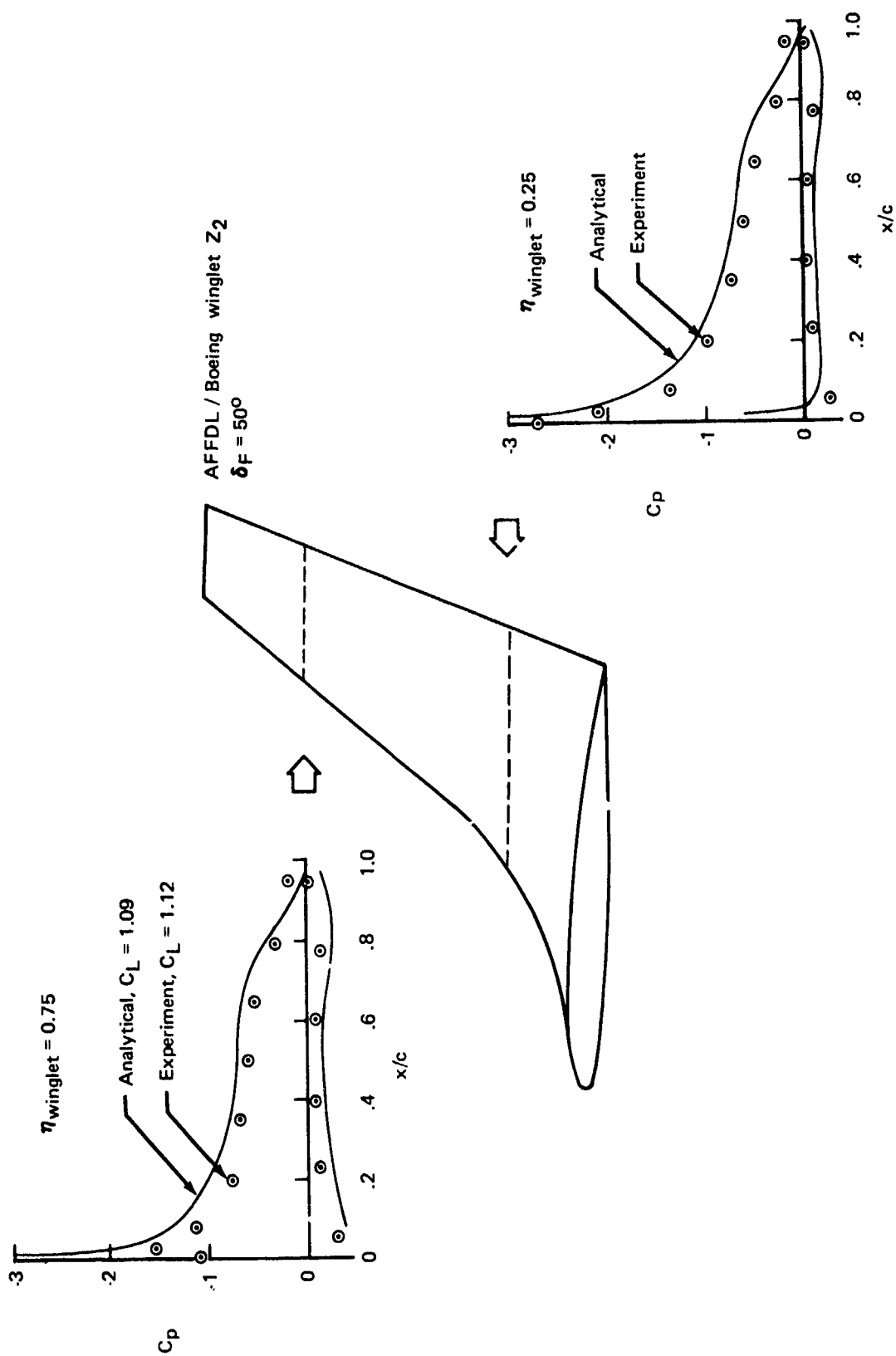
Figure 11. — Comparison of Analytical and Experimental Winglet Pressures
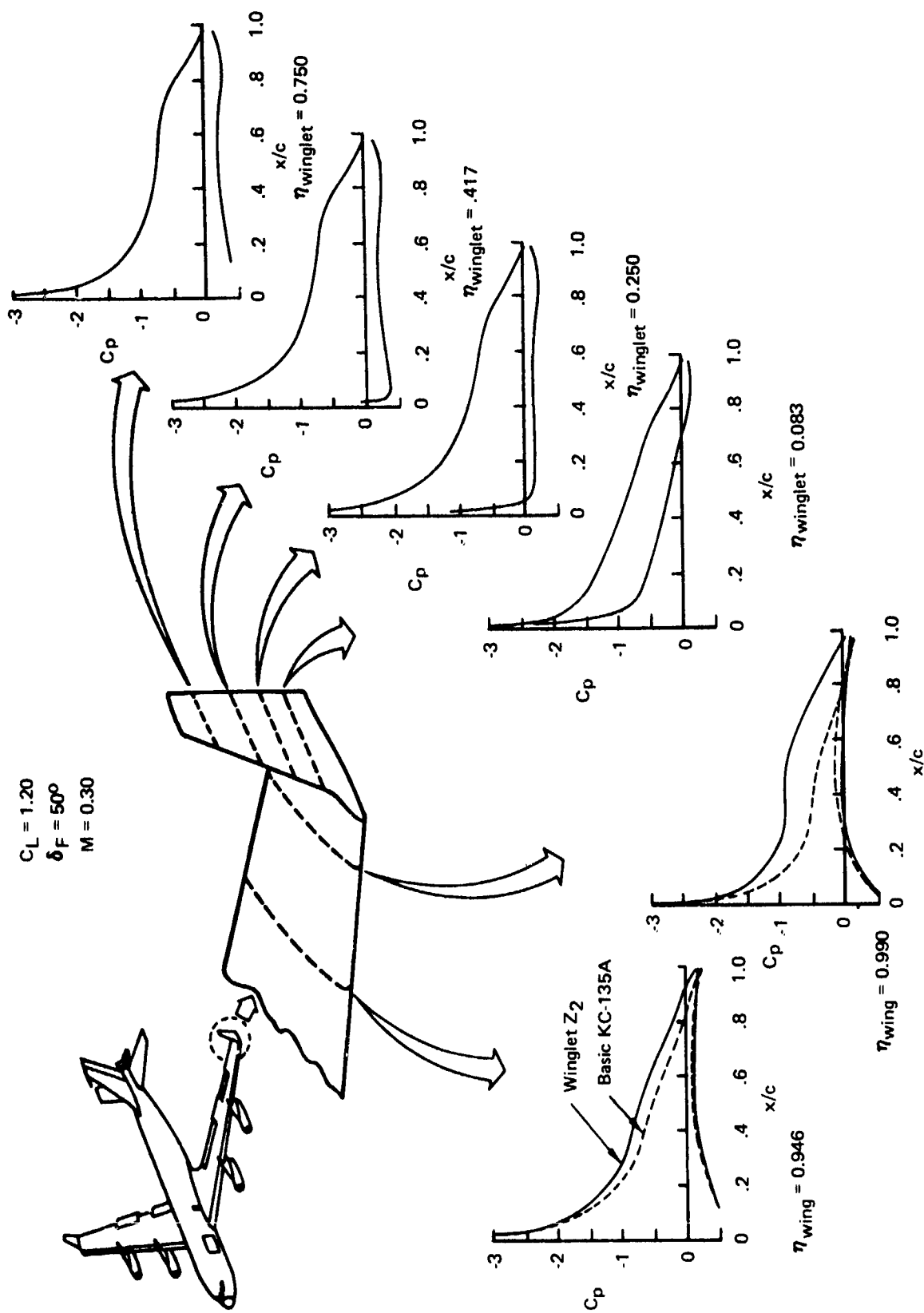
Figure 12. — Surface Pressures on Wing and Winglet at Touchdown

$C_L = 1.20$
$\delta_F = 50°$
$M = 0.30$

$\eta_{winglet} = 0.750$

$\eta_{winglet} = .417$

$\eta_{winglet} = 0.250$

$\eta_{winglet} = 0.083$

$\eta_{wing} = 0.990$

$\eta_{wing} = 0.946$

Winglet Z_2

Basic KC-135A

35
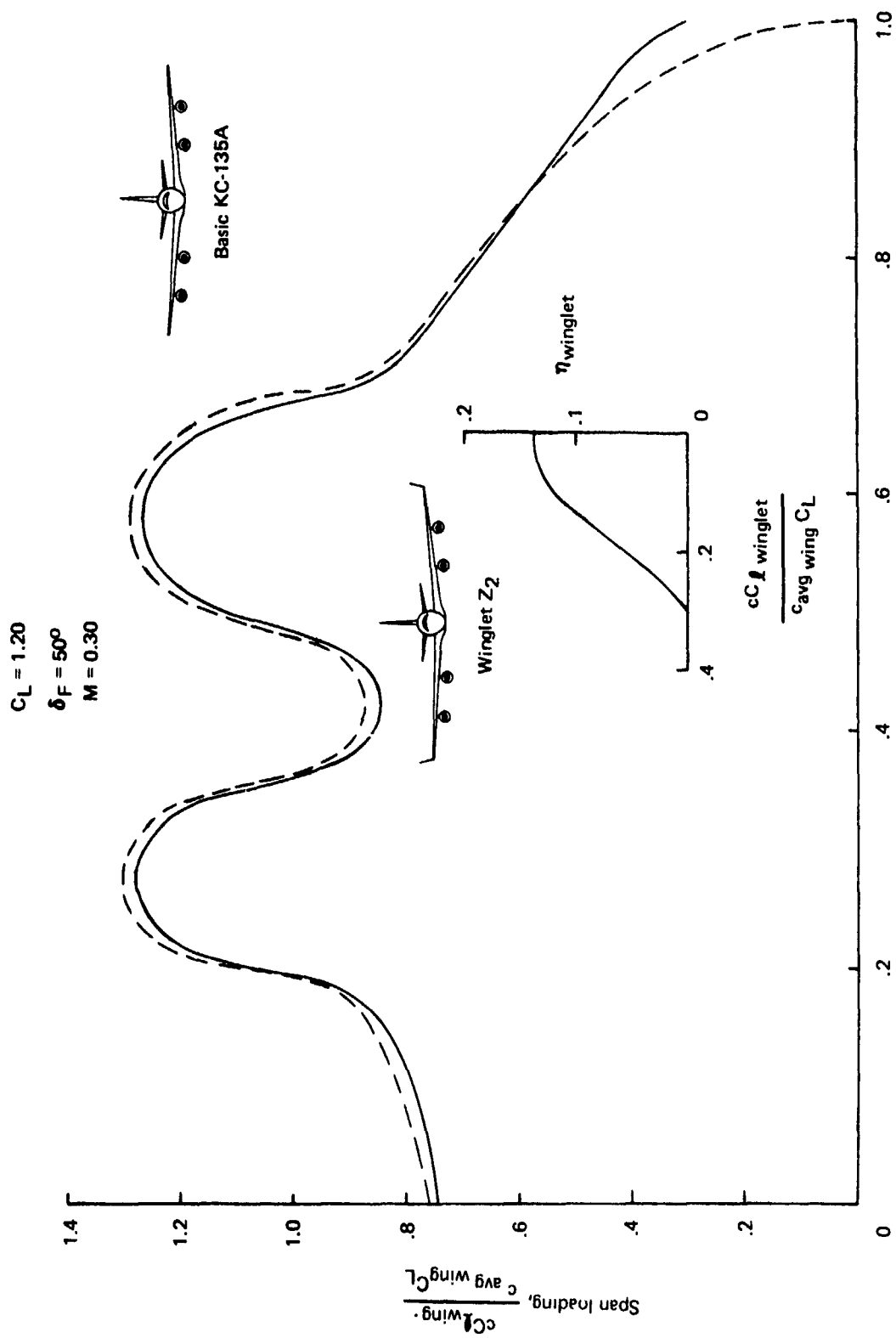
Figure 13. – Span Loading at Touchdown

$C_L = 1.20$
$\delta_F = 50^o$
$M = 0.30$

Basic KC-135A

Winglet Z_2

$\eta_{winglet}$

$\dfrac{cC\ell_{winglet}}{c_{avg\ wing}C_L}$

Span loading, $\dfrac{cC\ell_{wing}}{c_{avg\ wing}C_L}$
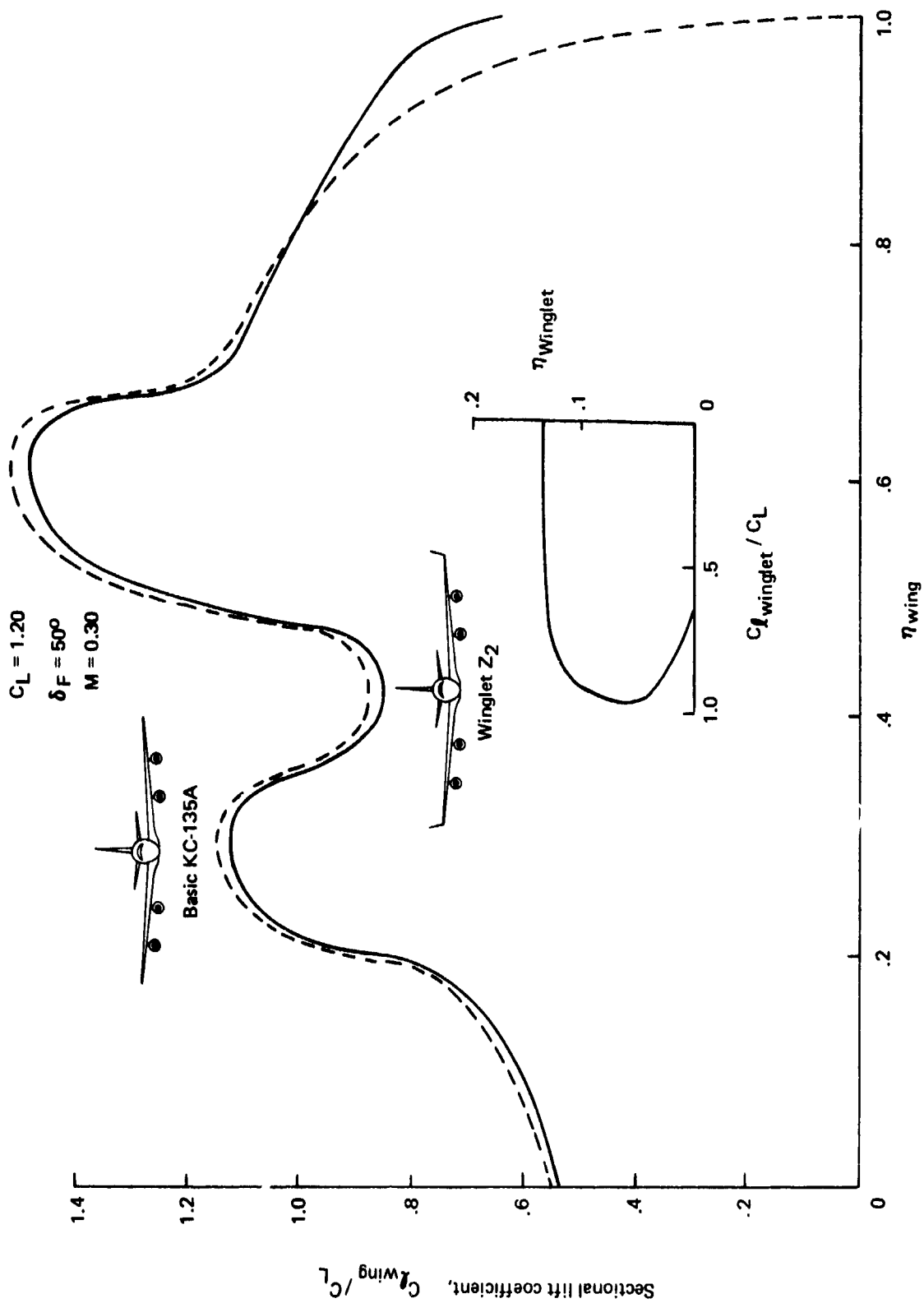
Figure 14. — Wing and Winglet Section C_ℓ 's at Touchdown

37
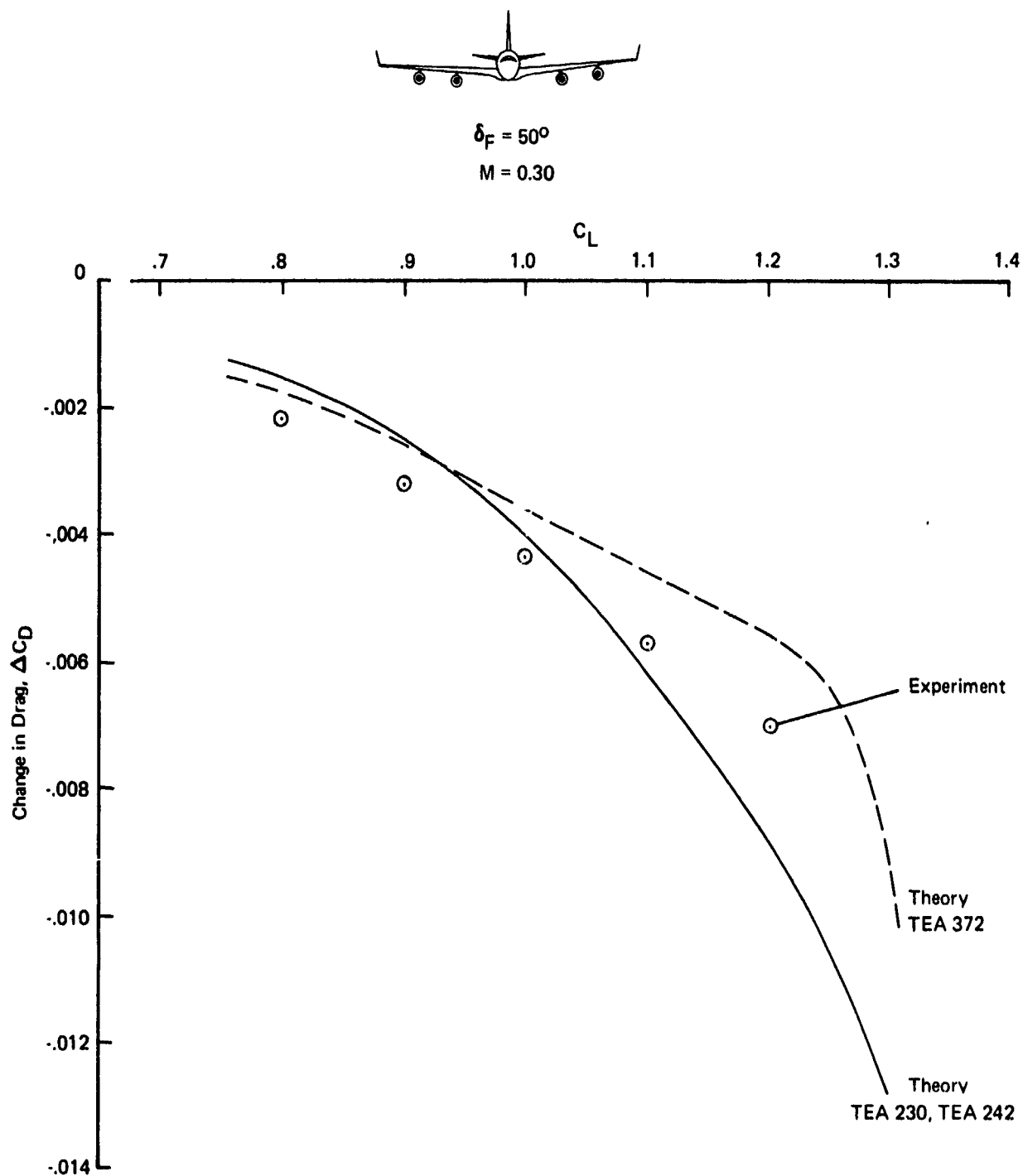
Figure 15. — Flaps 50º Reduction in Drag With High-Speed AFFDL/Boeing Winglets
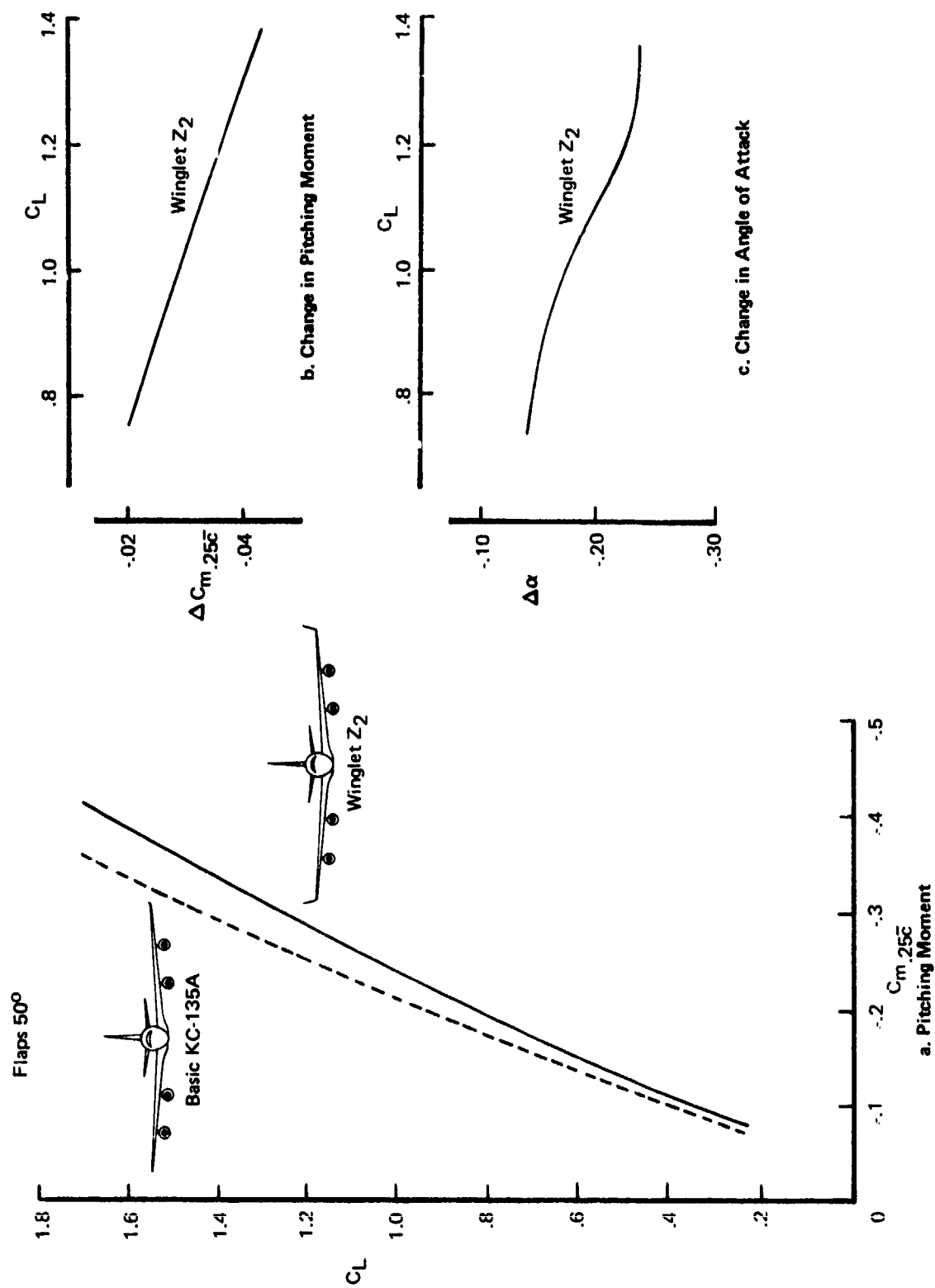
Figure 16. — Effect of AFFDL/Boeing Winglets on KC-135A Aerodynamics With Flaps 50°

39
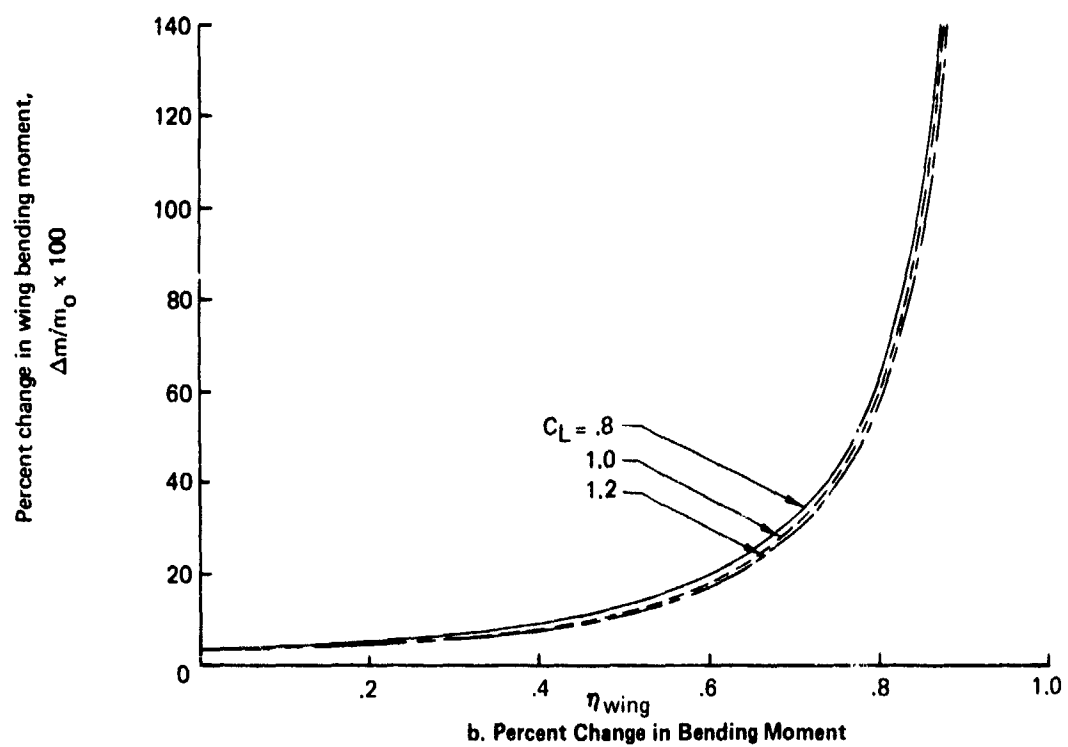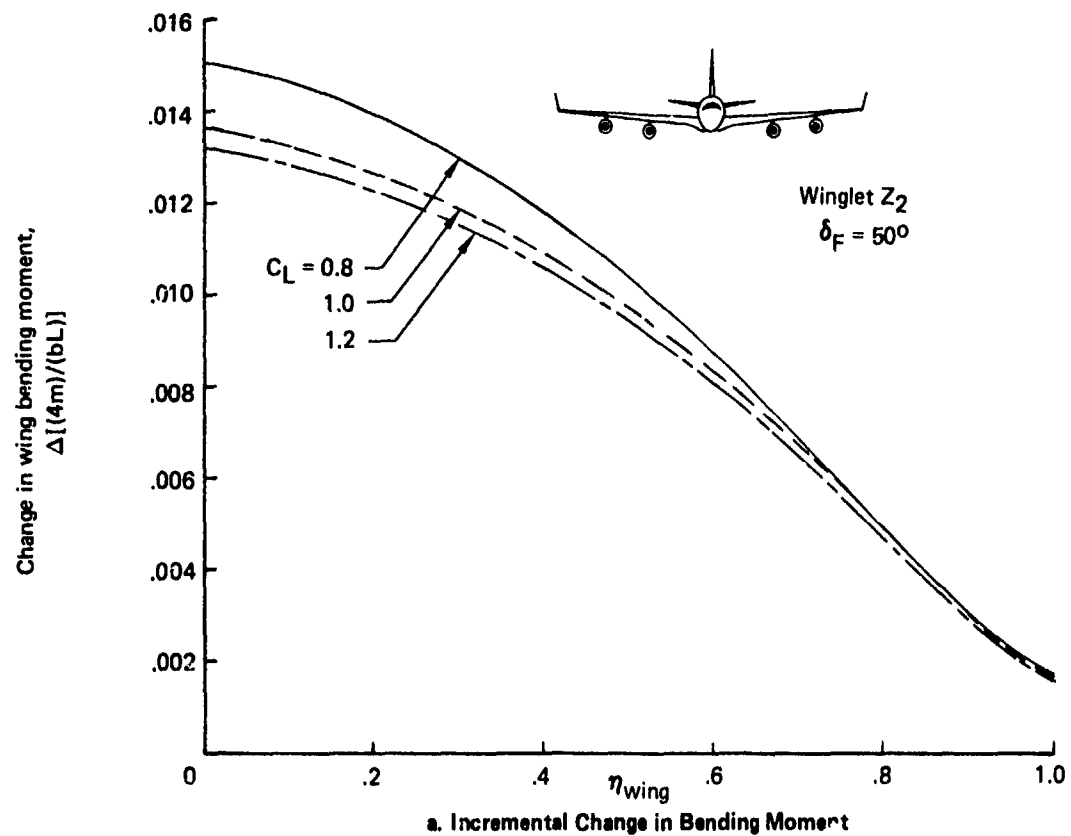
Figure 17. — Effect of AFFDL/Boeing Winglets on KC-135A Wing Bending Moment With Flaps 50°

40

b. Typical Cross Section of 747-Type Krueger

Flexible panel

Wing leading edge devices

a. Planform of Wing Leading-Edge Device

Figure 18. — Geometry of KC-135 Wing Leading-Edge Device Used for the Theoretical Analysis

41
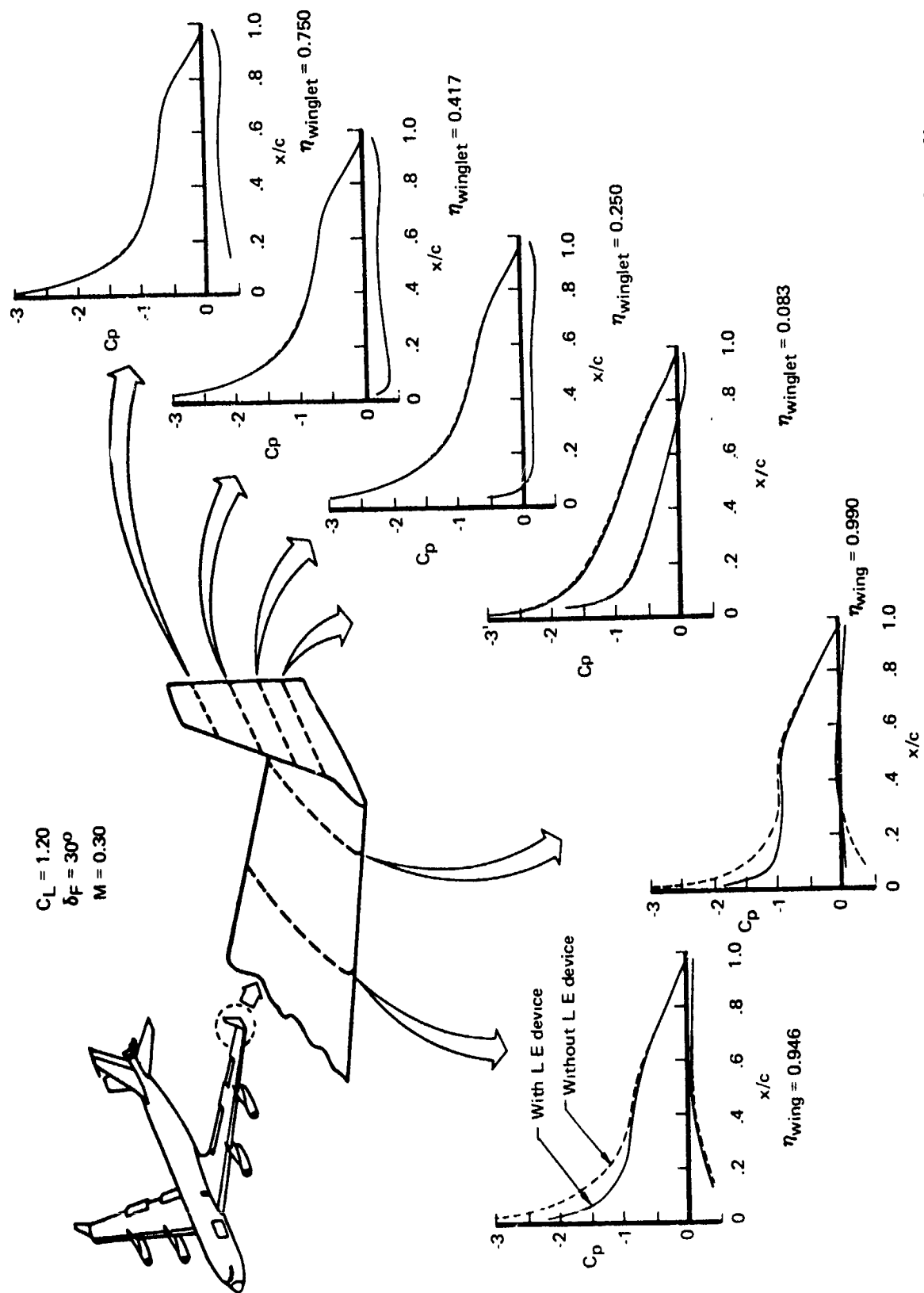
Figure 19. — Surface Pressures on Wing With Leading-Edge Device and AFFDL/Boeing Winglets at Takeoff

42
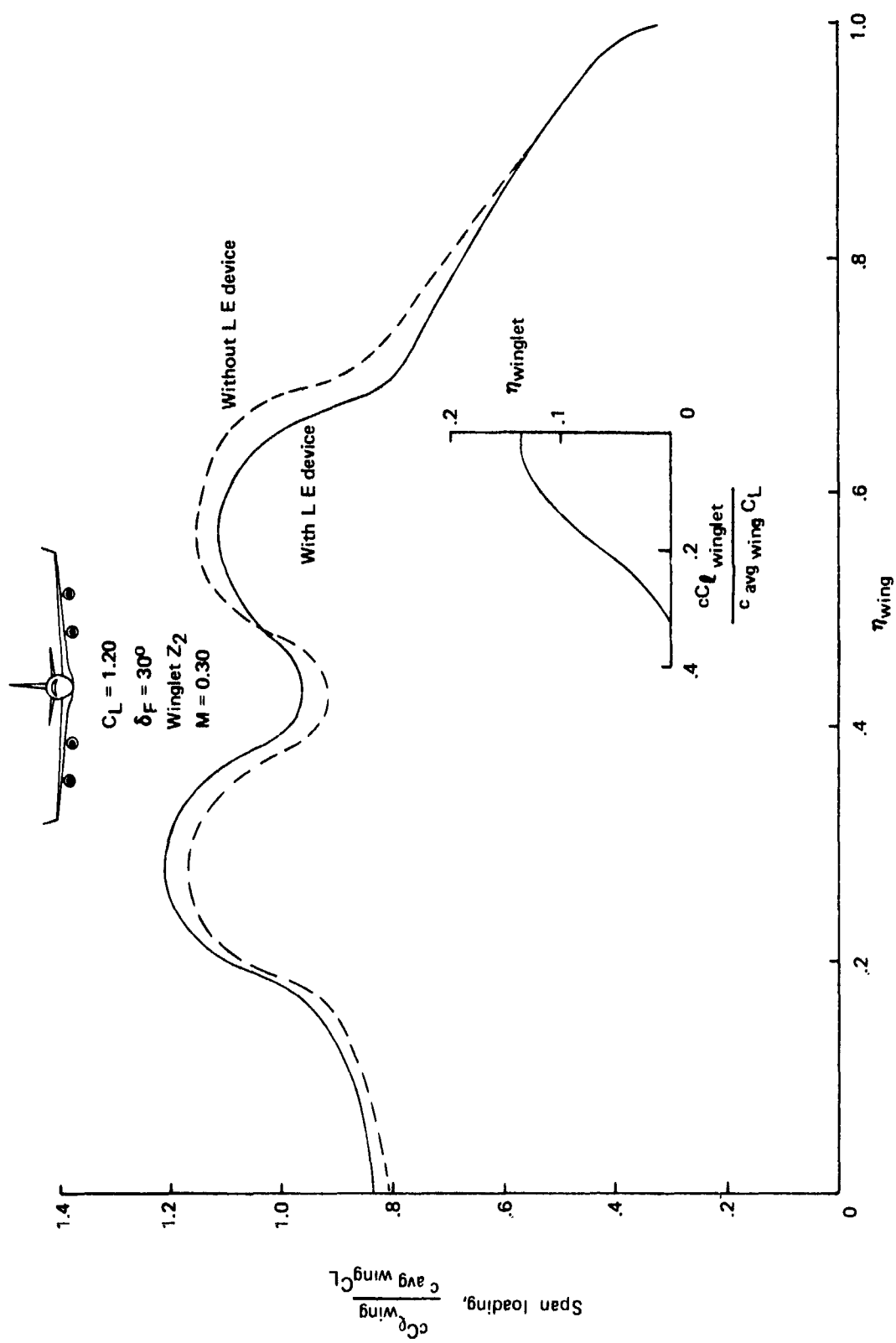
Figure 20. – Span Loading With Wing Leading-Edge Device

43
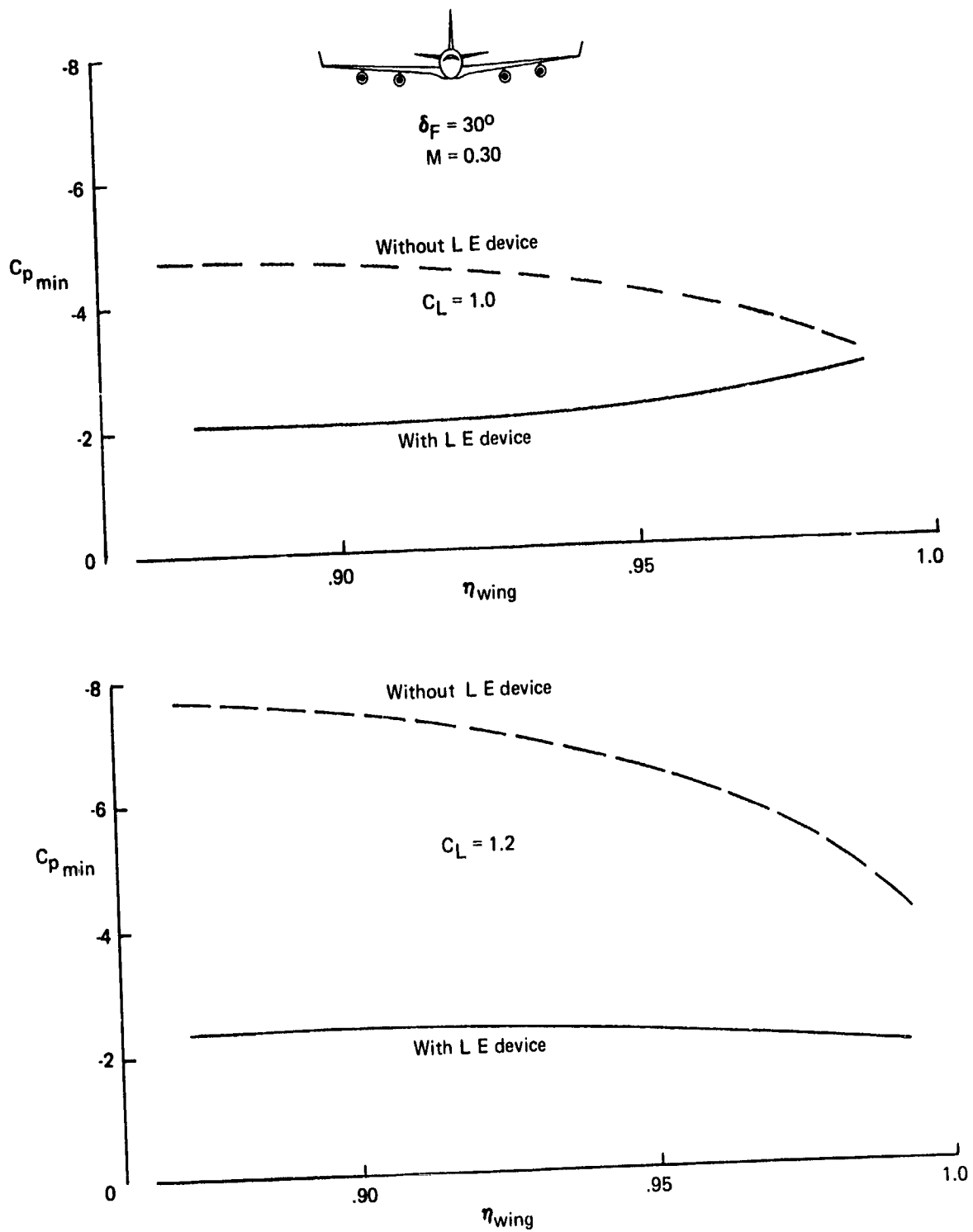
Figure 21. — Minimum Pressures on Outboard Wing
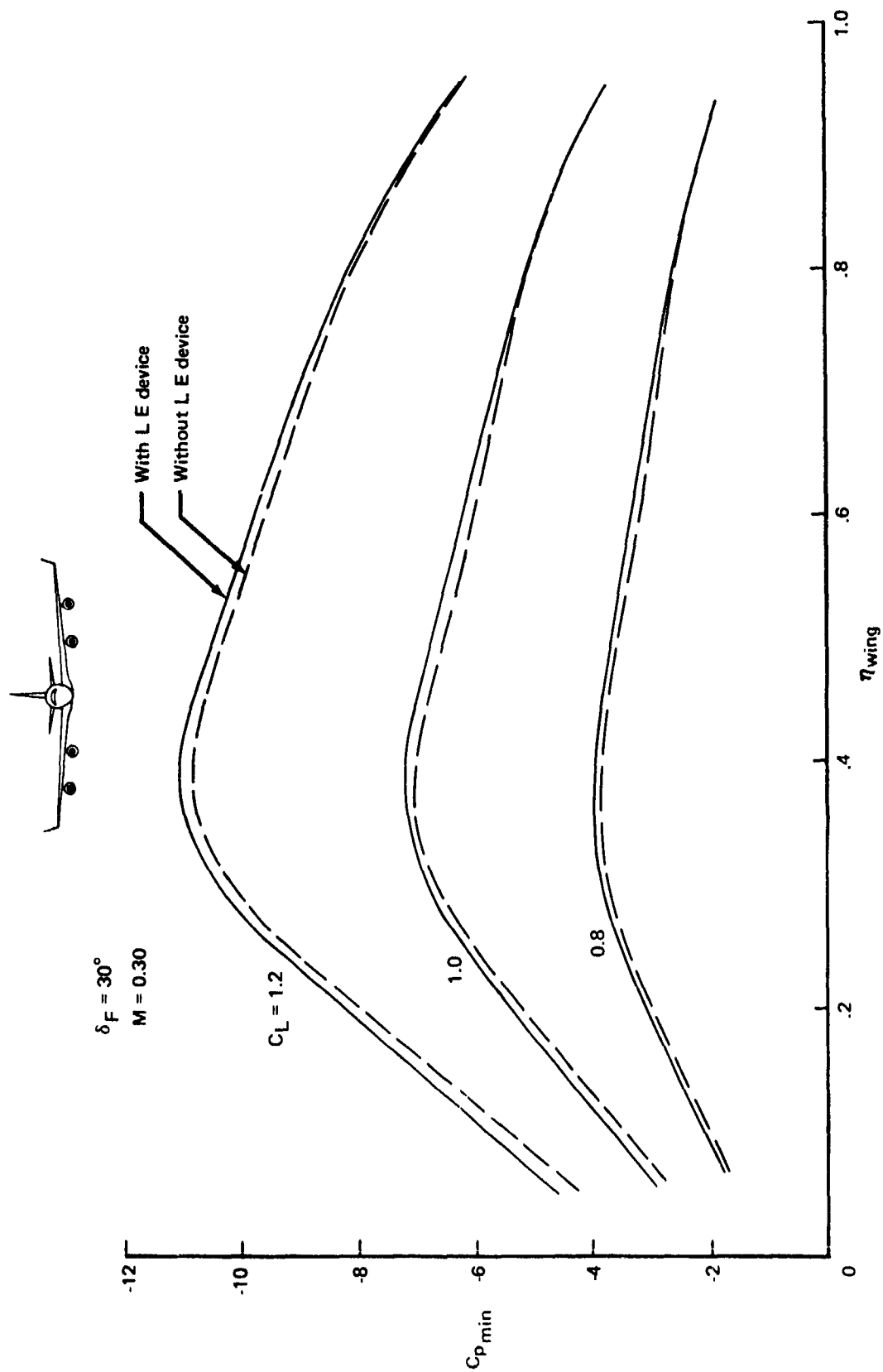
Figure 22. -- Minimum Pressures on AFFDL/Boeing Winglets

$\delta_F = 30°$
$M = 0.30$

With L E device
Without L E device

$C_L = 1.2$
1.0
0.8

η_{wing}

$C_{p_{min}}$

-12
-10
-8
-6
-4
-2
0

0   .2   .4   .6   .8   1.0

45
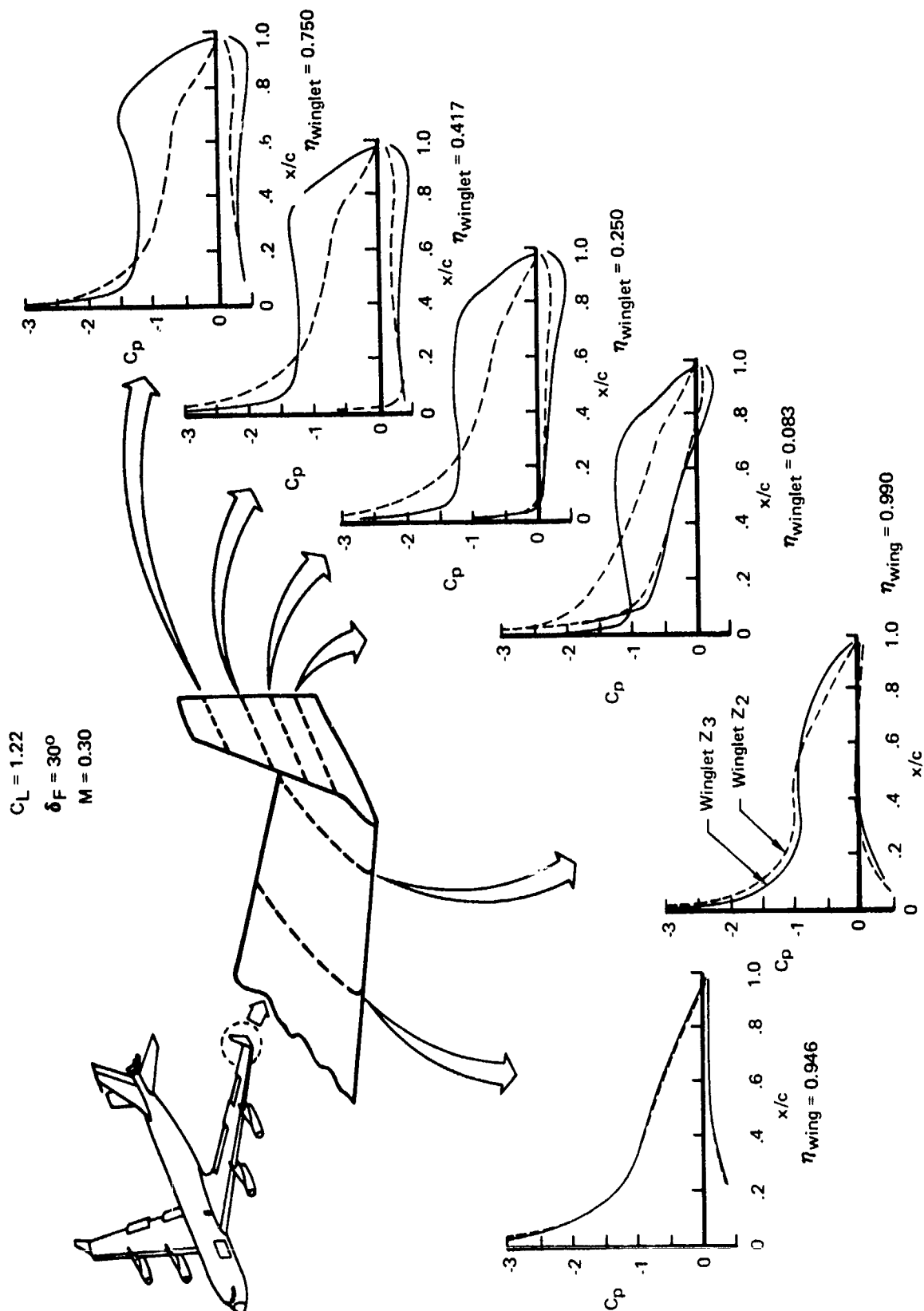
Figure 23. — Low-Speed Surface Pressures on Wing and Winglet Z_3

46
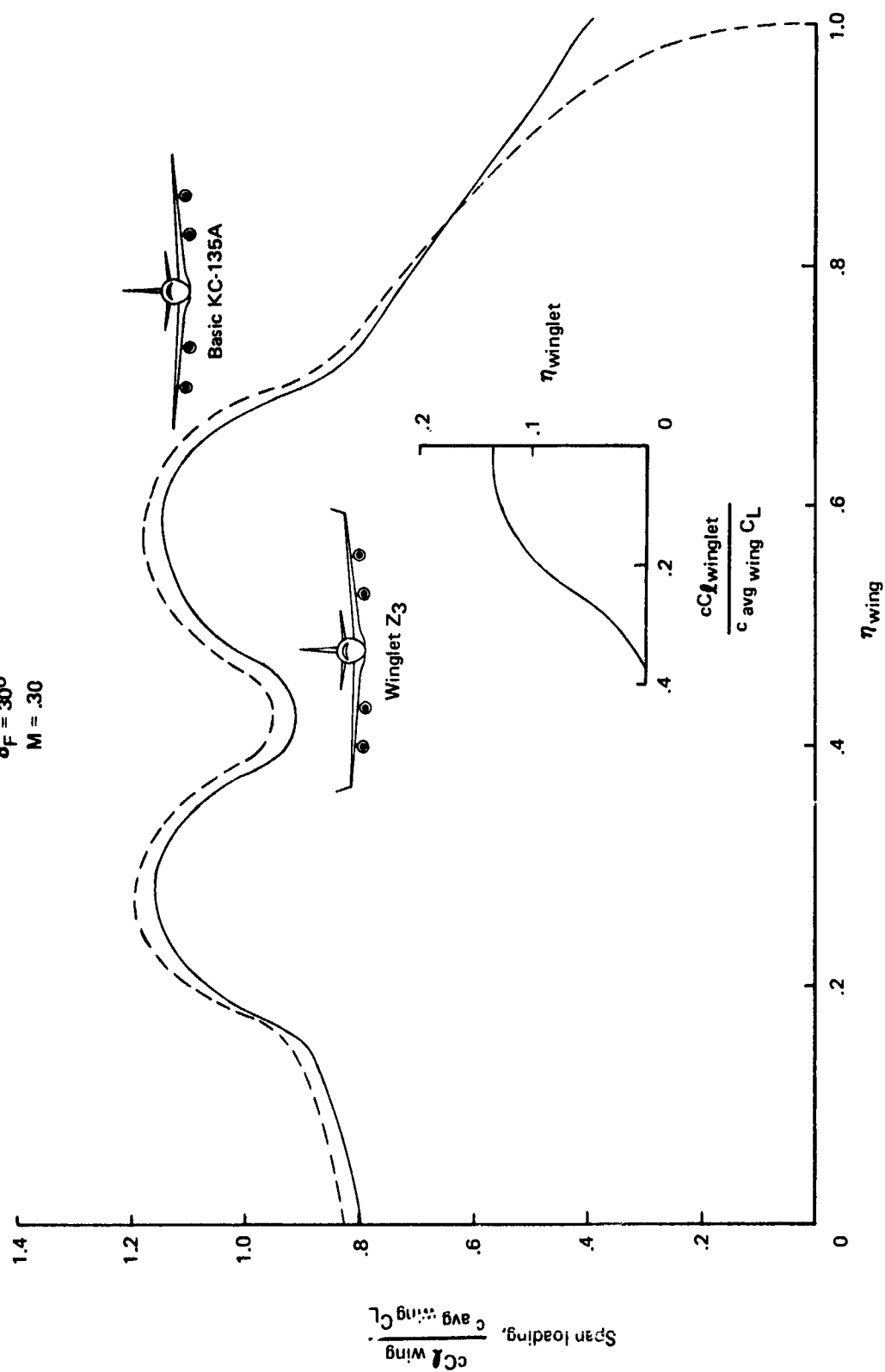
Figure 24. — Span Loading With Low-Speed Winglet Z₃

47

Figure 25. – Section C_l's With Low-Speed Winglet Z_3

$C_L = 1.22$
$\delta_F = 30^\circ$
$M = 0.30$

Basic KC-135A

Winglet Z_3

$\eta_{winglet}$

$C_{l_{winglet}}/C_L$

η_{wing}

Sectional lift coefficient, $C_{l_{wing}}/C_L$
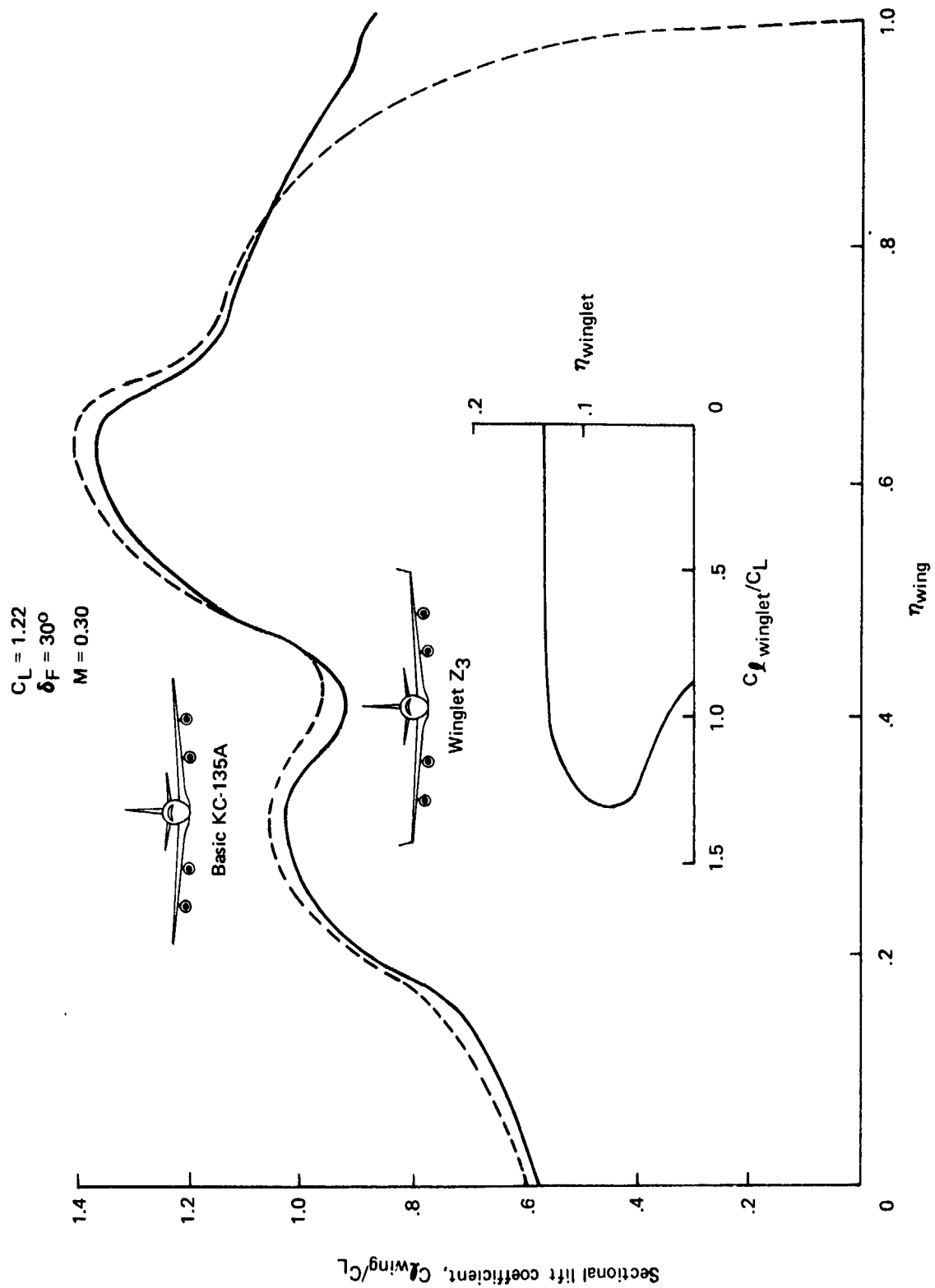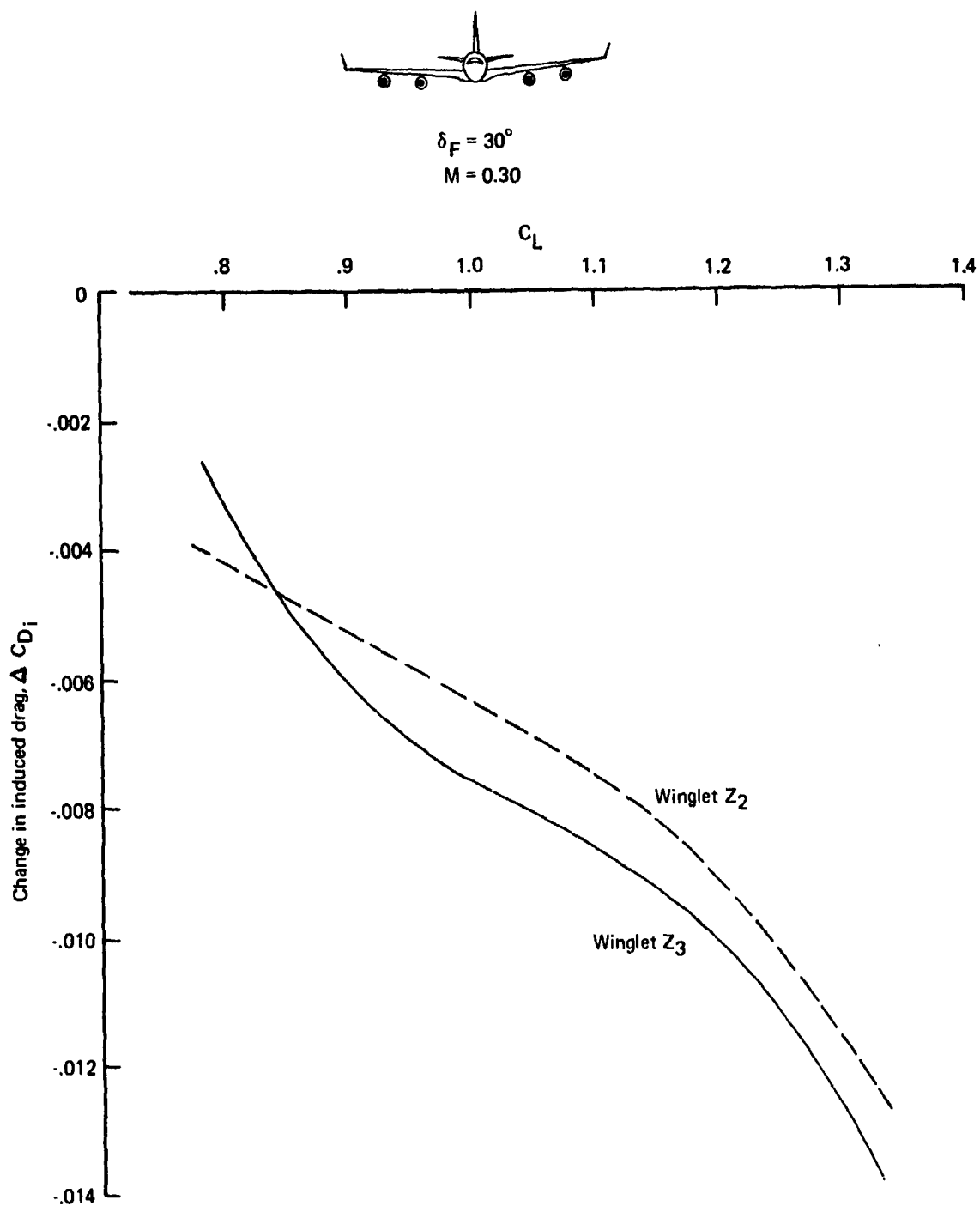
Figure 26. — Reduction in Induced Drag With Low-speed Winglet Z_3
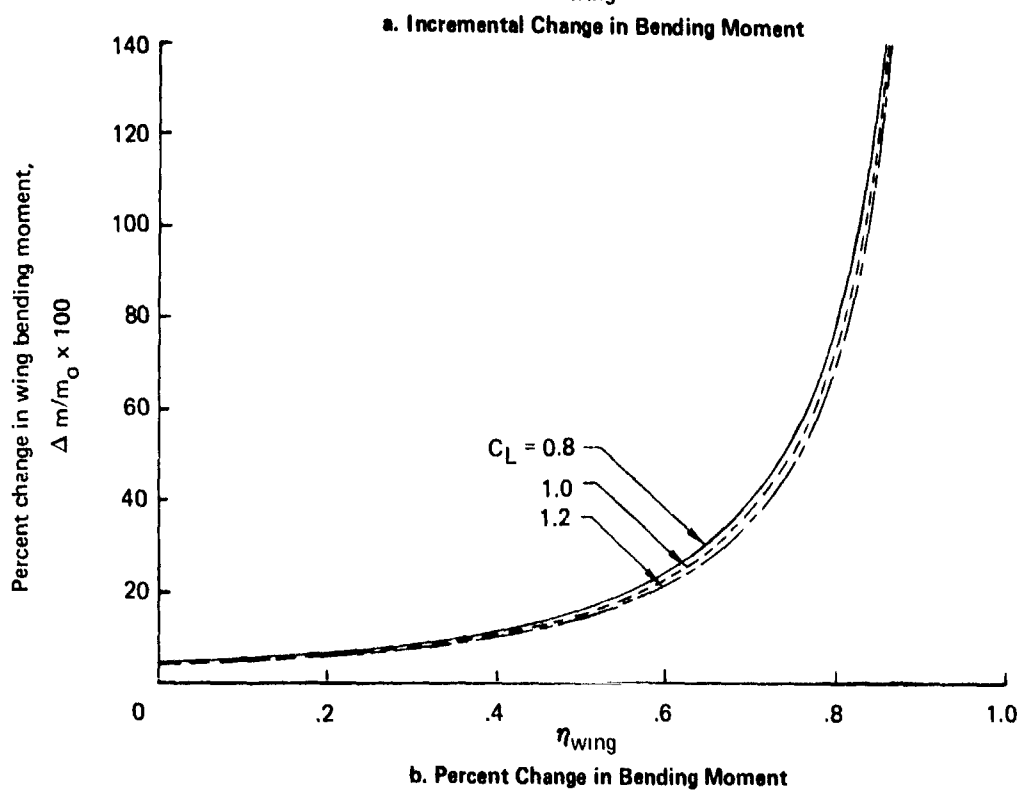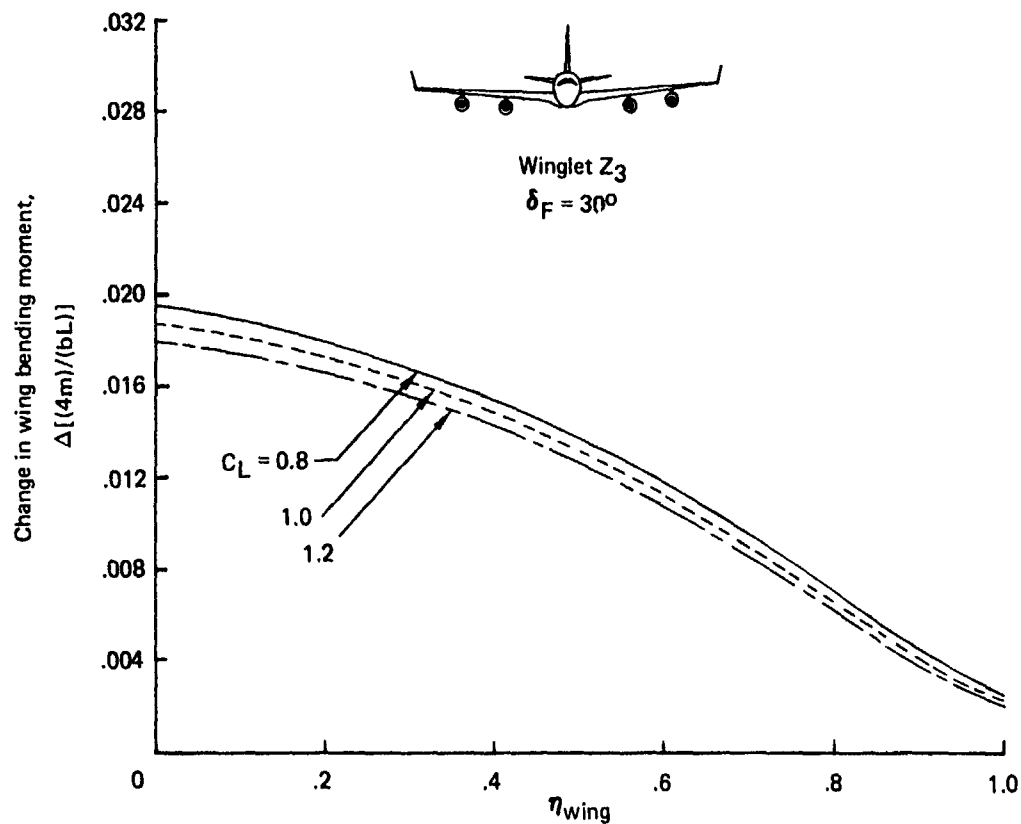
Figure 27. — Effect of Low-Speed Winglet Z_3 on KC-135A Wing Bending Moment With Flaps 30°

50
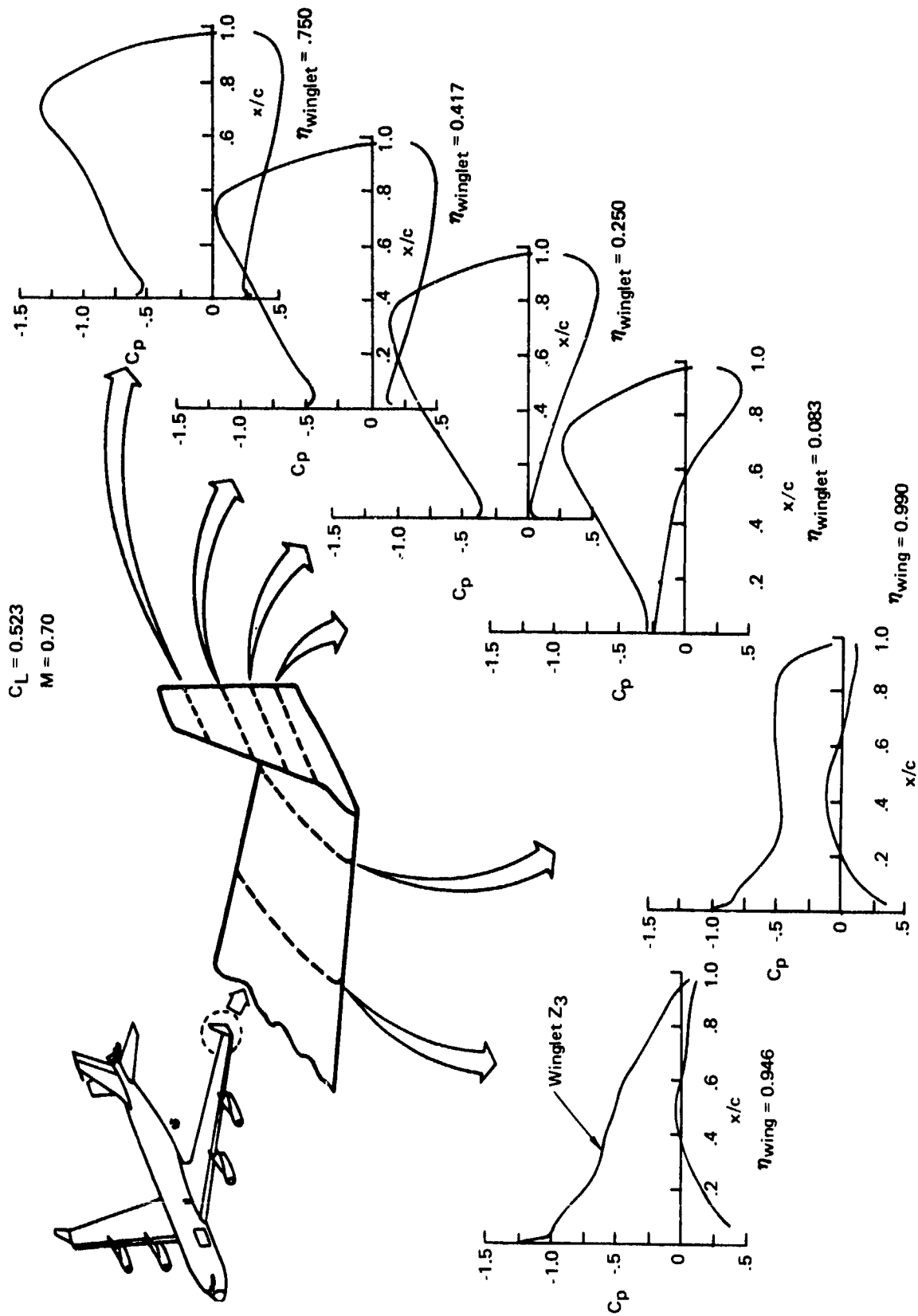
Figure 28. — High-Speed Surface Pressures on Wing and Winglet Z_3

51
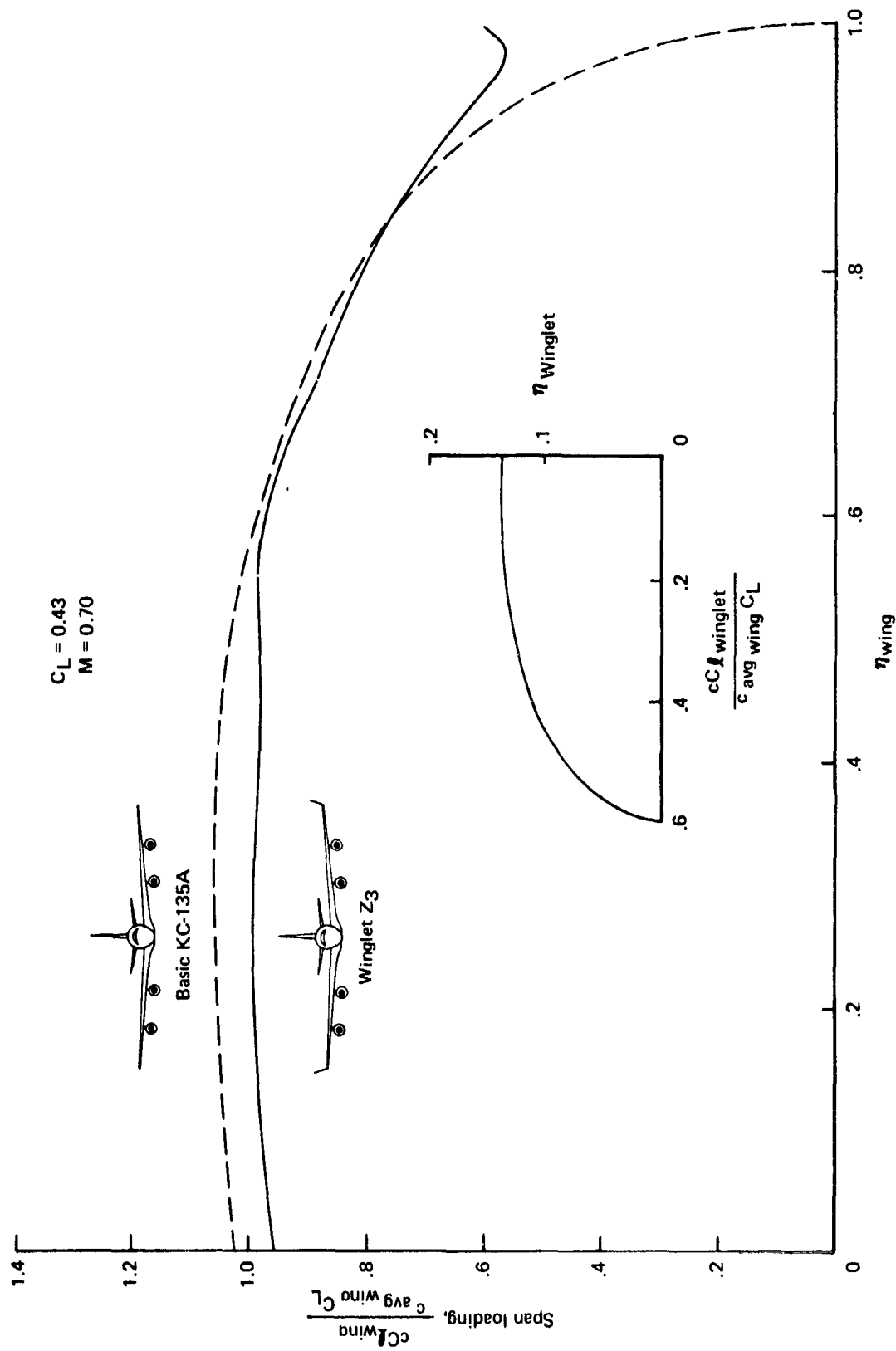
Figure 29. — High-Speed Span Loading With Winglet Z_3

$\delta_F = 30^\circ$
$C_L = 1.22$
$M = 0.30$

$\eta_{winglet} = 0.25$

Winglet Z_2
Winglet Z_4

C_p

x/c

$\eta_{winglet} = 0.75$

Winglet Z_2
Winglet Z_4

C_p

x/c
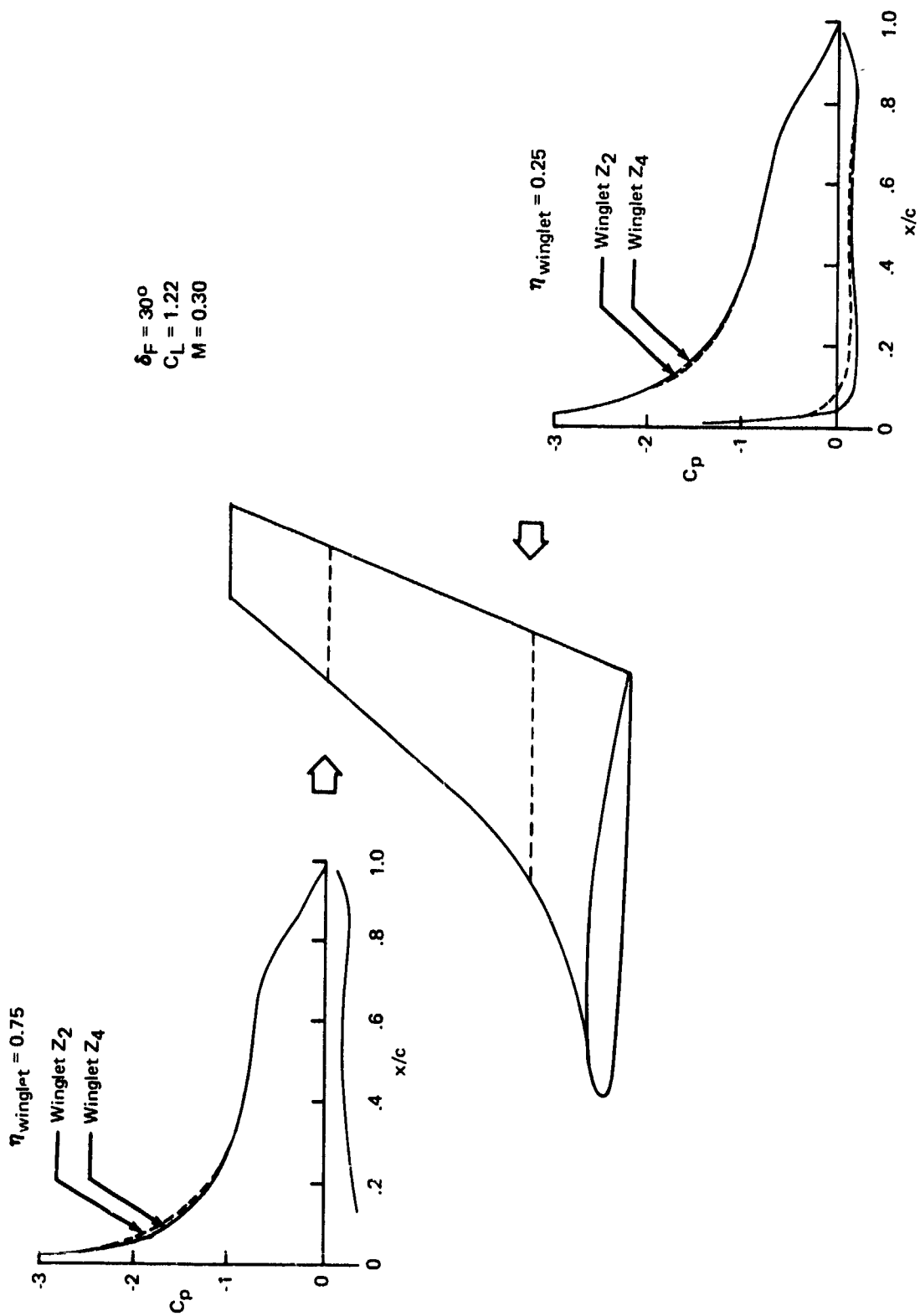
Figure 30. – Low-Speed Surface Pressures With Compromise Winglet Z_4
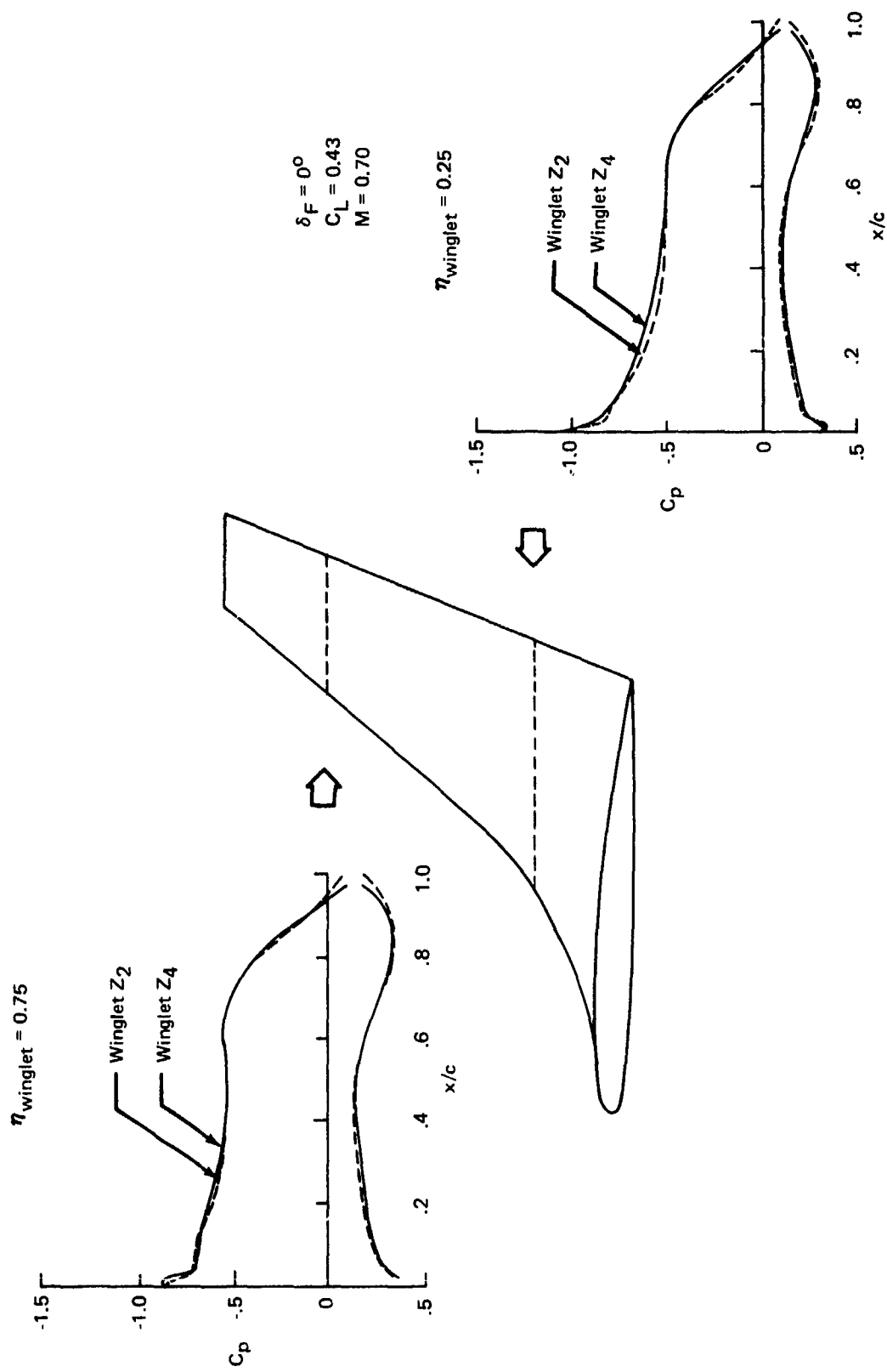
Figure 31. – High-Speed Surface Pressures With Compromise Winglet 7_4

$\delta_F = 0^{\circ}$
$C_L = 0.43$
$M = 0.70$

$\eta_{winglet} = 0.25$

$\eta_{winglet} = 0.75$

Winglet Z_2
Winglet Z_4

54
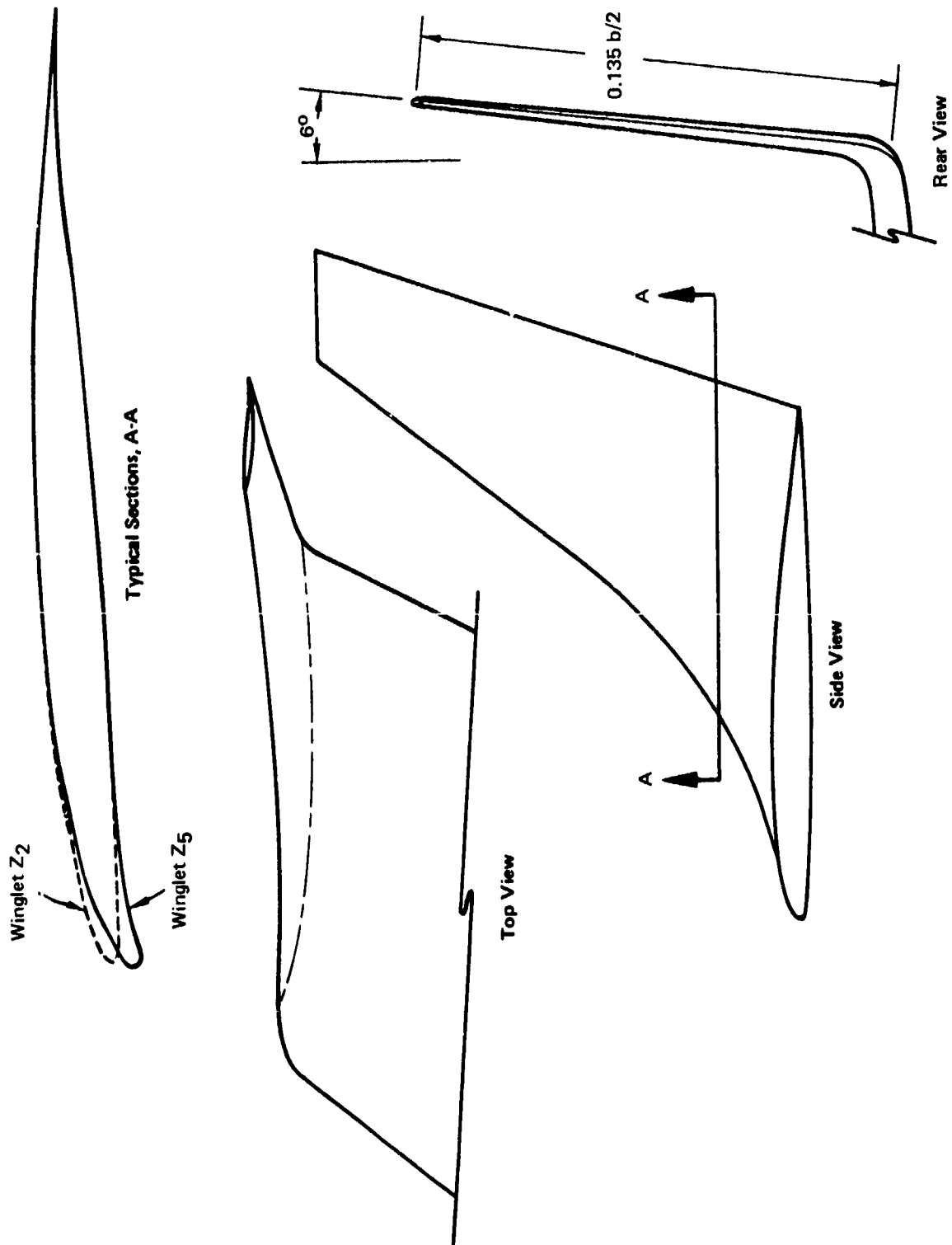
Figure 32. — Geometry of Compromise Winglet Z_5

Winglet Z_2

Winglet Z_5

Typical Sections, A-A

Top View

Side View

Rear View

0.135 b/2

6°

A

A

55
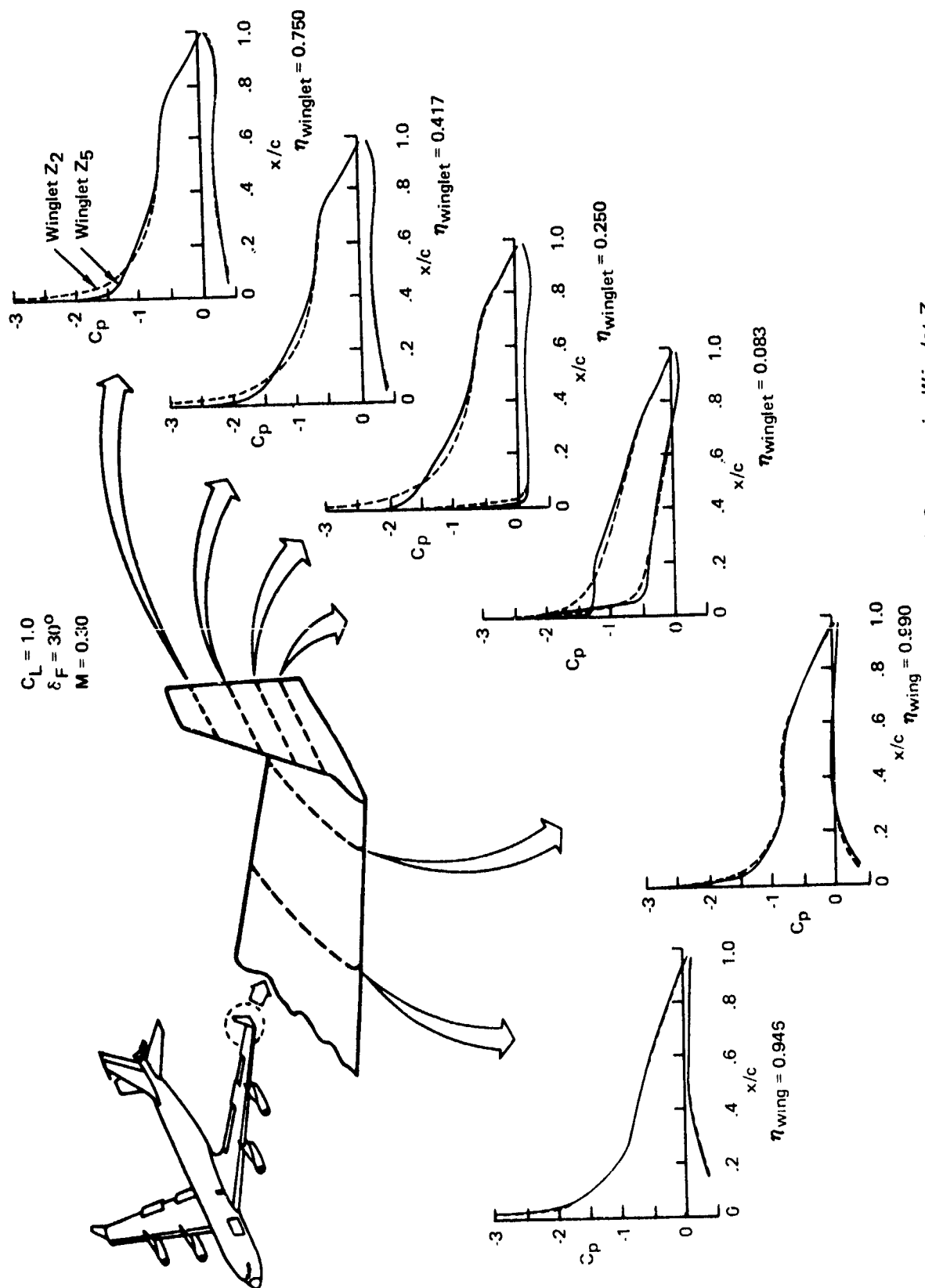
Figure 33. — Low-Speed Surface Pressures With Compromise Winglet Z5

$C_L = 1.0$
$\varepsilon_F = 30°$
$M = 0.30$

Winglet Z_2
Winglet Z_5

$\eta_{winglet} = 0.750$
$\eta_{winglet} = 0.417$
$\eta_{winglet} = 0.250$
$\eta_{winglet} = 0.083$
$\eta_{wing} = 0.990$
$\eta_{wing} = 0.945$
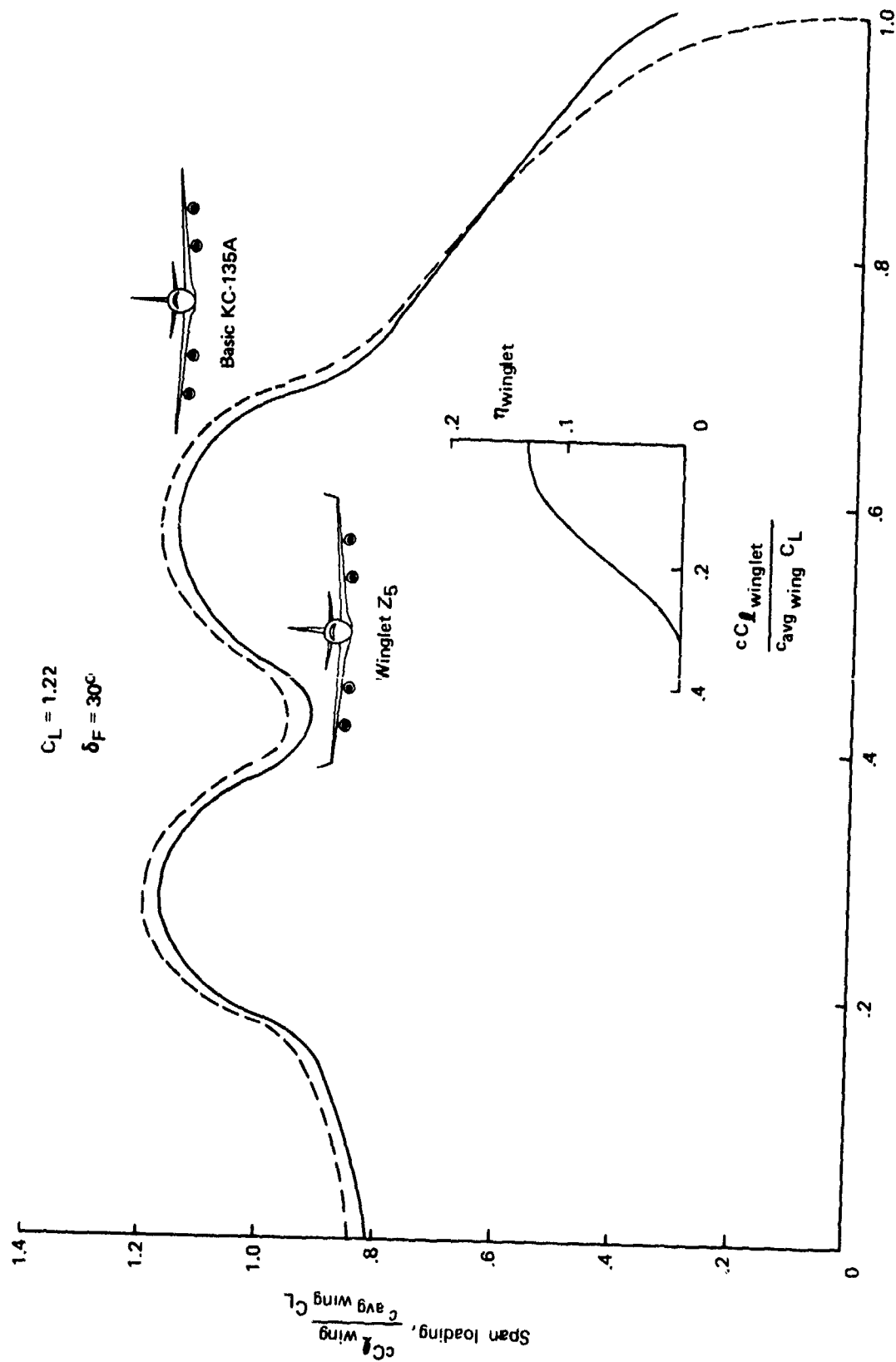
Figure 34. — Span Loading at Takeoff With Compromise Winglet Z_5

$\delta_F = 30^\circ$

M = 0.30
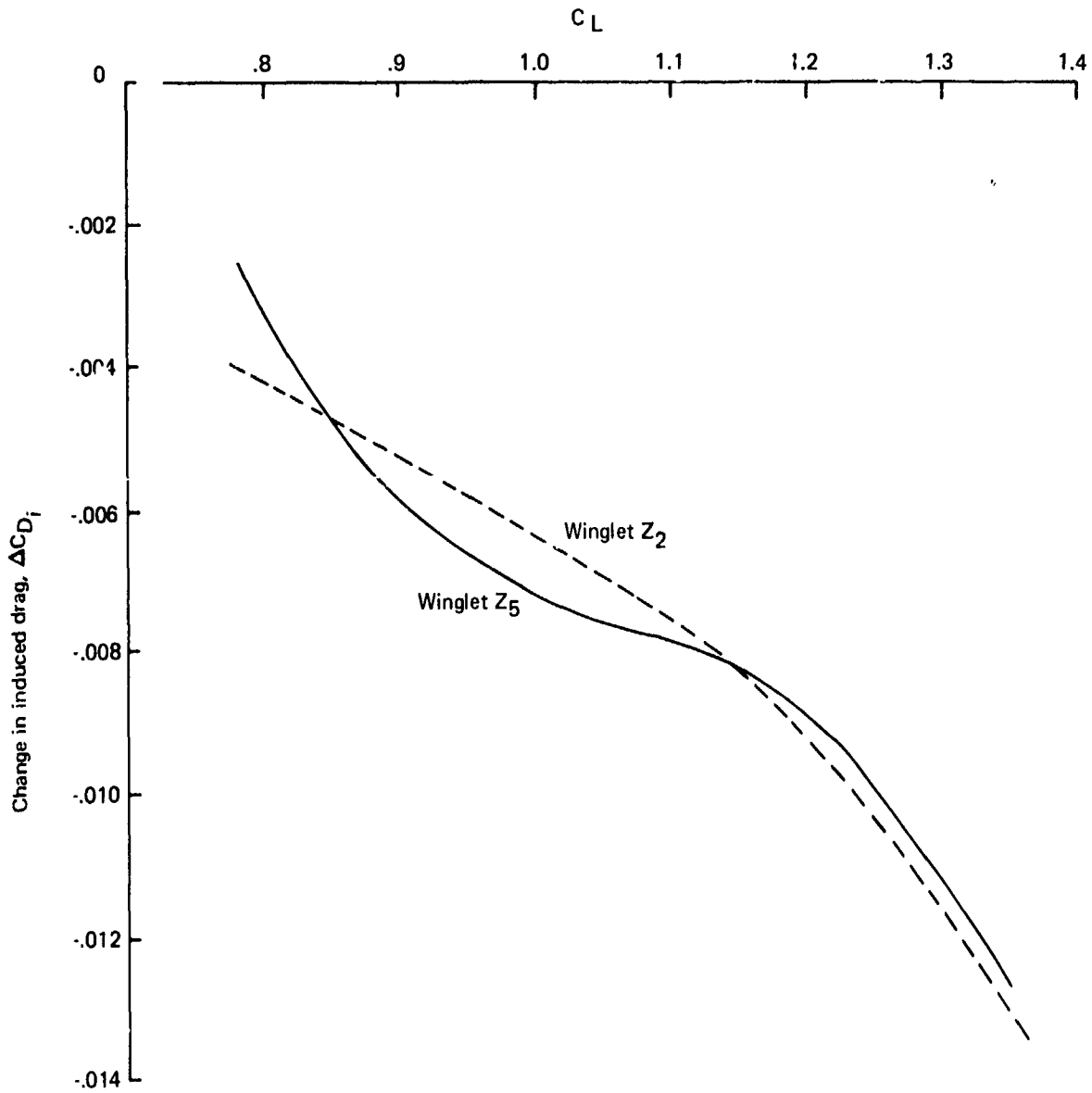
Figure 35. — Reduction in Induced Drag With Compromise Winglet Z_5
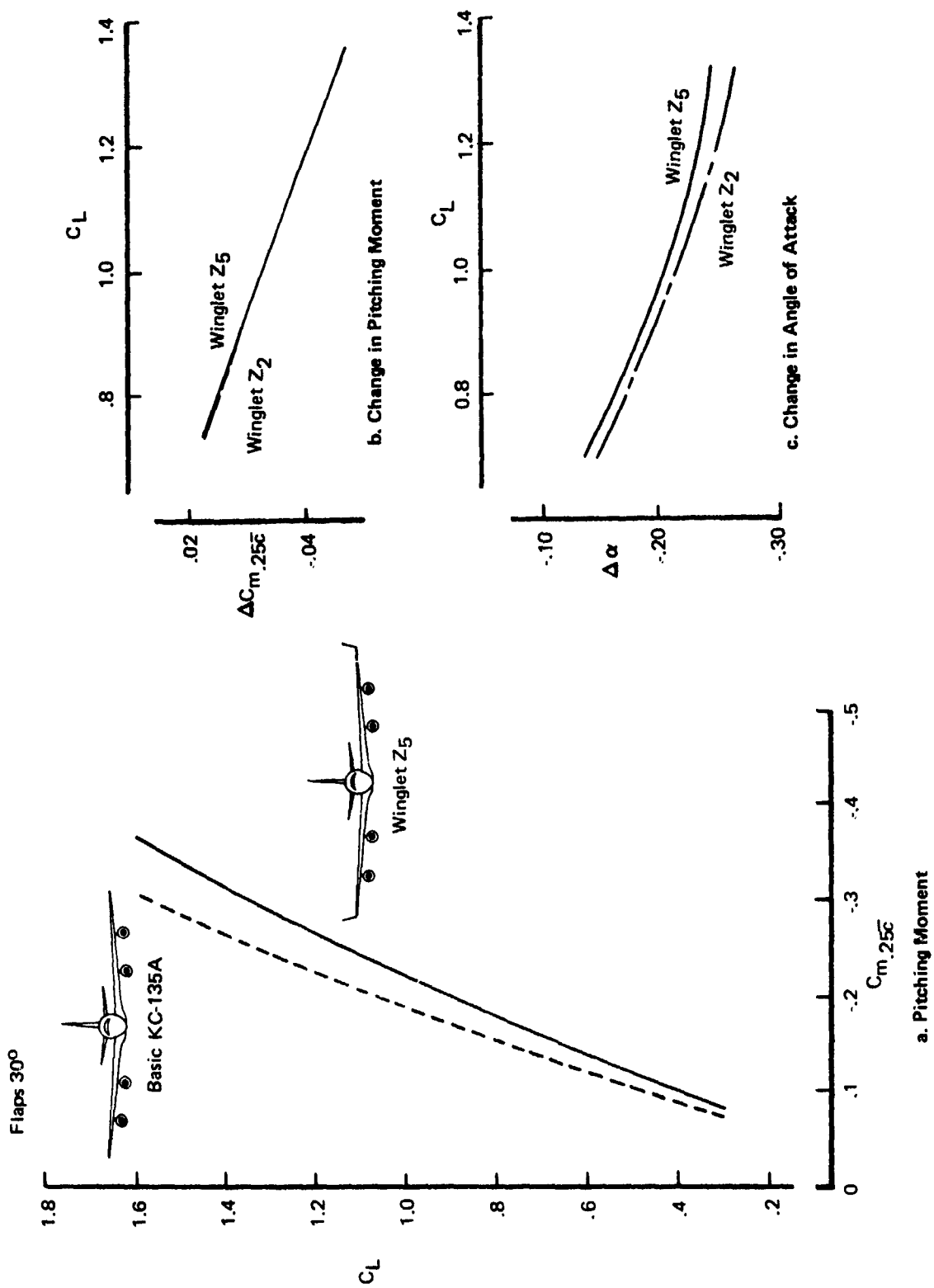
Figure 36. — Effect of Winglet Z_5 on KC-135A Aerodynamics With Flaps 30°

59
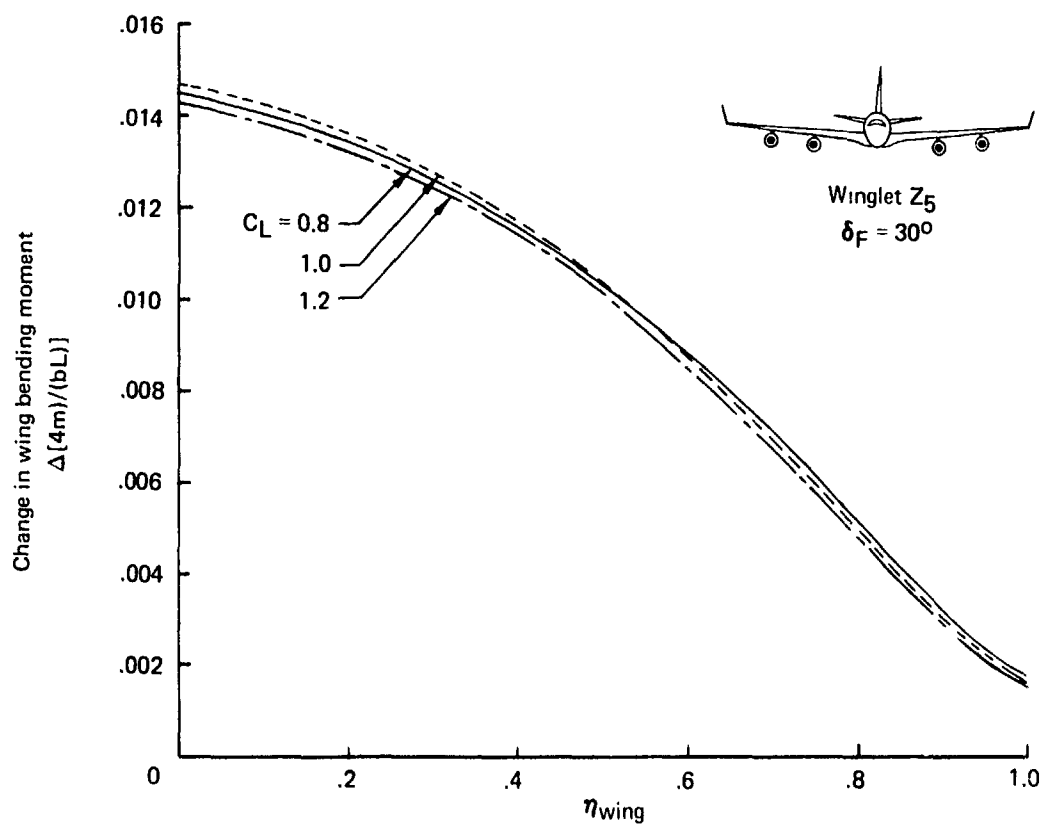
a. Incremental Change in Bending Moment
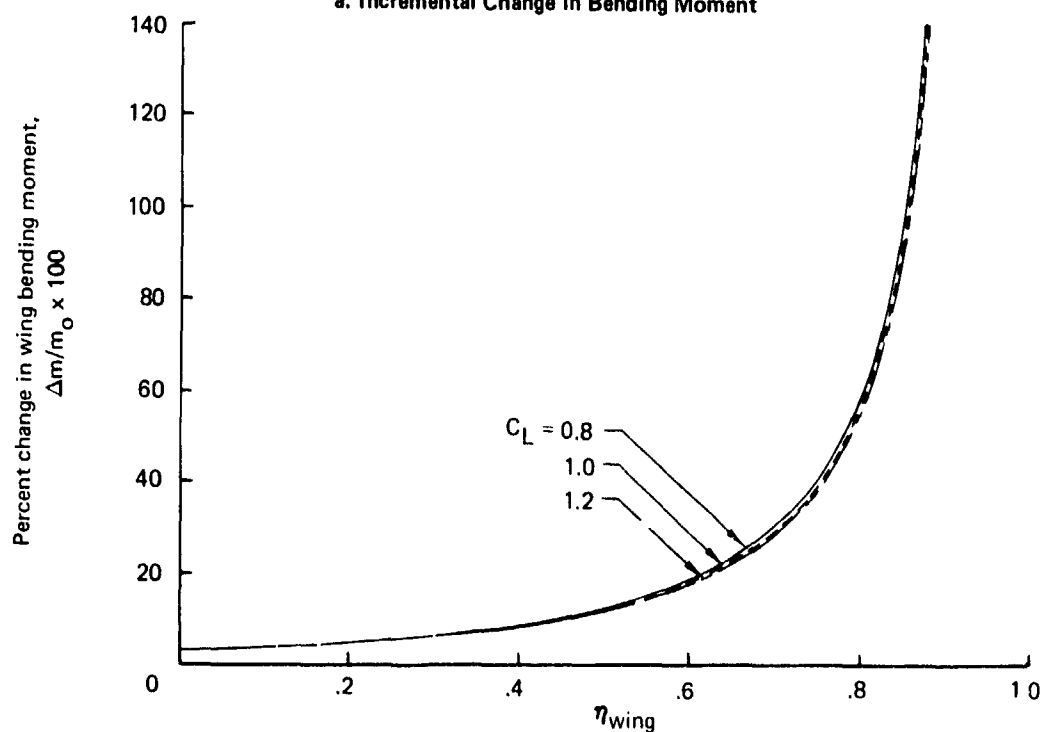
b. Percent Change in Bending Moment

Figure 37. — Effect of Winglet Z_5 on KC-135A Wing Bending Moment With Flaps 30°
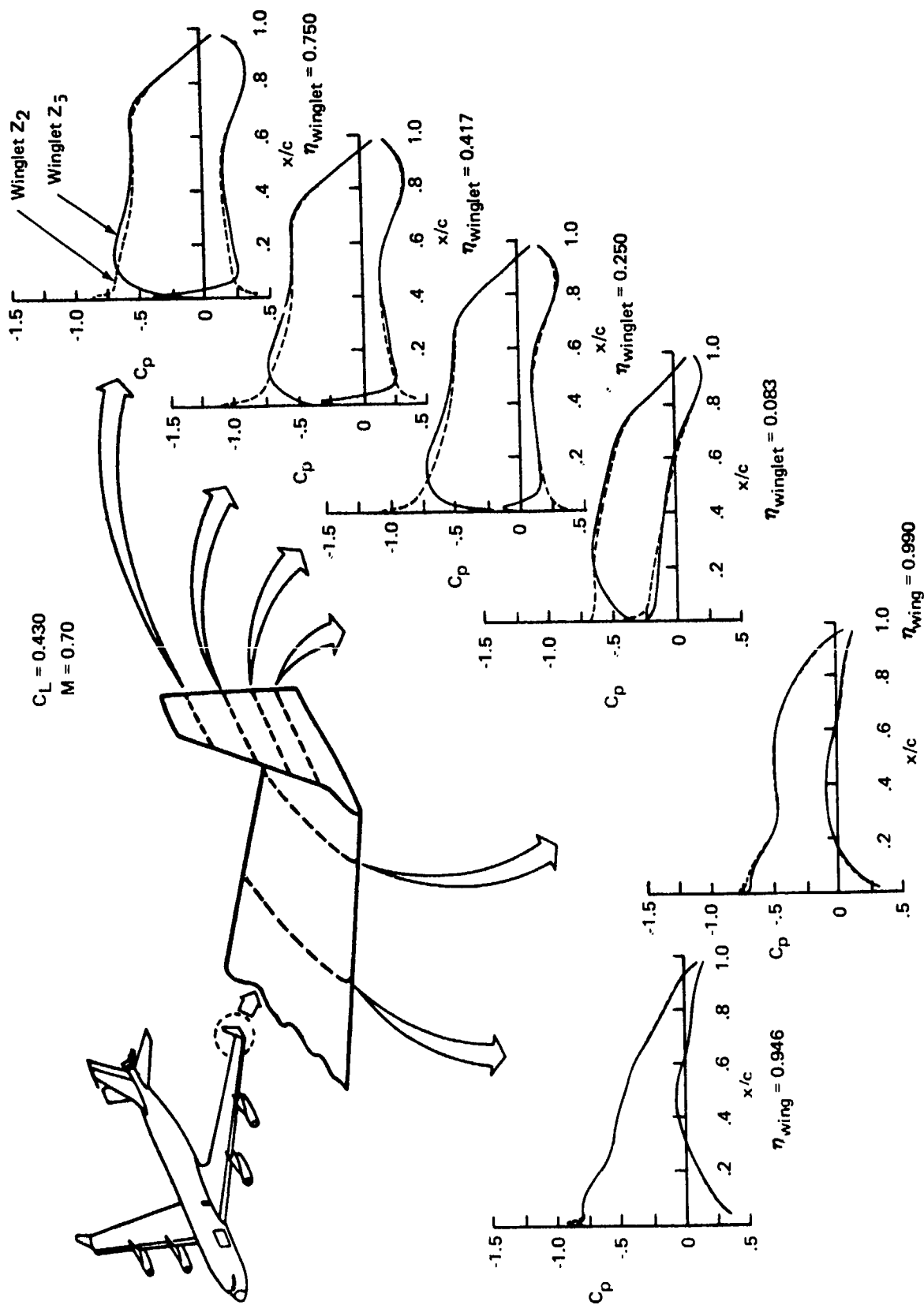
Figure 38. — High-Speed Surface Pressures With Compromise Winglet Z_5

61
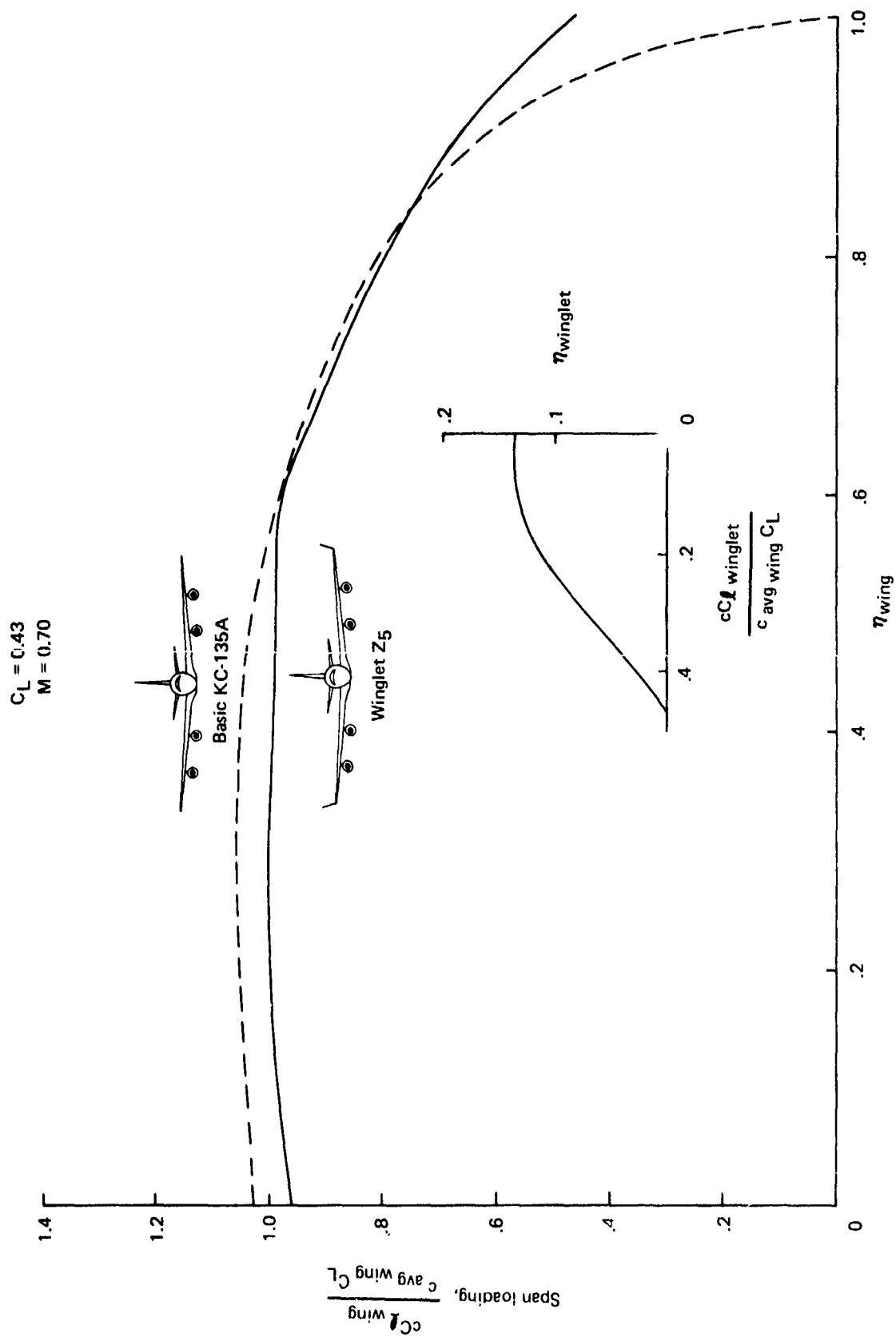
Figure 39. — High-Speed Span Loading With Winglet Z5
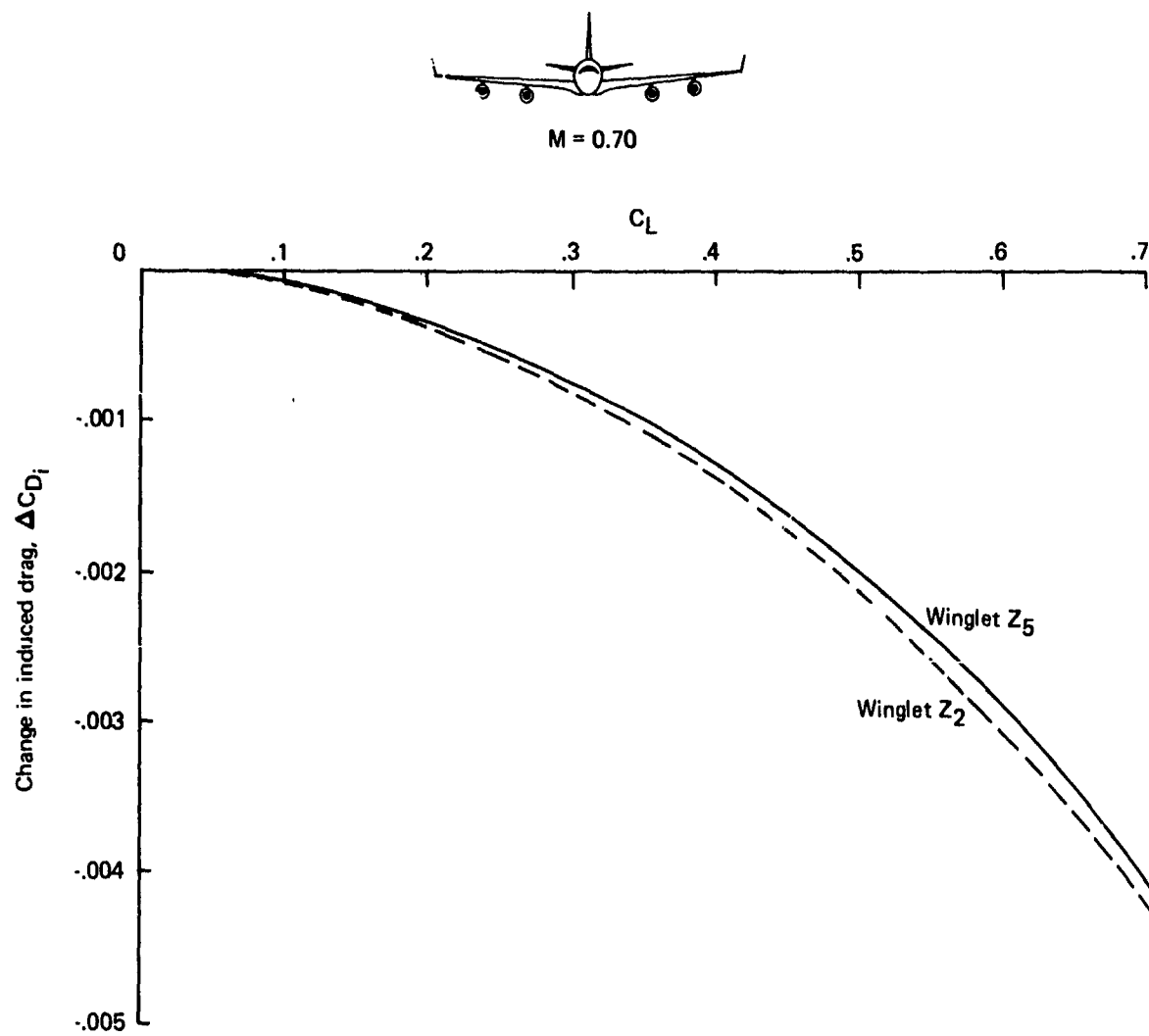
Figure 40. — Reduction in High-Speed Induced Drag With Winglet Z_5
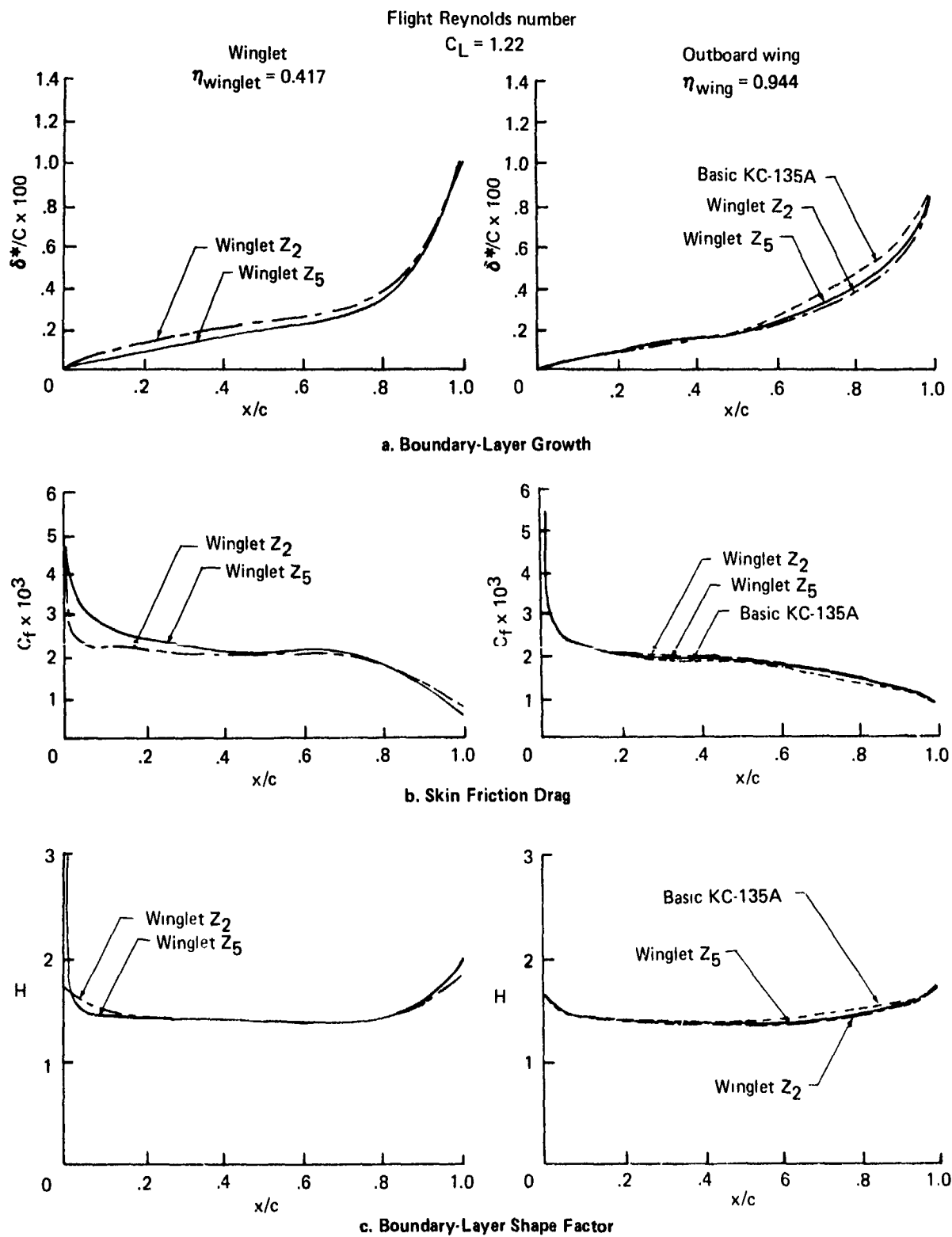
Figure 41. — Comparison of AFFDL/Boeing Winglet and Winglet Z_5 Boundary-Layer Characteristics

64
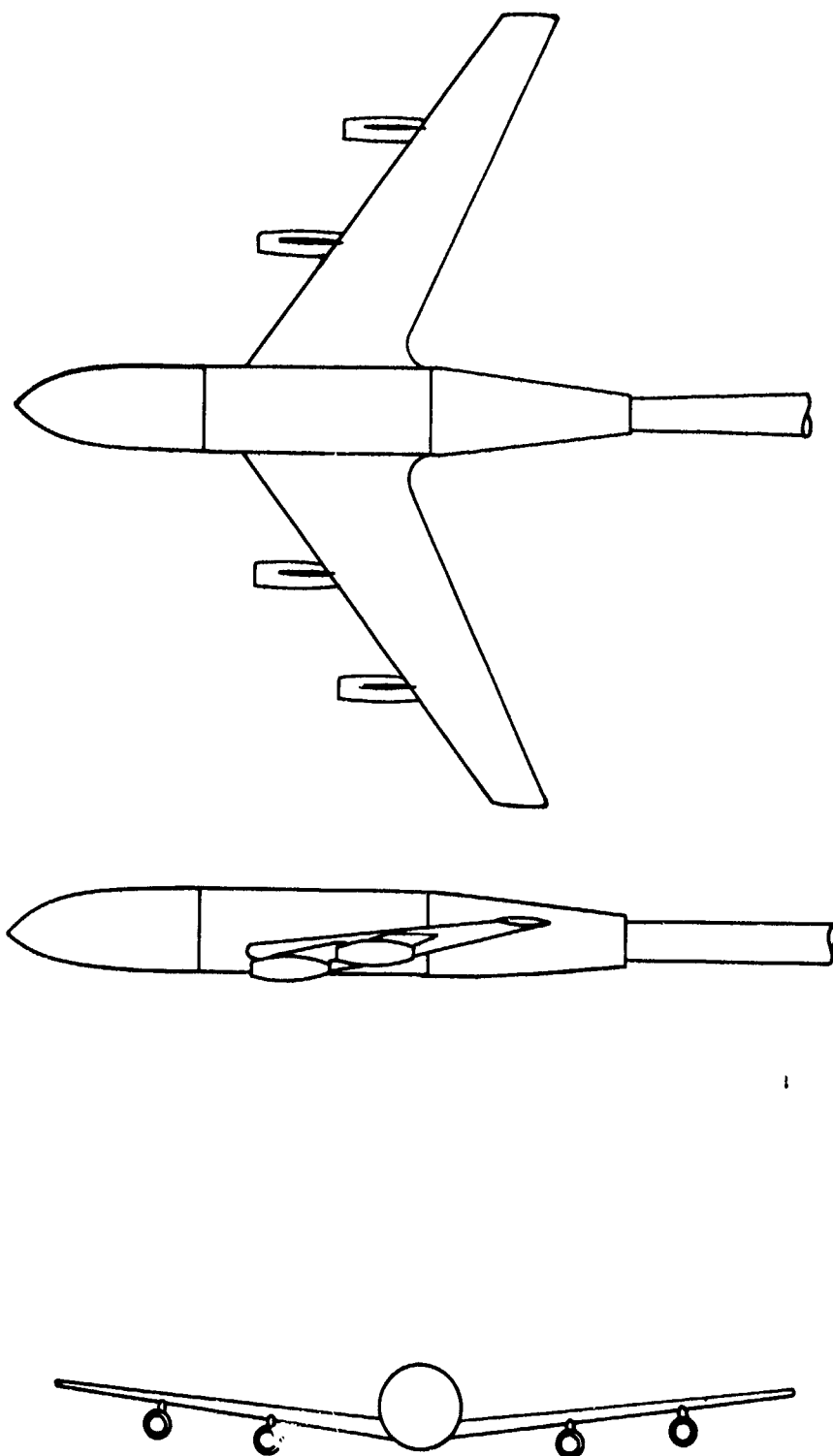
Figure 42. — High-Speed Wind Tunnel Model
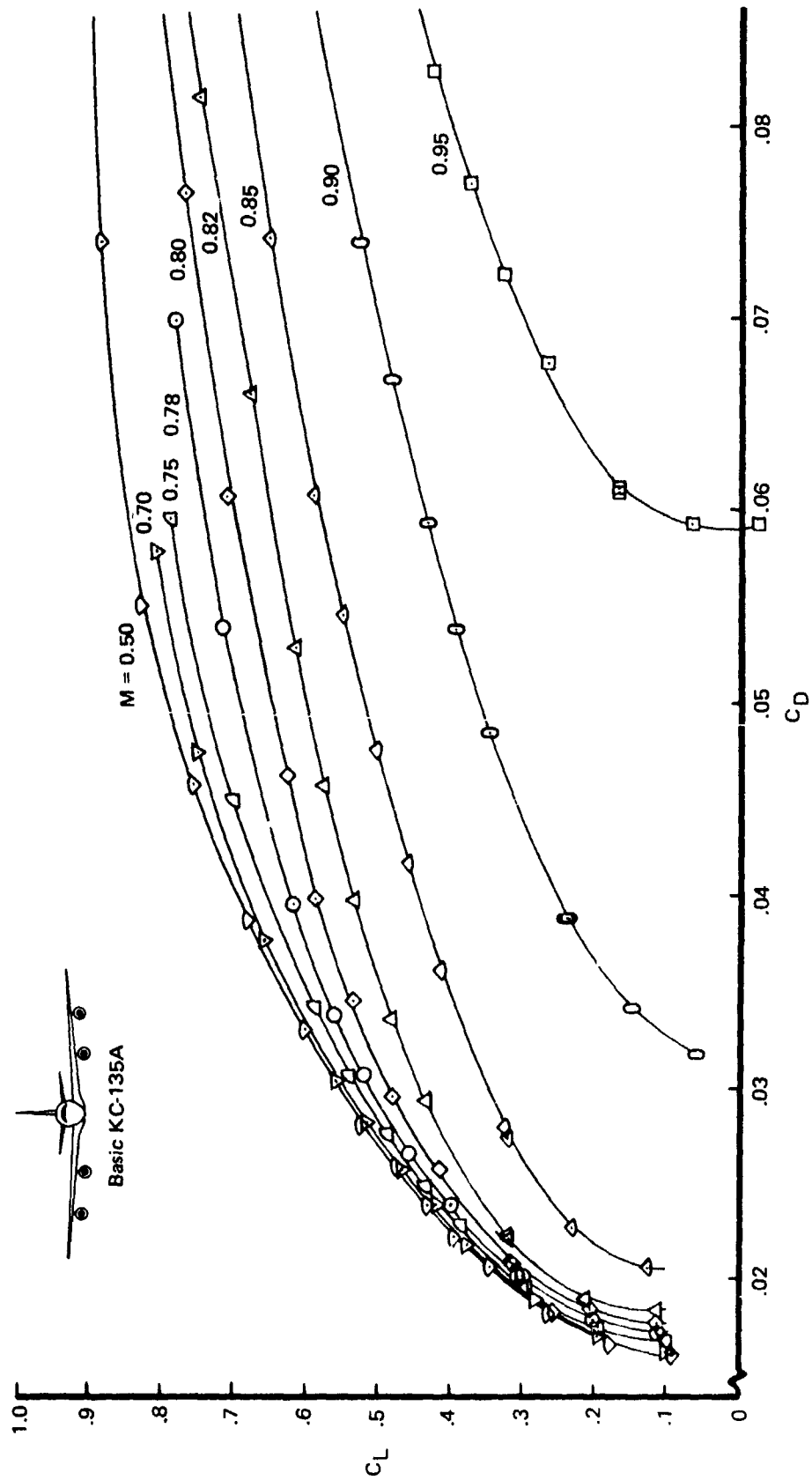
Figure 43. — High-Speed Drag Polars of Basic KC-135A
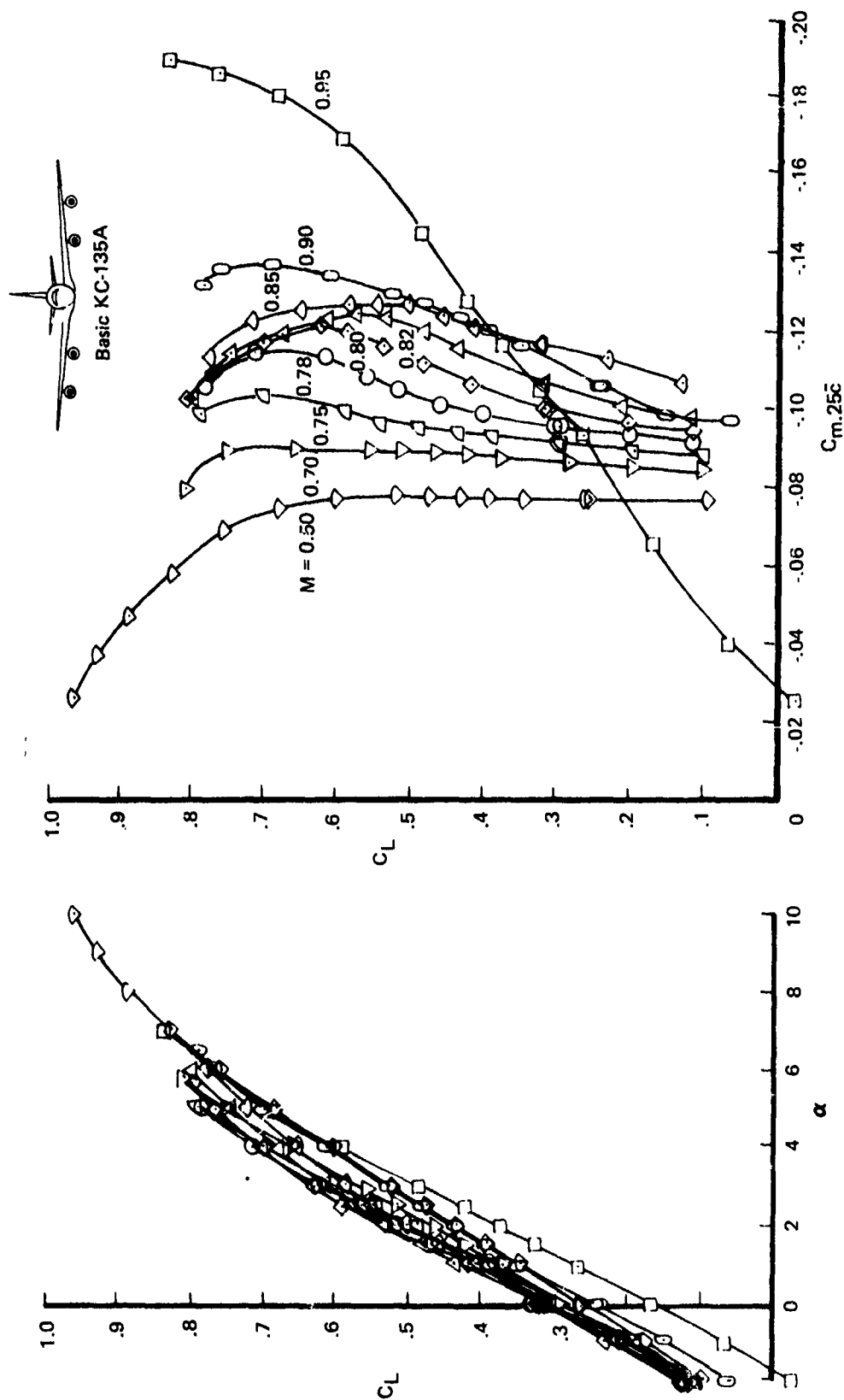
Figure 44. — *High-Speed Lift and Pitching Moment of Basic KC-135A*
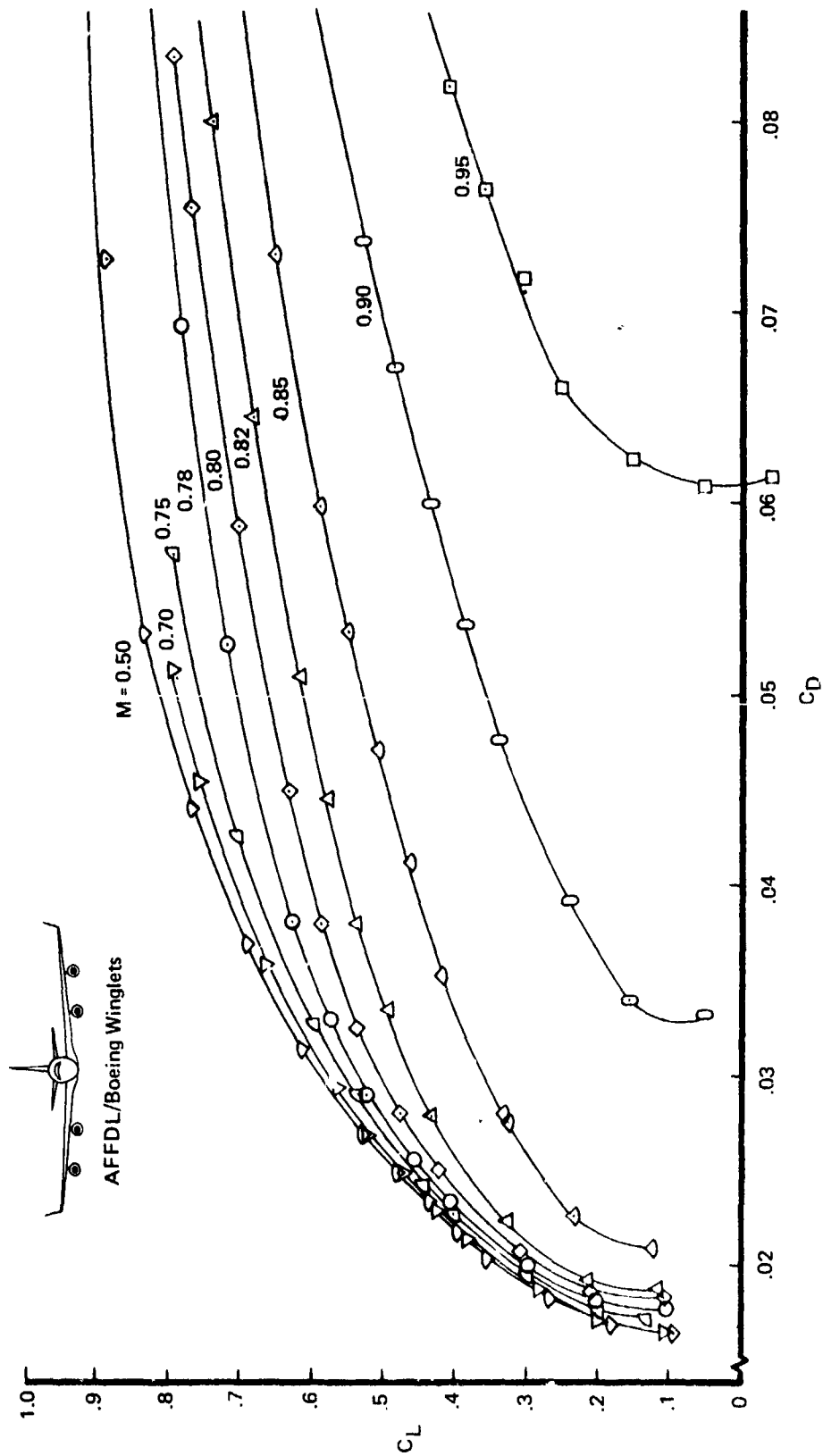
Figure 45. — High-Speed Drag Polars of KC-135A With AFFDL/Boeing Winglets

68
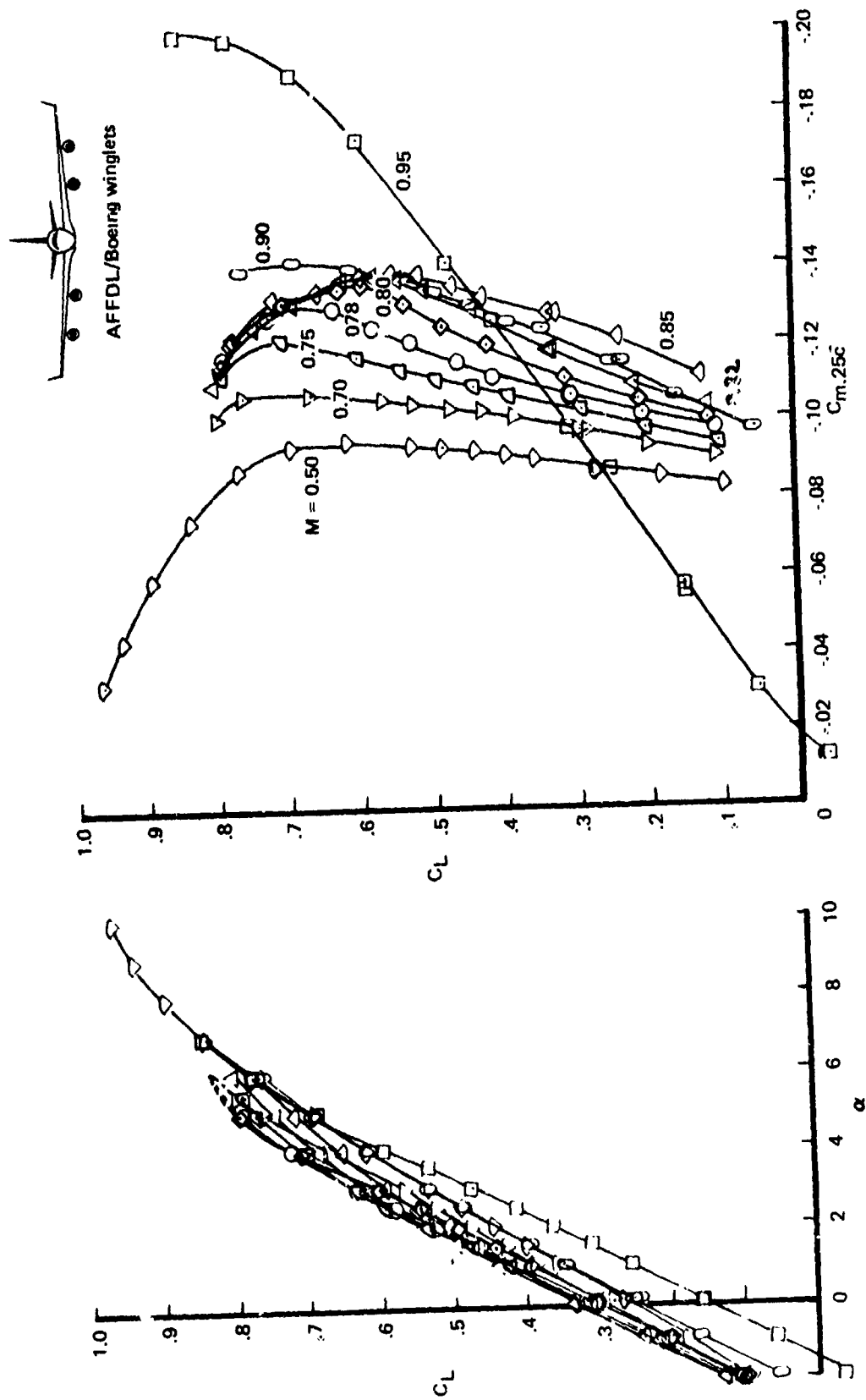
Figure 46. — High-Speed Lift and Pitching Moment of KC-135A With AFFDL/Boeing Winglets
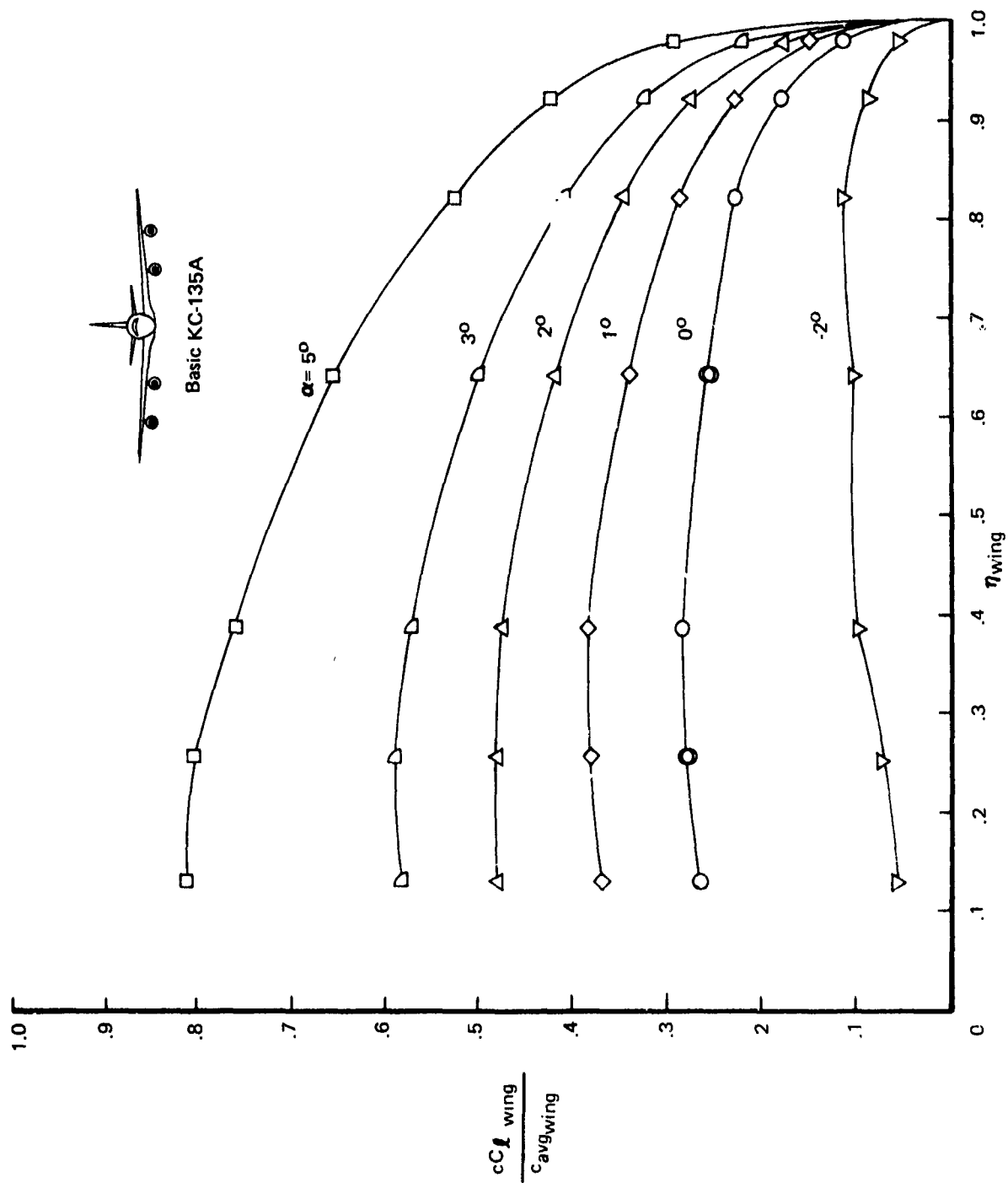
Figure 47. – Basic KC-135A Span Load, Mach 0.50
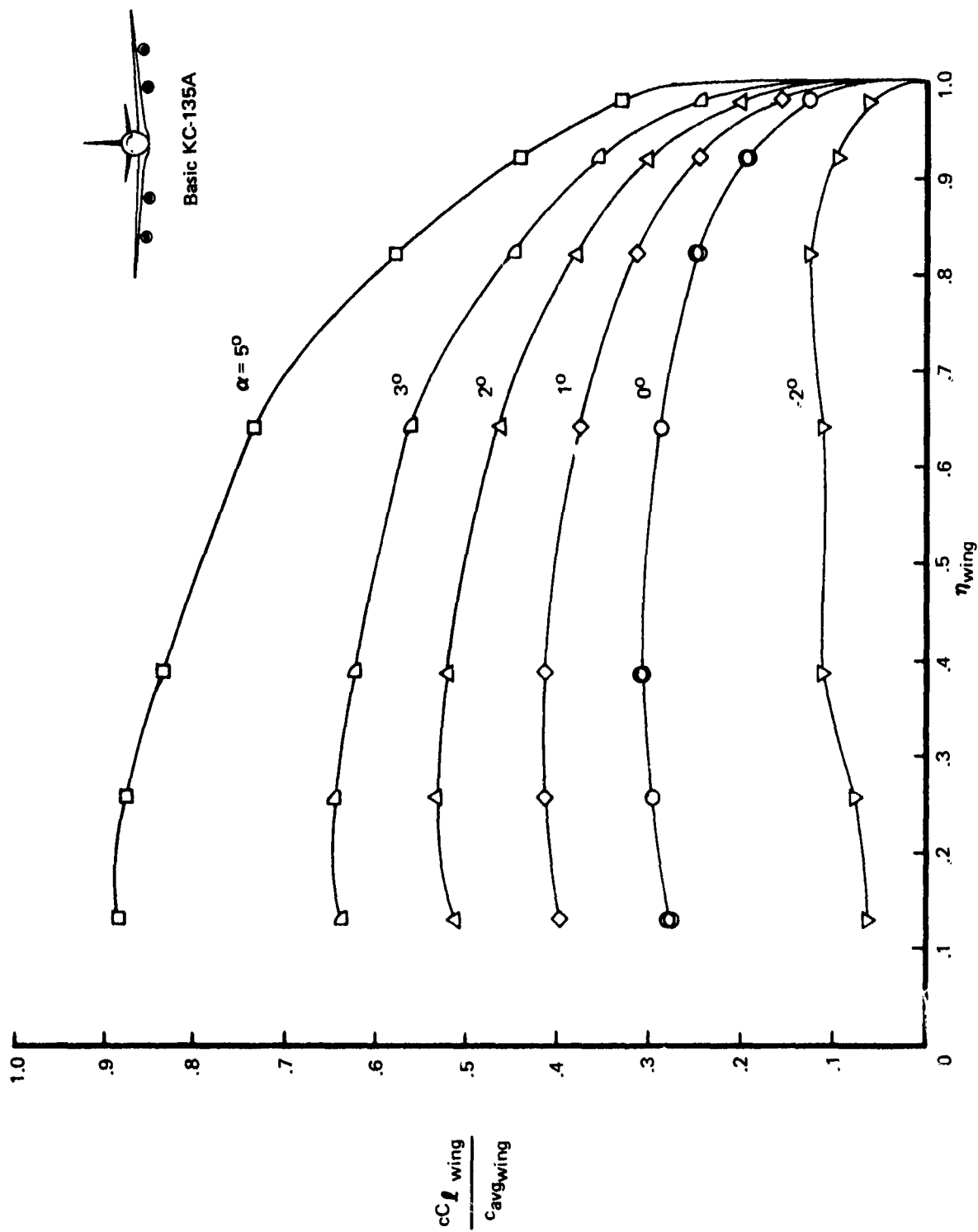
Figure 48. — Basic KC-135A Span Load, Mach 0.70

71

Basic KC-135A

$\alpha = 5^o$

3°

2°

1°

0°

-2°

η_{wing}

$\dfrac{cC_{l\ wing}}{c_{avg_{wing}}}$
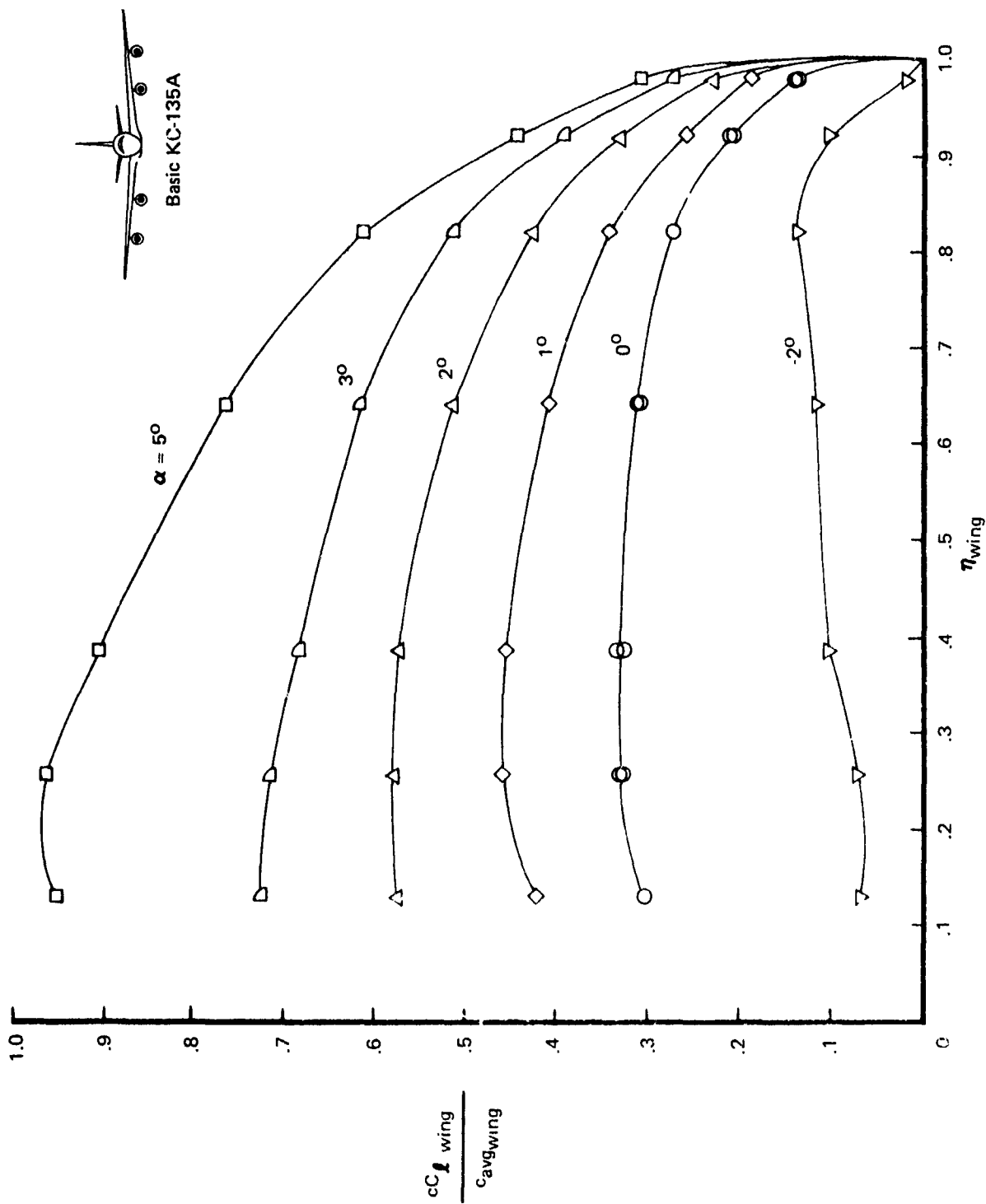
Figure 49. — Basic KC-135A Span Load, Mach 0.78

72
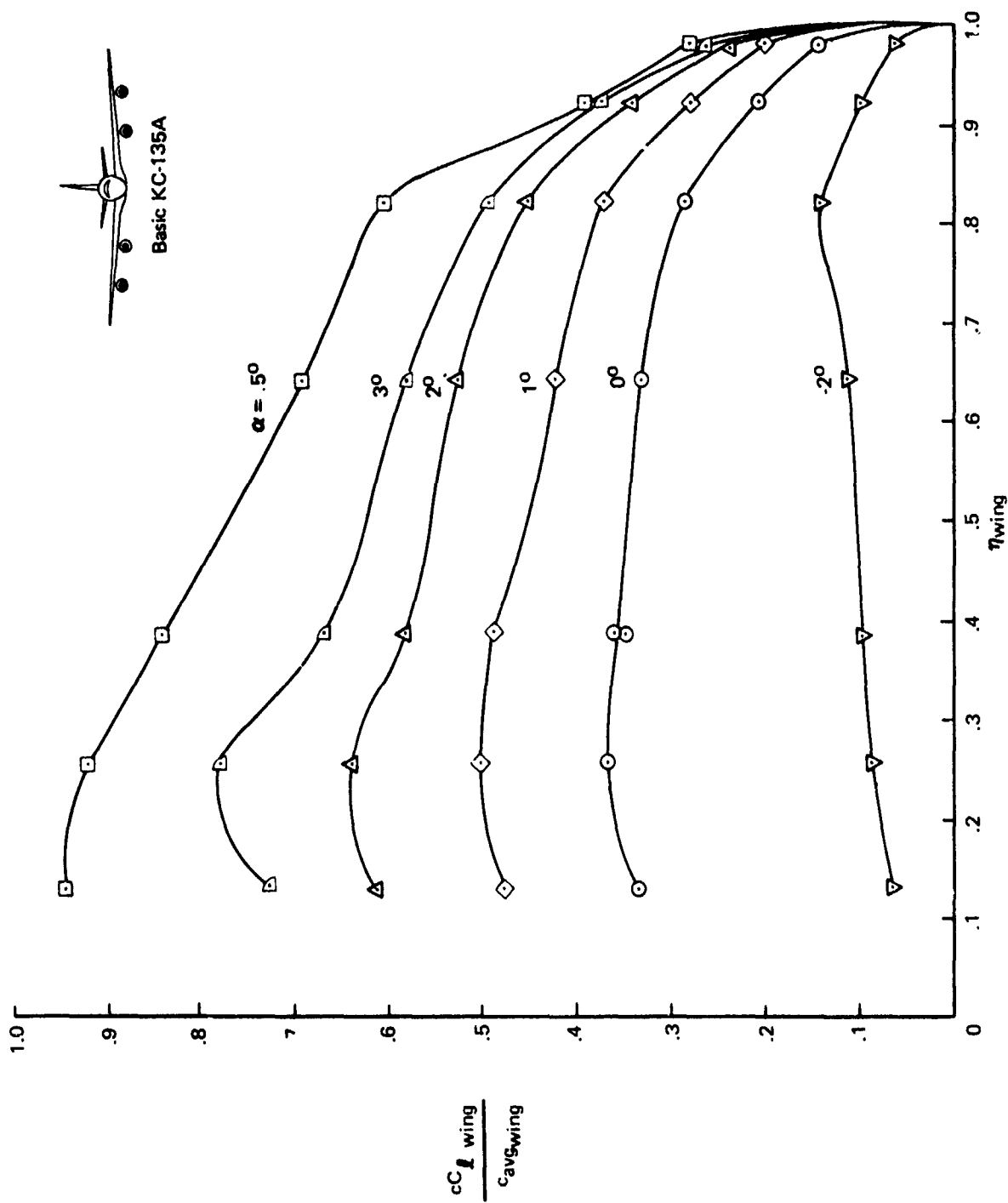
Figure 50.— Basic KC-135A Span Load, Mach 0.82

73
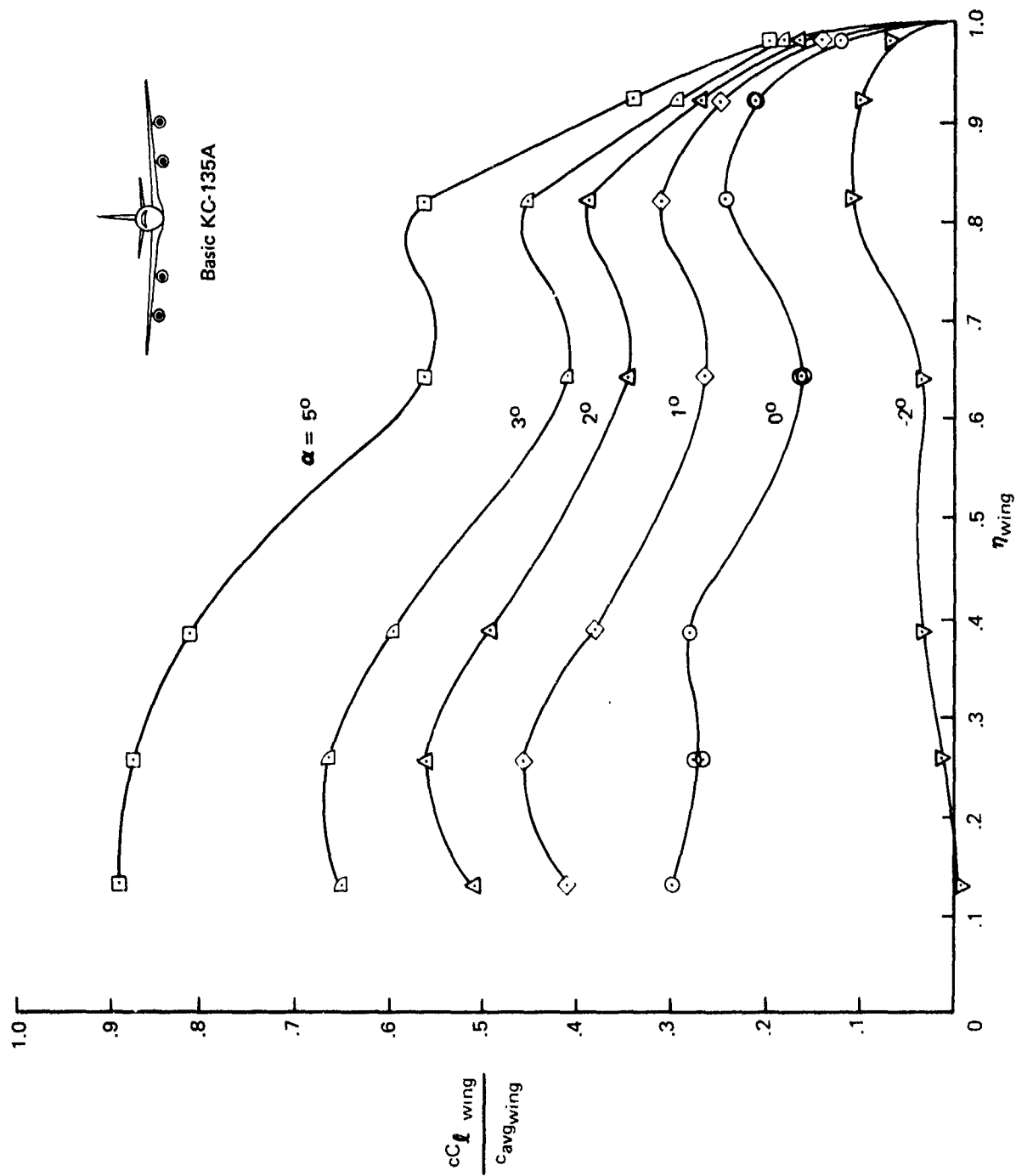
Figure 51. — Basic KC-135A Span Load, Mach 0.90
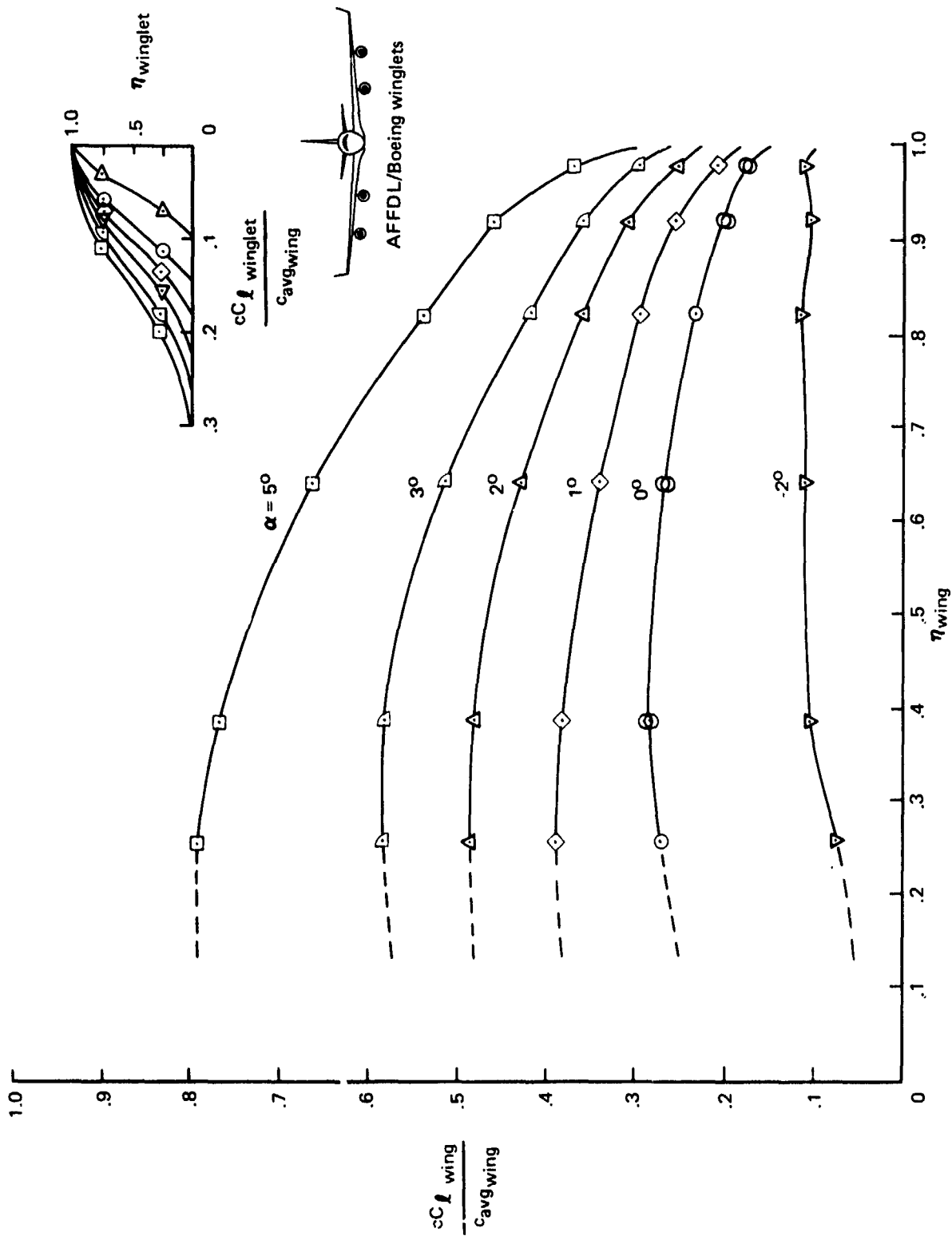
Figure 52. — KC-135A With AFFDL/Boeing Winglet Span Load, Mach 0.50

75
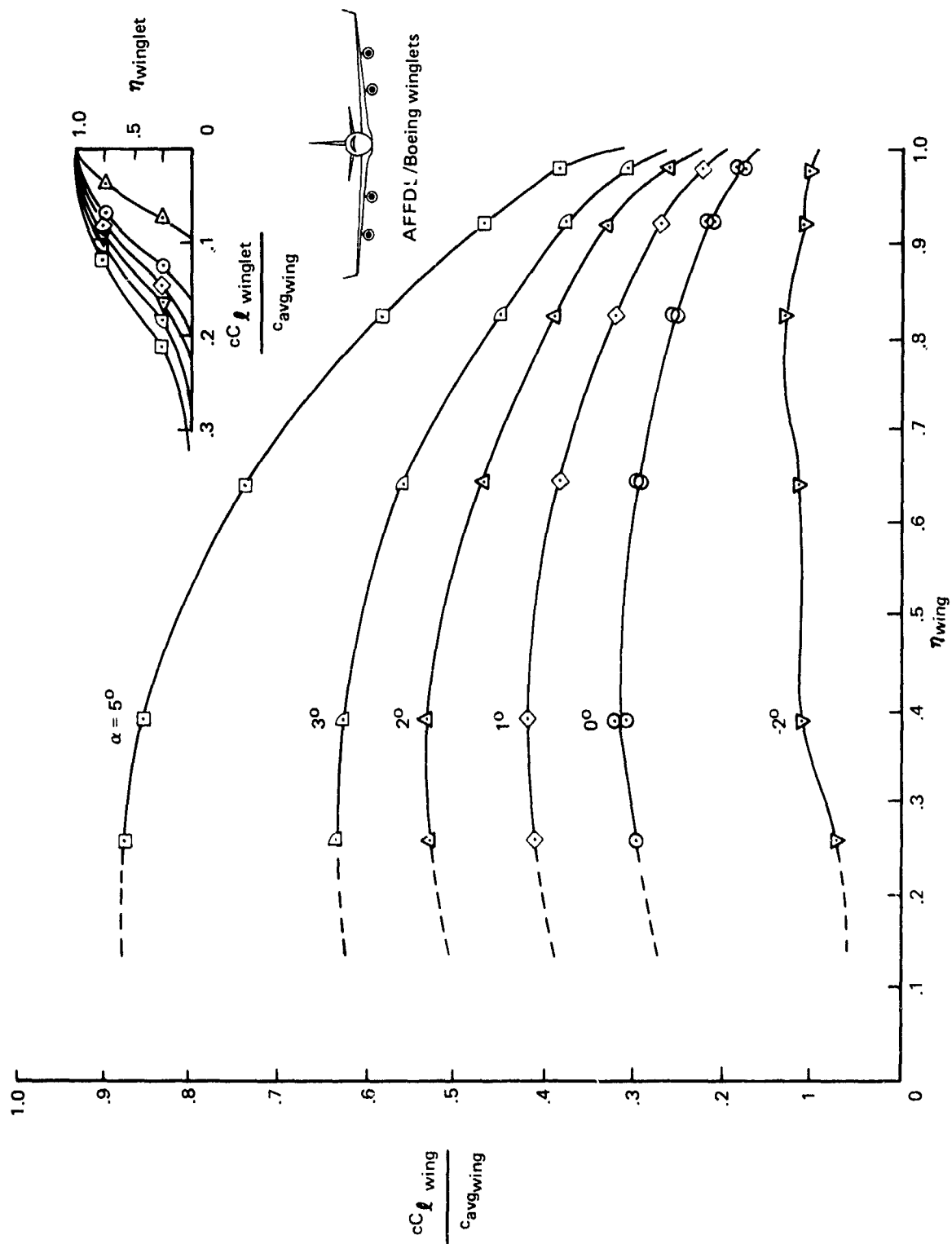
Figure 53. – KC-135A With AFFDL/Boeing Winglet Span Load, Mach 0.70
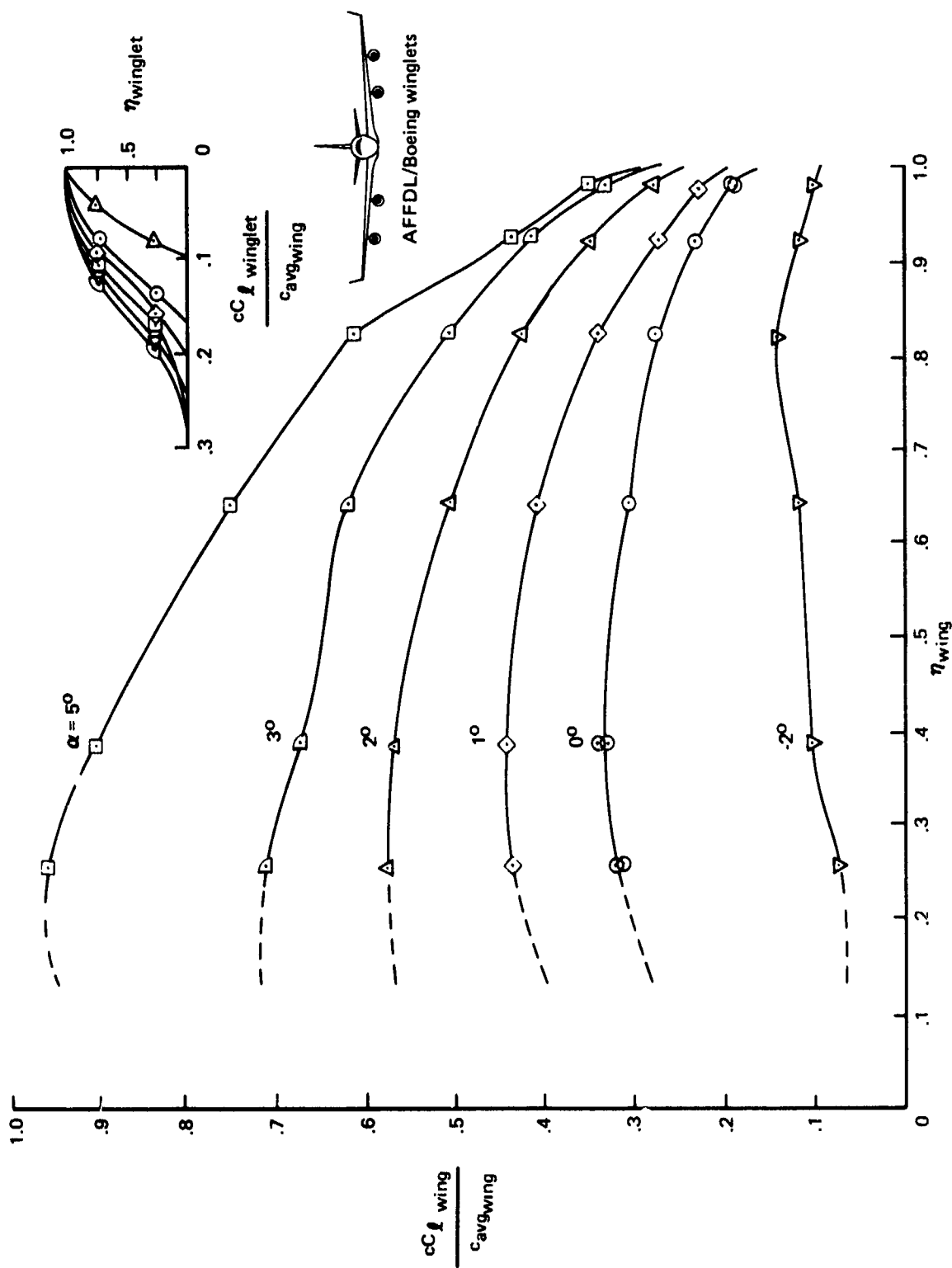
Figure 54. — KC-135A With AFFDL/Boeing Winglet Span Load, Mach 0.78

77
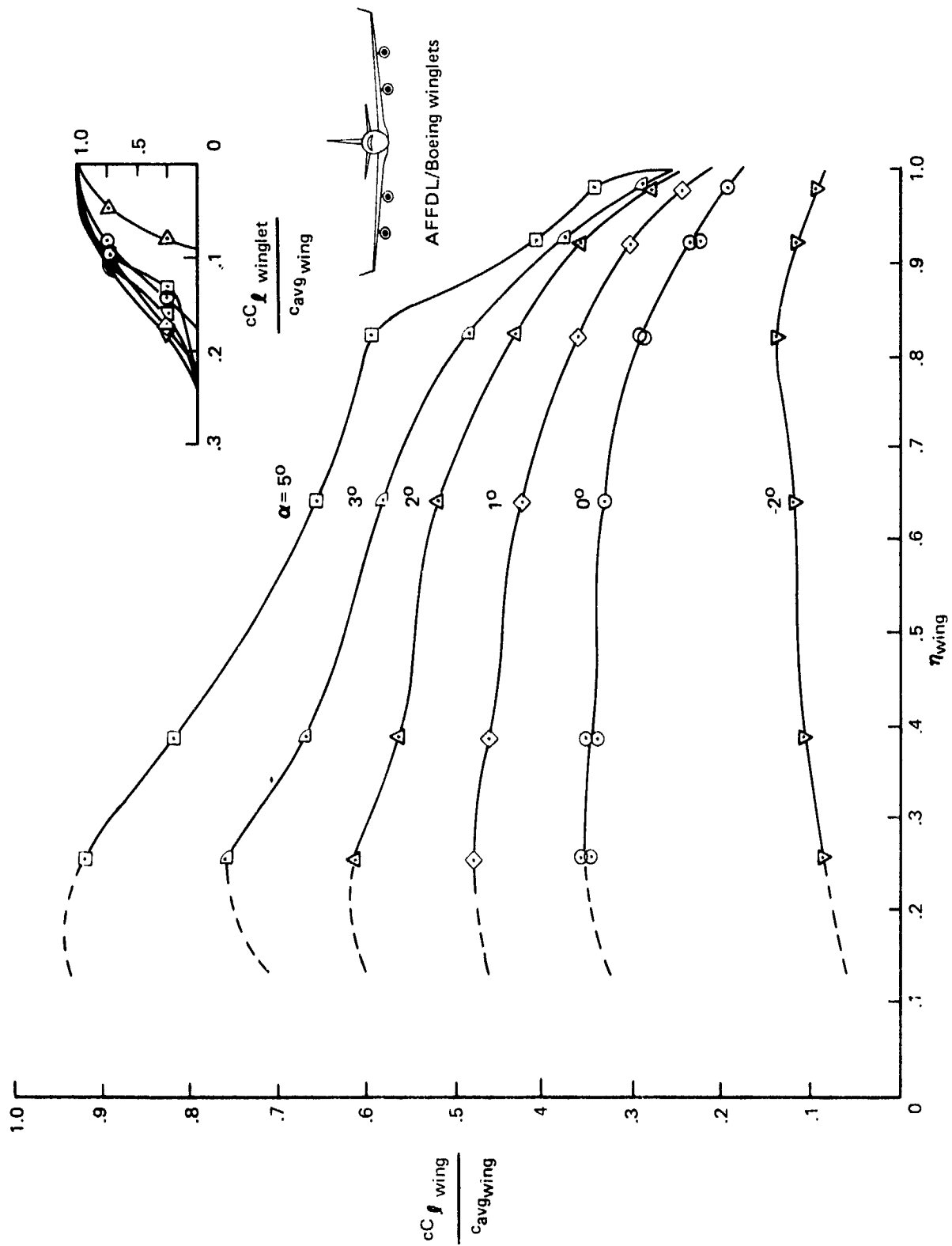
Figure 55. — KC-135A With AFFDL/Boeing Winglet Span Load, Mach 0.82

78
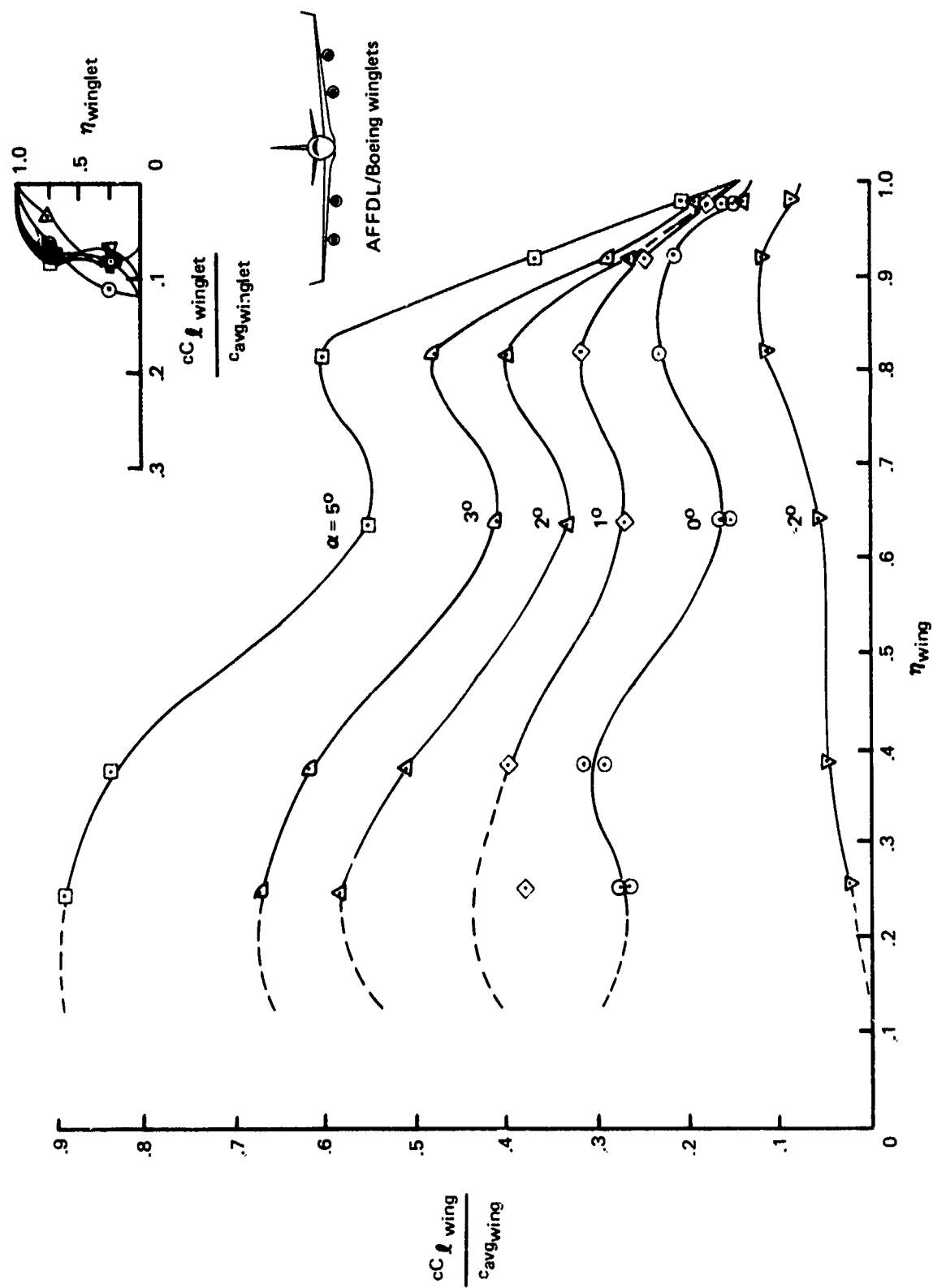
Figure 56. – KC-135A With AFFDL/Boeing Winglet Span Load, Mach 0.90

79
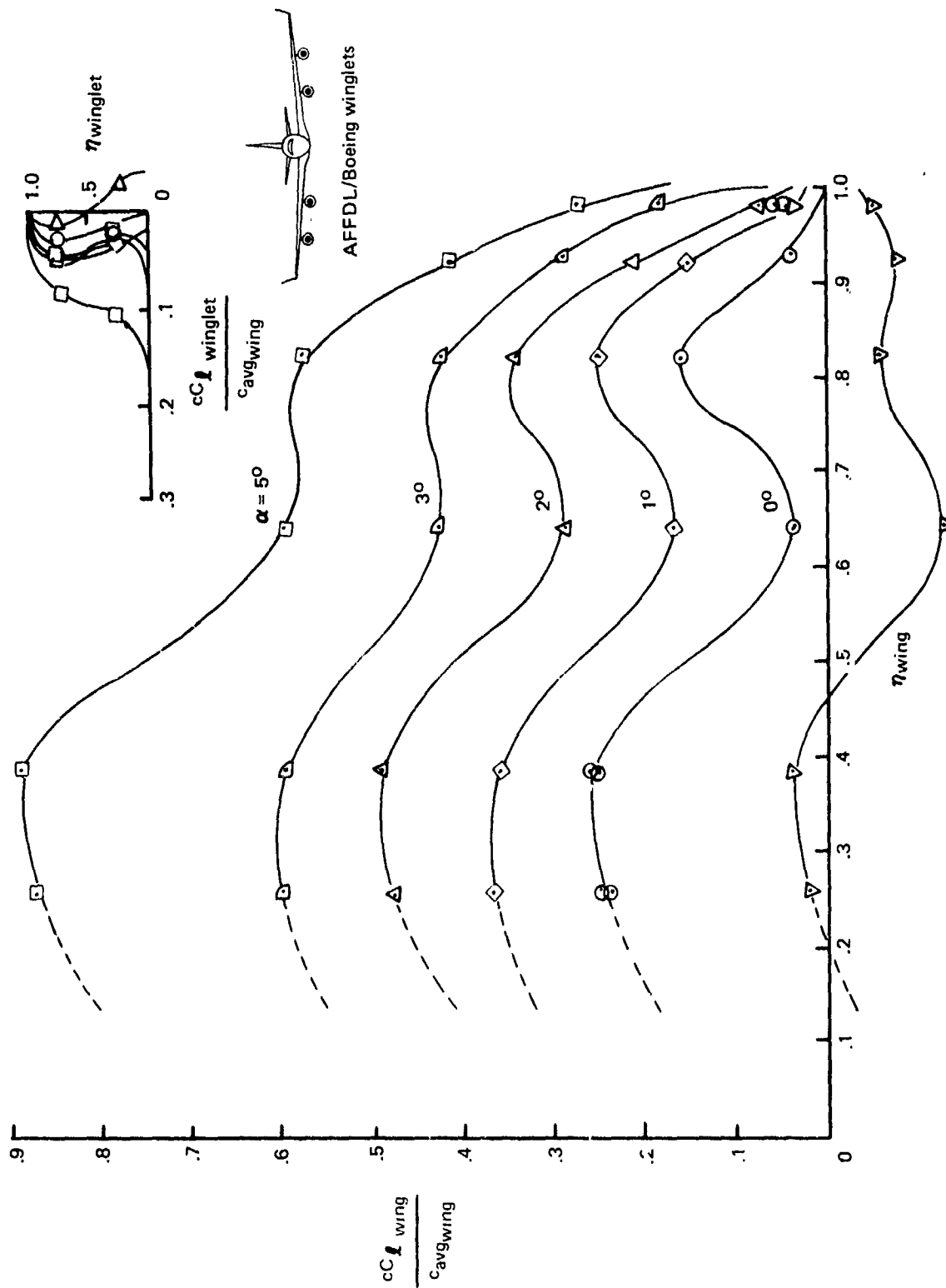
Figure 57. – KC-135A With AFFDL/Boeing Winglet Span Load, Mach 0.95
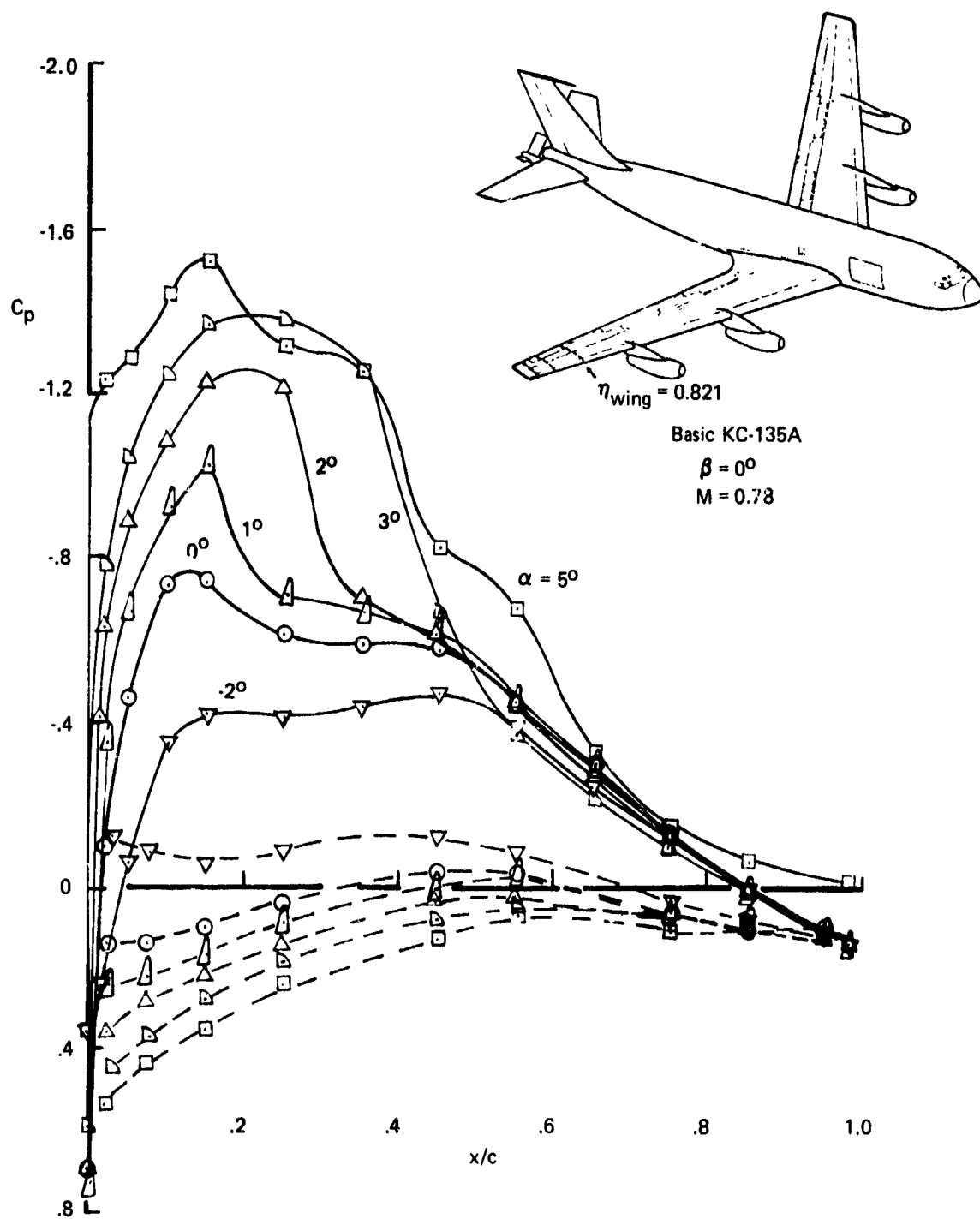
Figure 58. — Basic KC-135A Chordwise Pressures, $\eta_{wing} = 0.821$

81
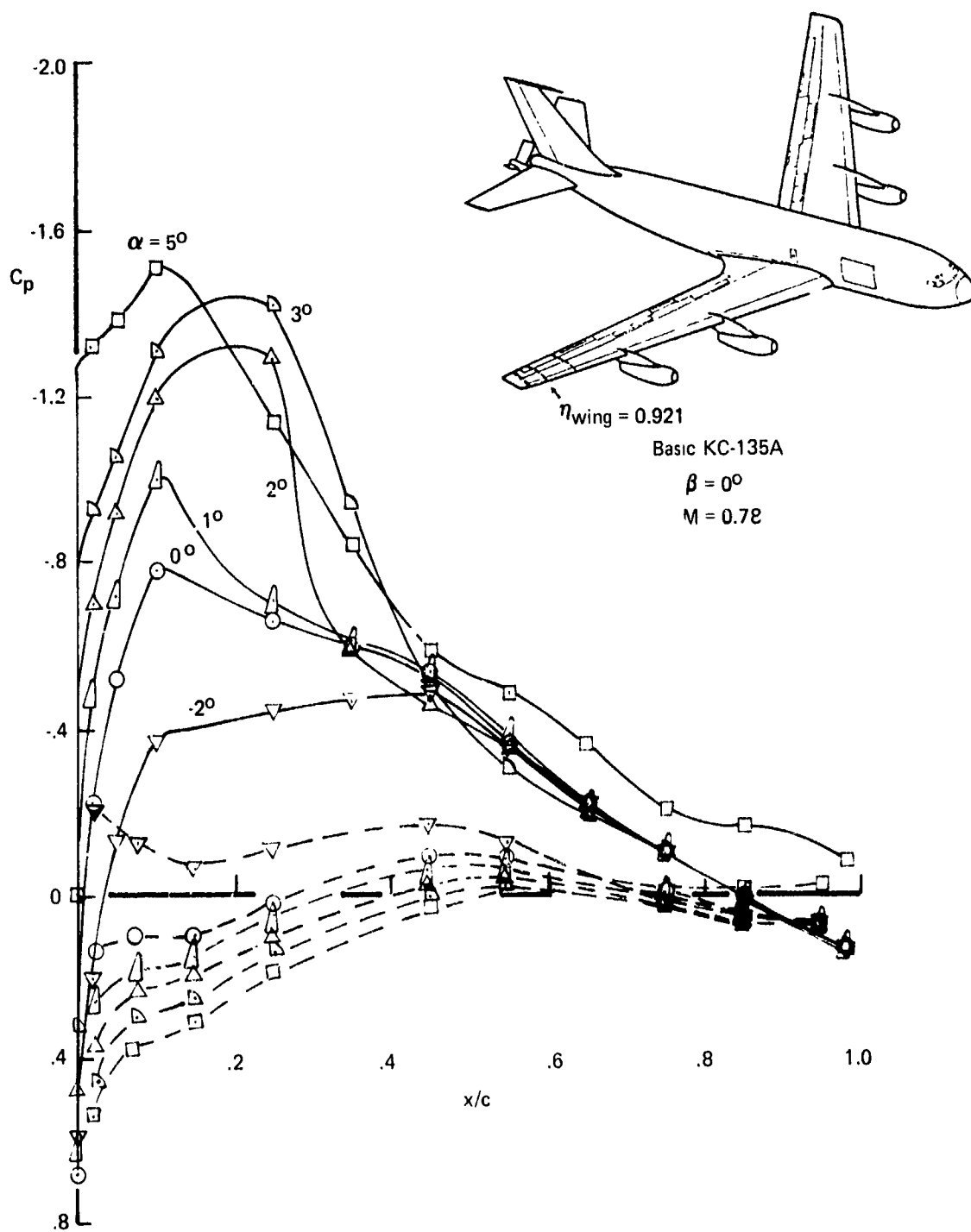
Figure 59. — Basic KC-135A Chordwise Pressures, $\eta_{wing} = 0.921$
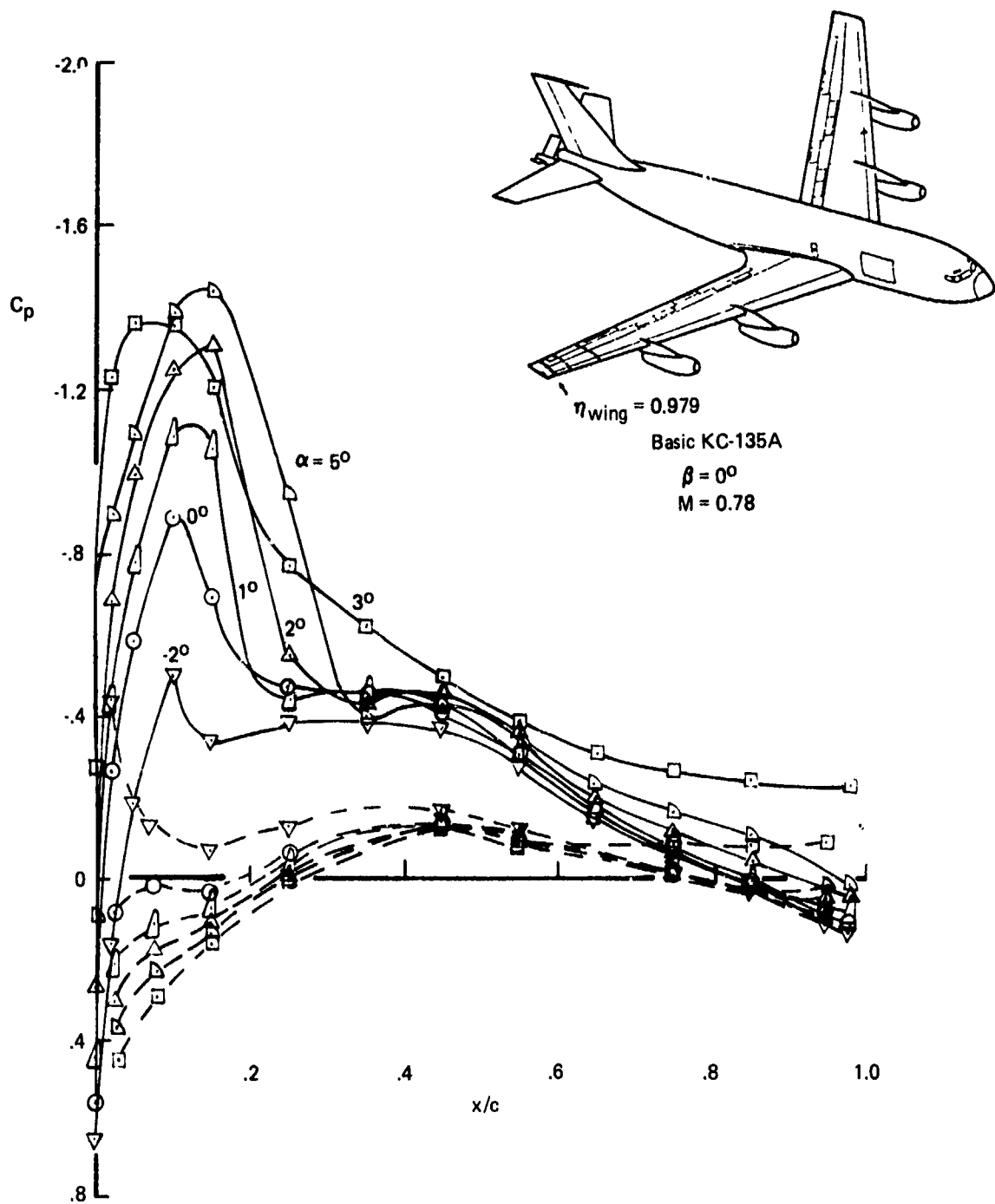
Figure 60. — Basic KC-135A Chordwise Pressures, $\eta_{wing} = 0.979$
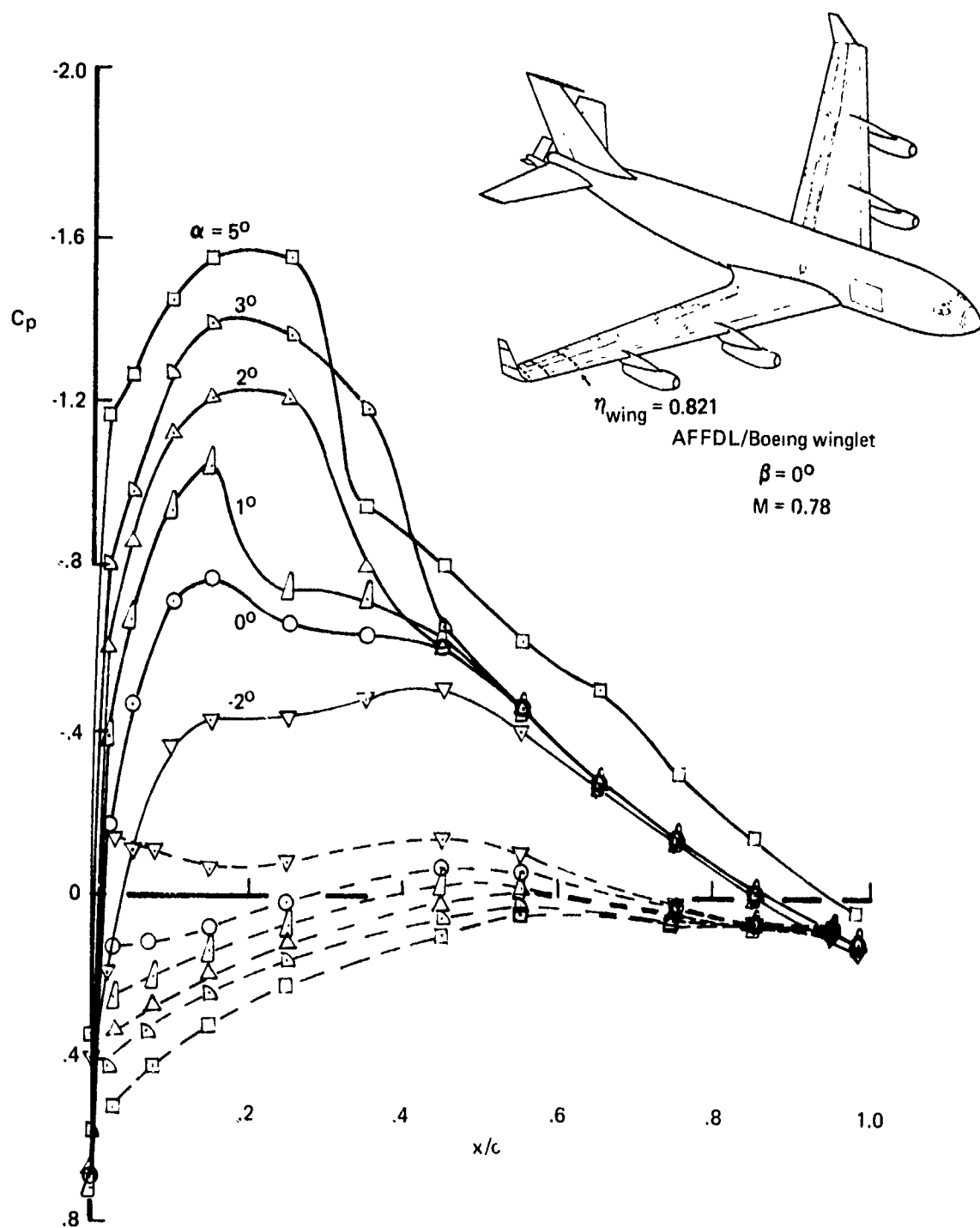
Figure 61. — KC-135A With AFFDL/Boeing Winglet Chordwise Pressures, η_{wing} = 0.821
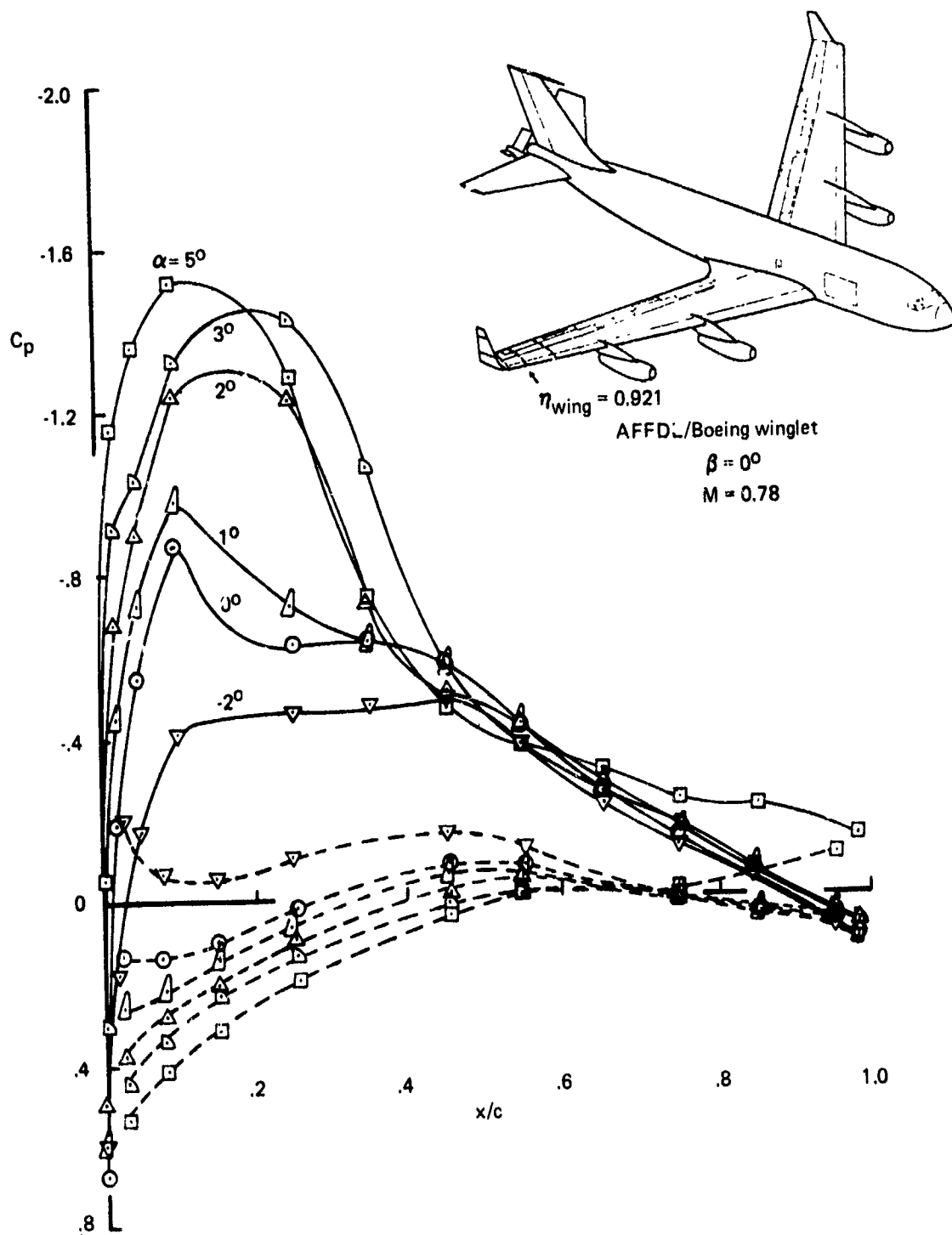
Figure 62. — *KC-135A With AFFDL/Boeing Winglet Chordwise Pressures,* $\eta_{wing} = 0.921$
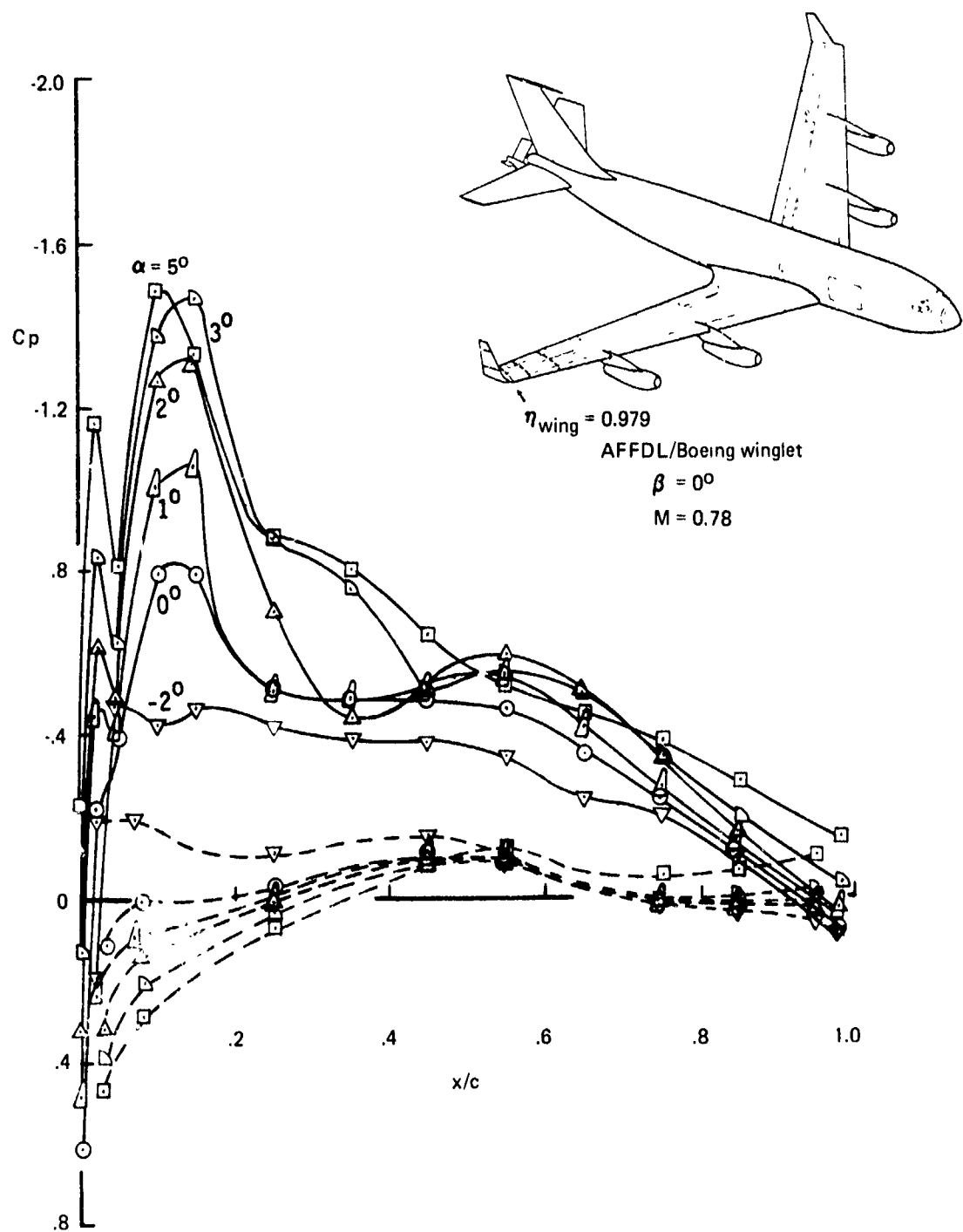
Figure 63. — KC-135A With AFFDL/Boeing Winglet Chordwise Pressures, $\eta_{wing} = 0.979$
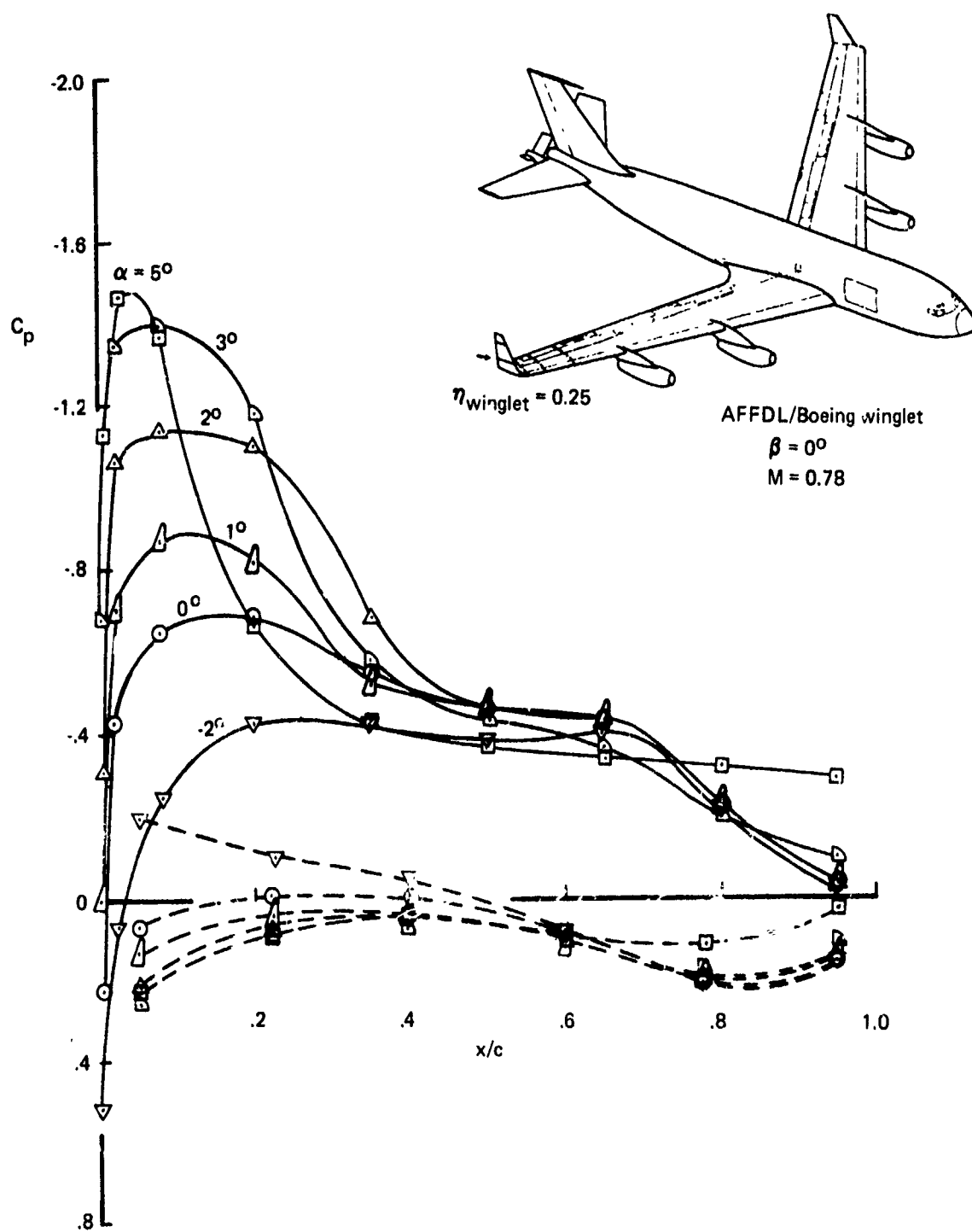
Figure 64. — KC-135A With AFFDL/Boeing Winglet Chordwise Pressures, $\eta_{winglet} = 0.25$
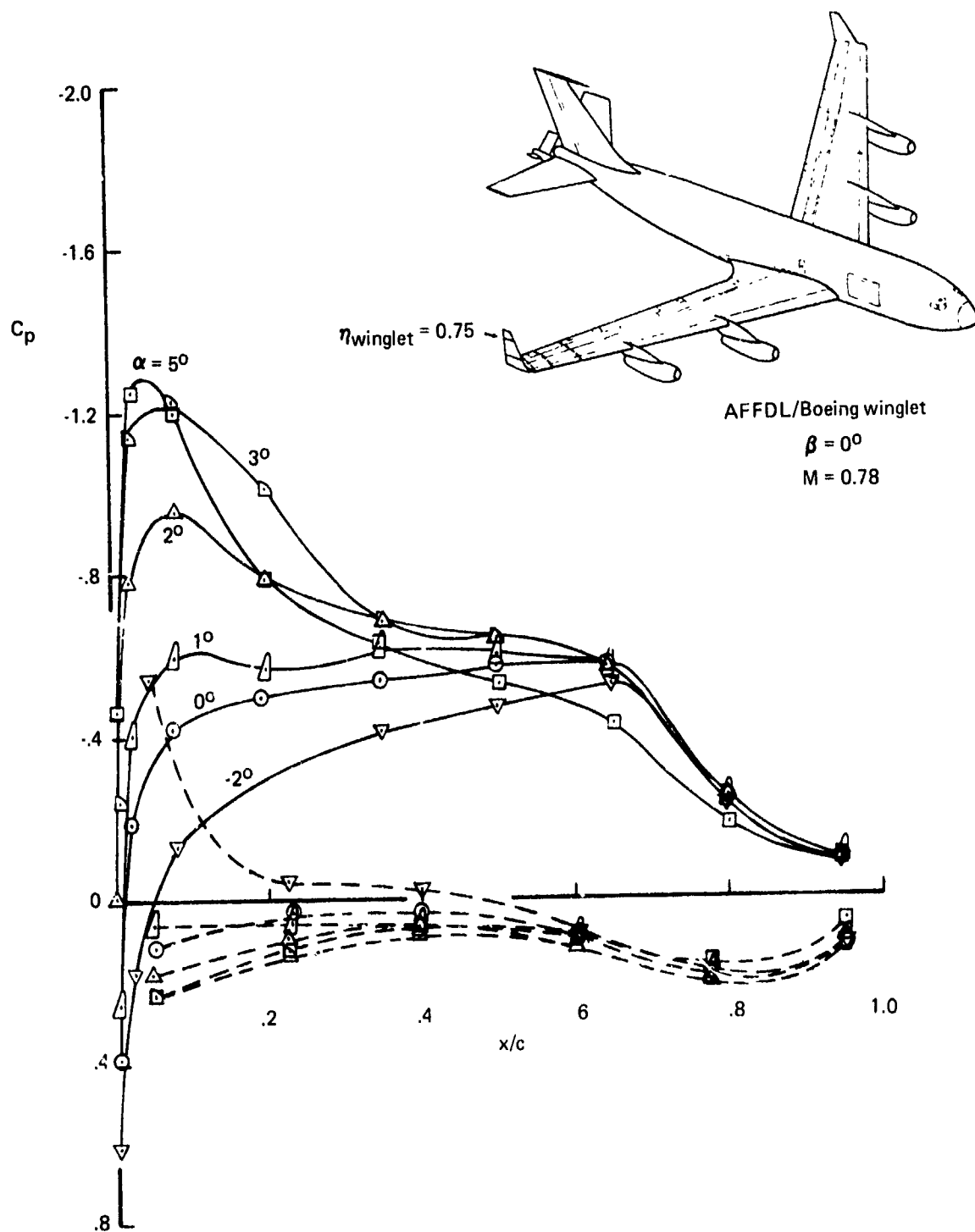
Figure 65. – KC-135A With AFFDL/Boeing Winglet Chordwise Pressures, $\eta_{winglet} = 0.75$
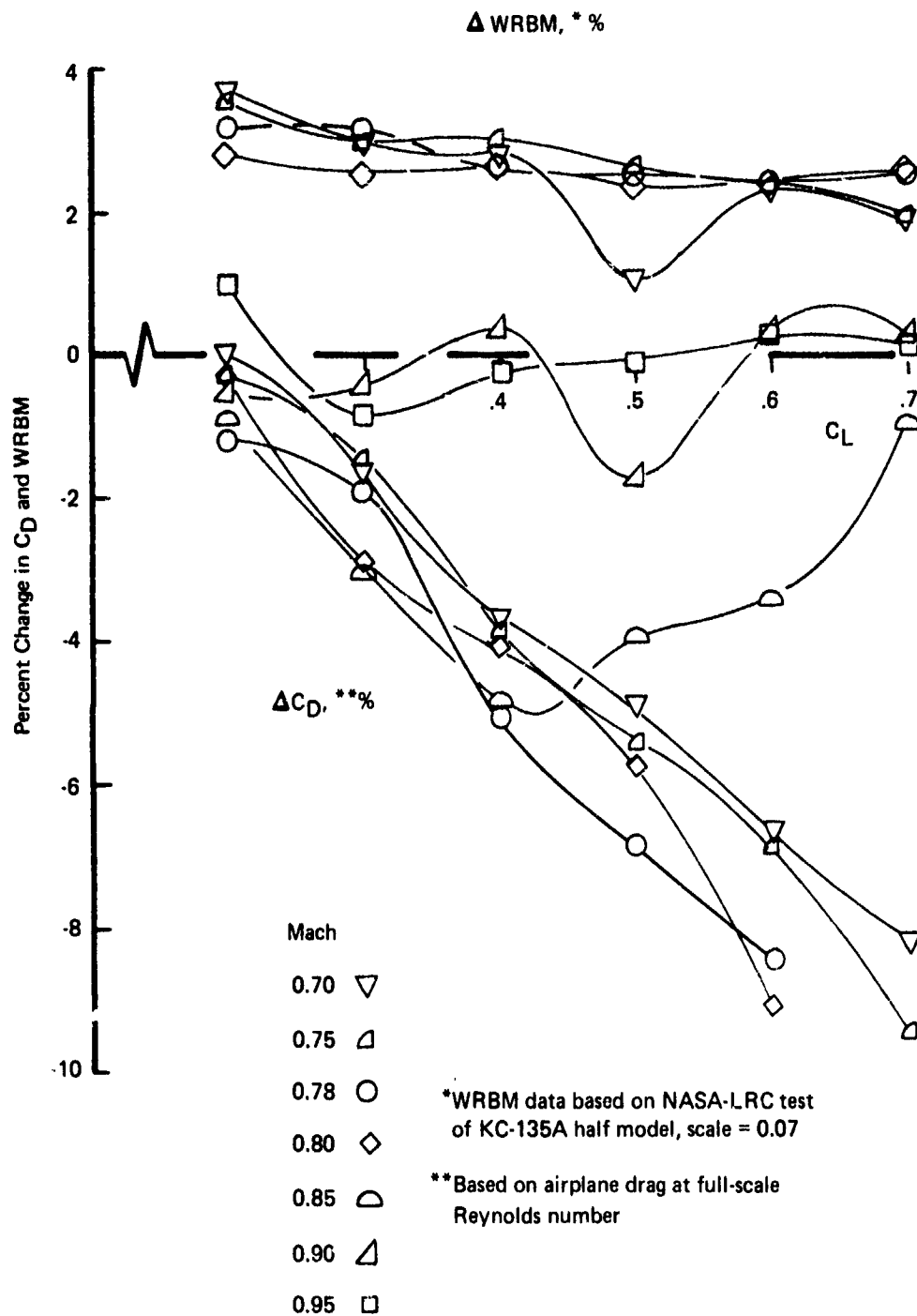
Figure 66. — Effect of AFFDL/Boeing Winglets on KC-135A Aerodynamic Performance
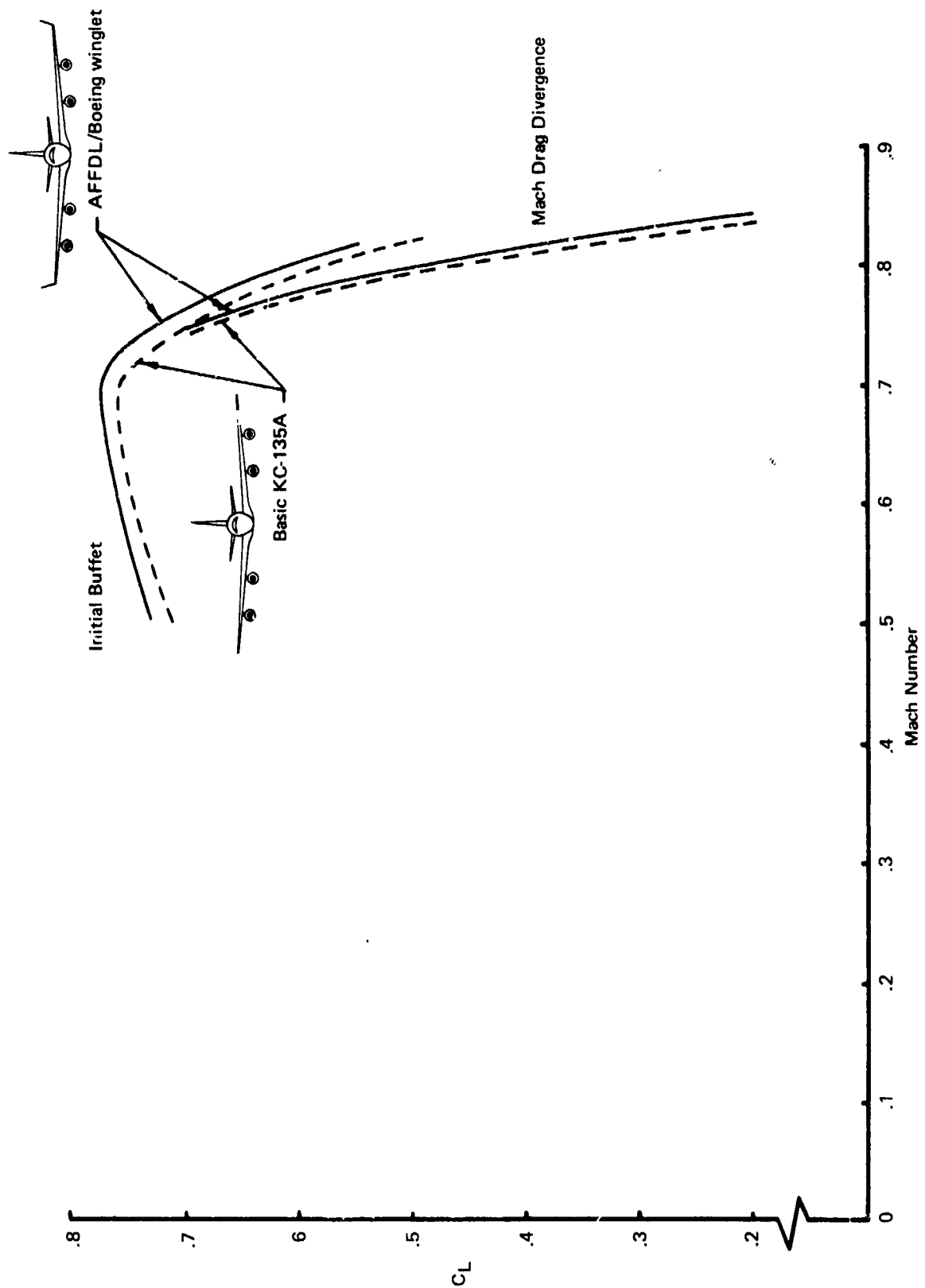
Figure 67. — *Effect of AFFDL/Boeing Winglets on KC-135A Initial Buffet and Drag Divergence Boundaries*
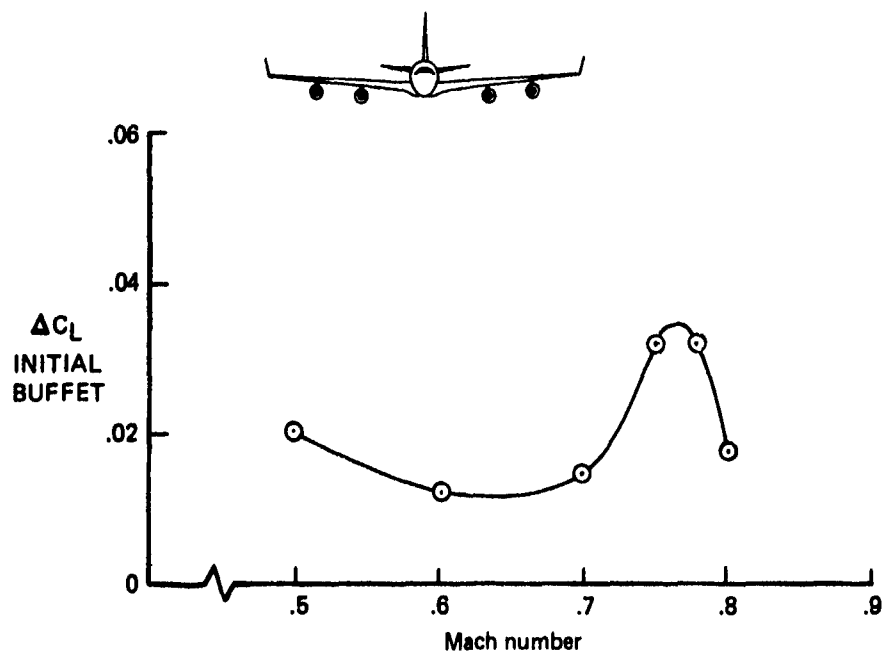
a. Effect of Winglets on Initial Buffet Boundary
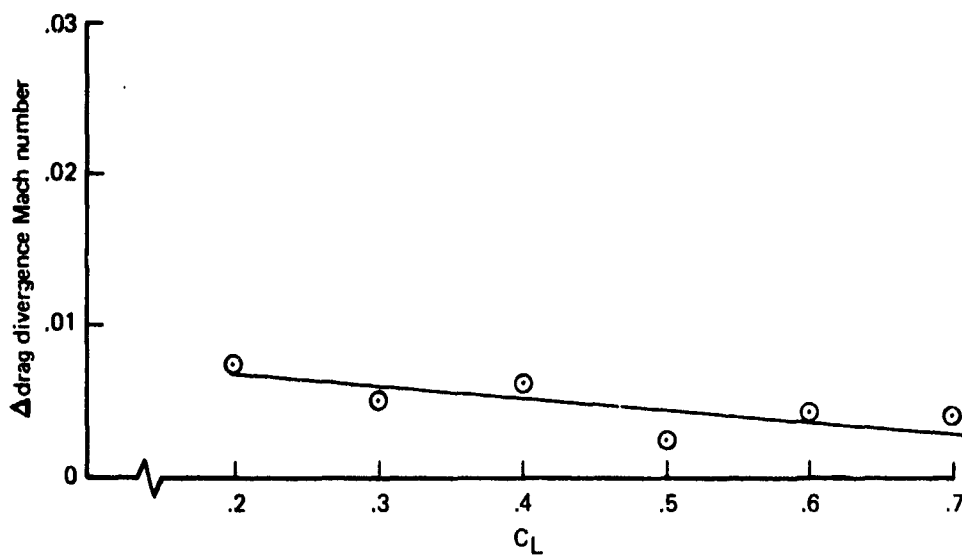
b. Effect of Winglets on Drag Divergence Mach Number

Figure 68. — Change of KC-135A High-Speed Boundaries
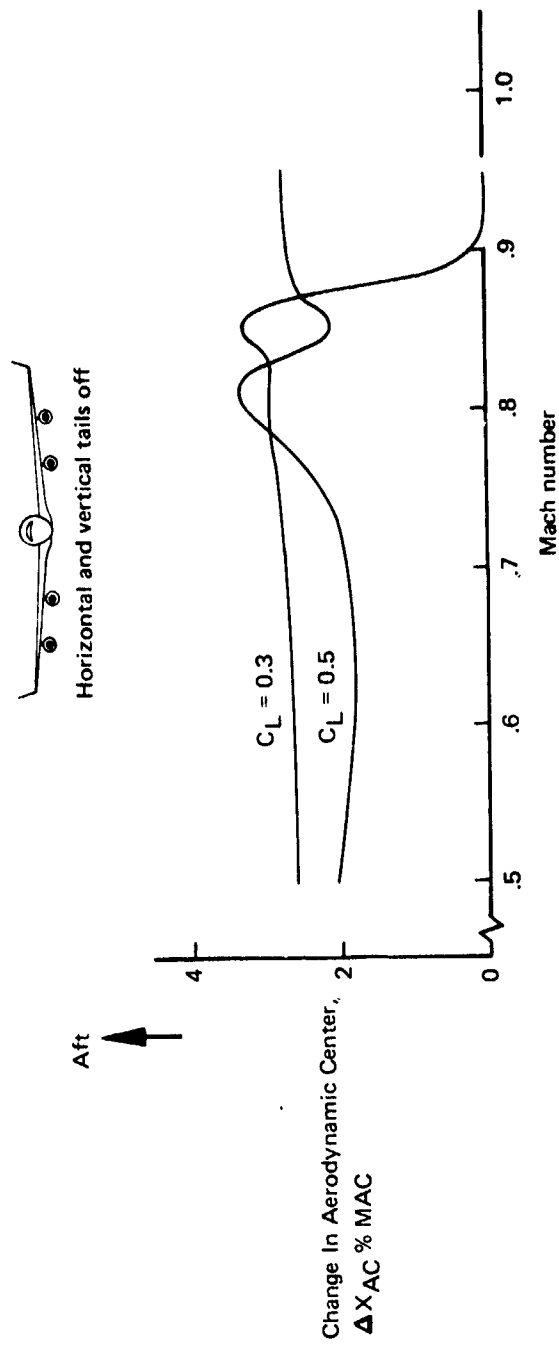
Figure 69. – Effect of AFFDL/Boeing Winglets on KC-135A Wing-Body Aerodynamic Center
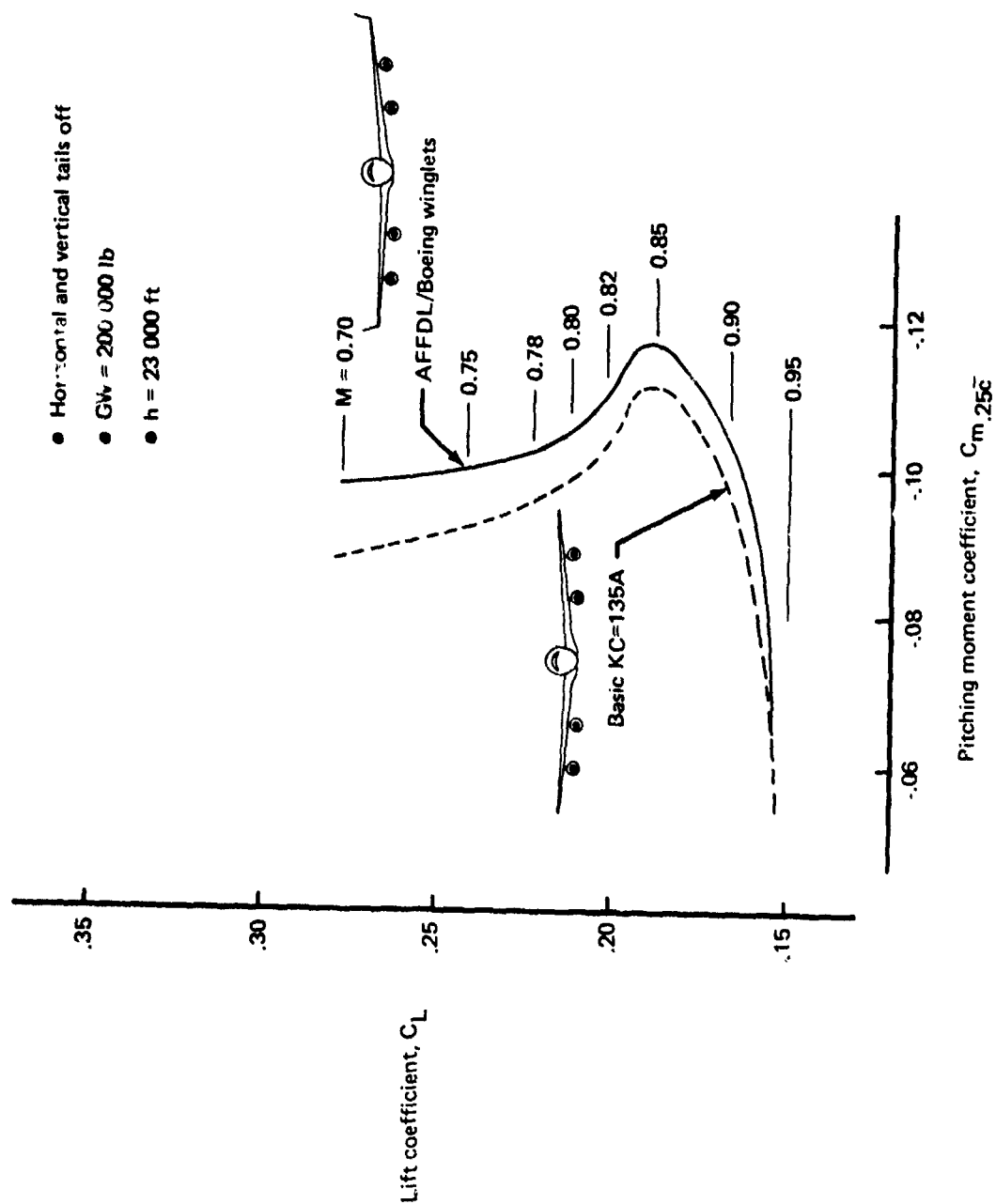
Figure 70. — Effect of AFFDL/Boeing Winglets on KC-135A High-Speed Longitudinal Stability
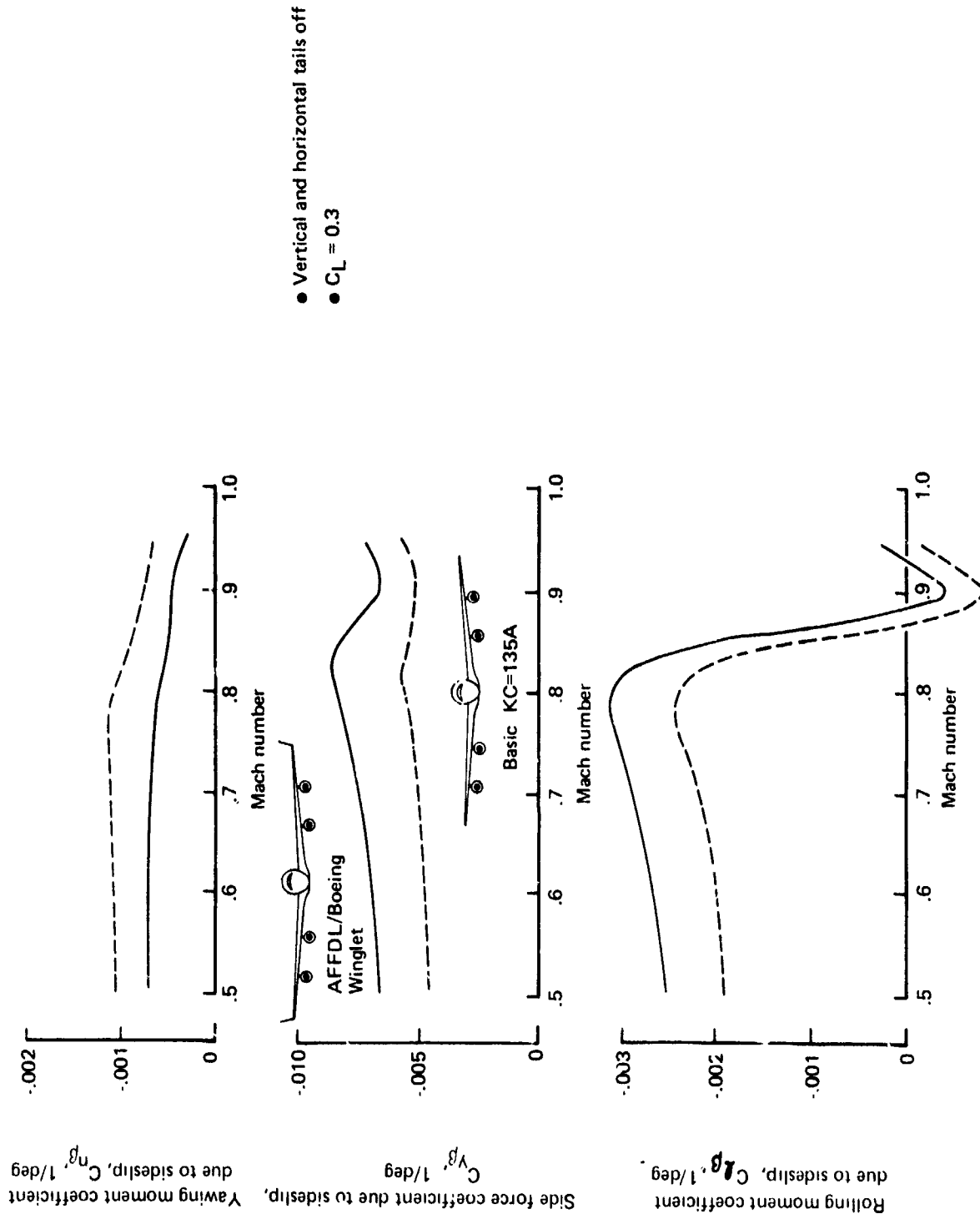
Figure 71. — Effect of AFFDL/Boeing Winglets on KC-135A Static Lateral-Directional Stability, Tail Off
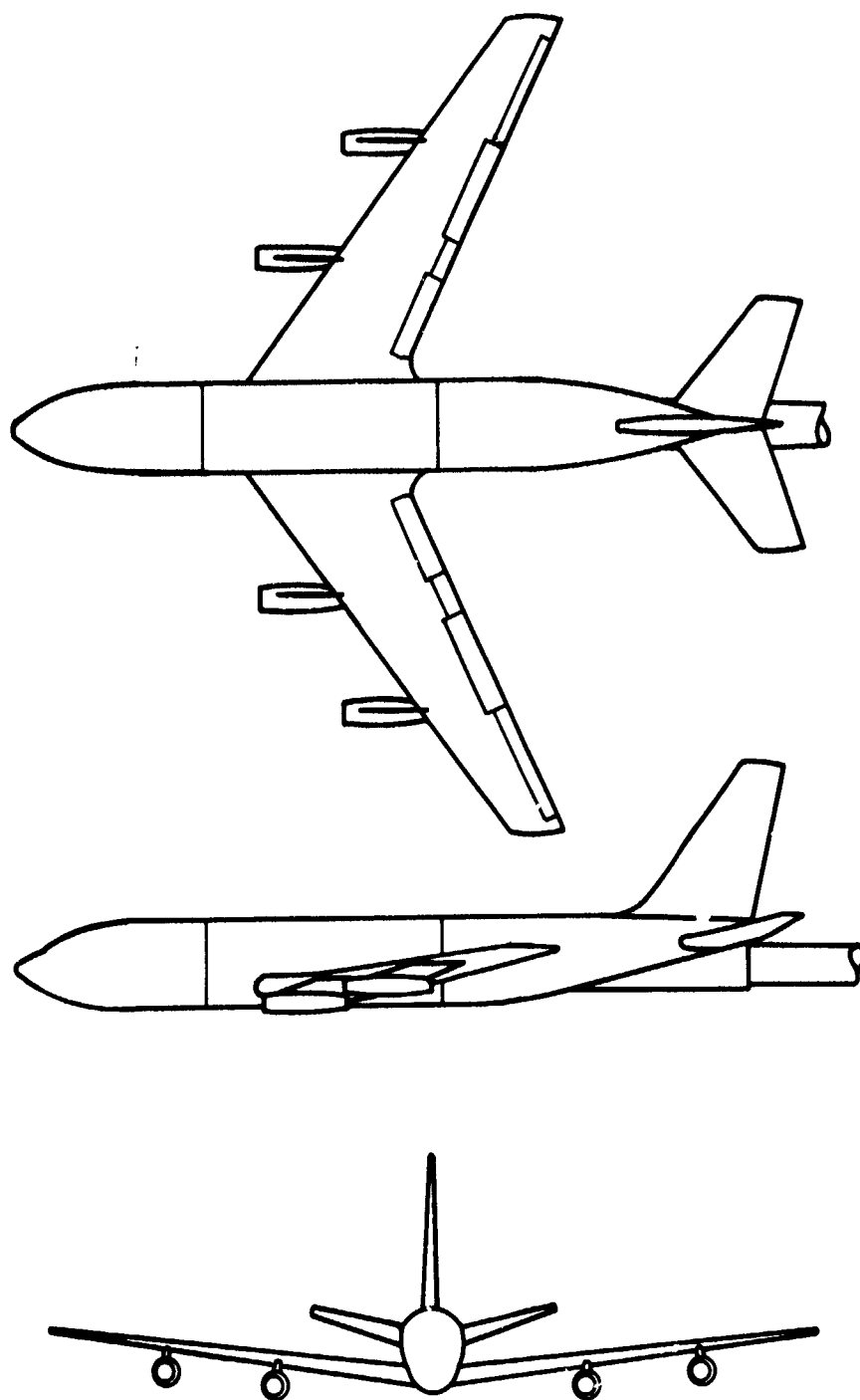
- Vertical and horizontal tails off
- $C_L = 0.3$

Yawing moment coefficient due to sideslip, C_{n_β}, 1/deg

Side force coefficient due to sideslip, C_{y_β}, 1/deg

Rolling moment coefficient due to sideslip, C_{l_β}, 1/deg

AFFDL/Boeing Winglet

Basic KC-135A

Mach number

94

Figure 72. — 0.035 Scale Model of KC-135A, FR-174I
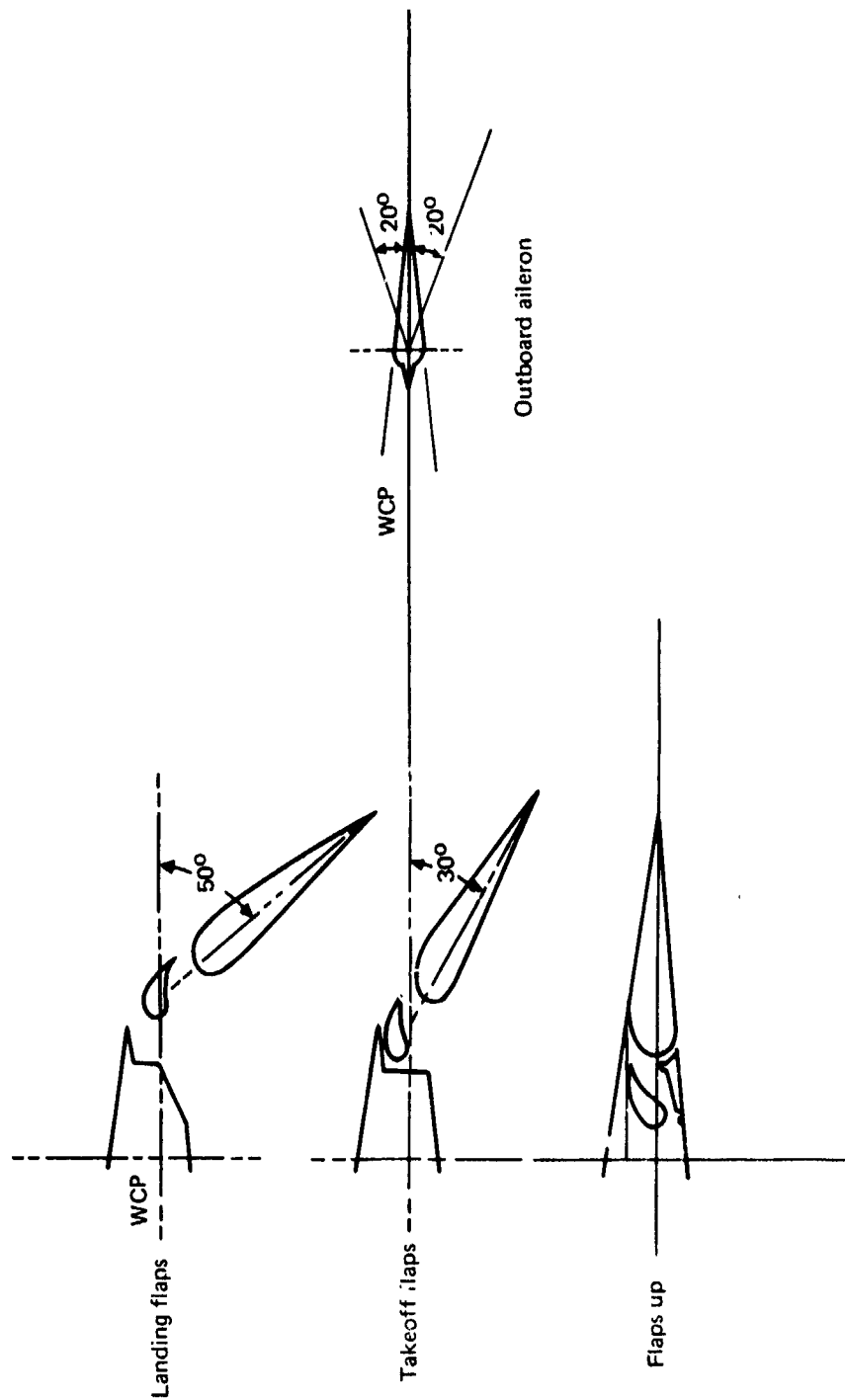
Figure 73. — KC-135A Model Wing Flap and Aileron Cross Section

KC-135A jet tanker
$\delta_A = 0°$, $\delta_H = -10°$
$M_\infty = 0.30$, Reynolds number $\approx 3.7 \times 10^6$

AFFDL/Boeing winglets

Basic KC-135A

$\delta_F = 30°$

$\delta_F = 50°$
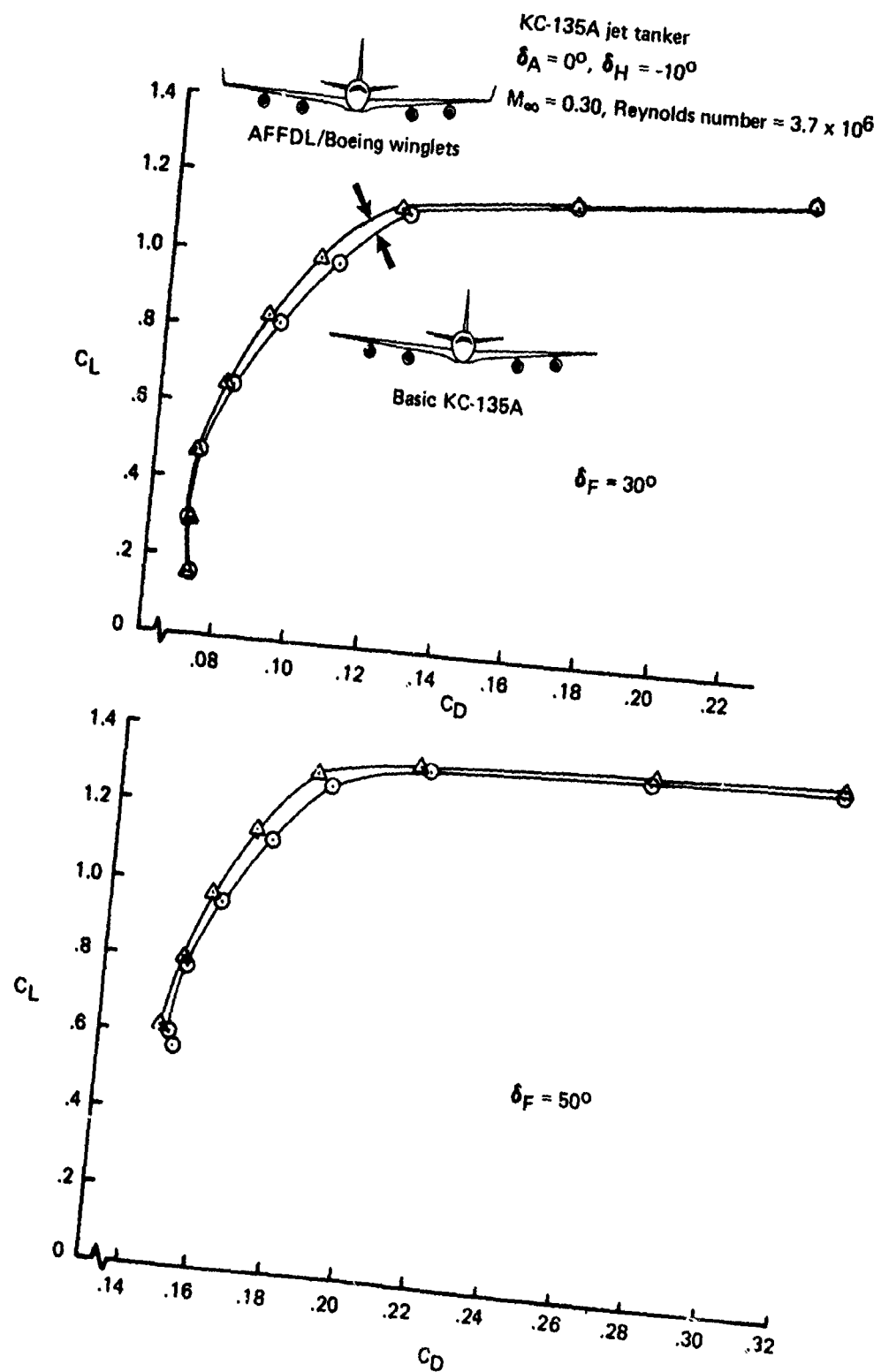
Figure 74. — Low-Speed Drag Polar Comparisons of KC-135A With and Without AFFDL/Boeing Winglets
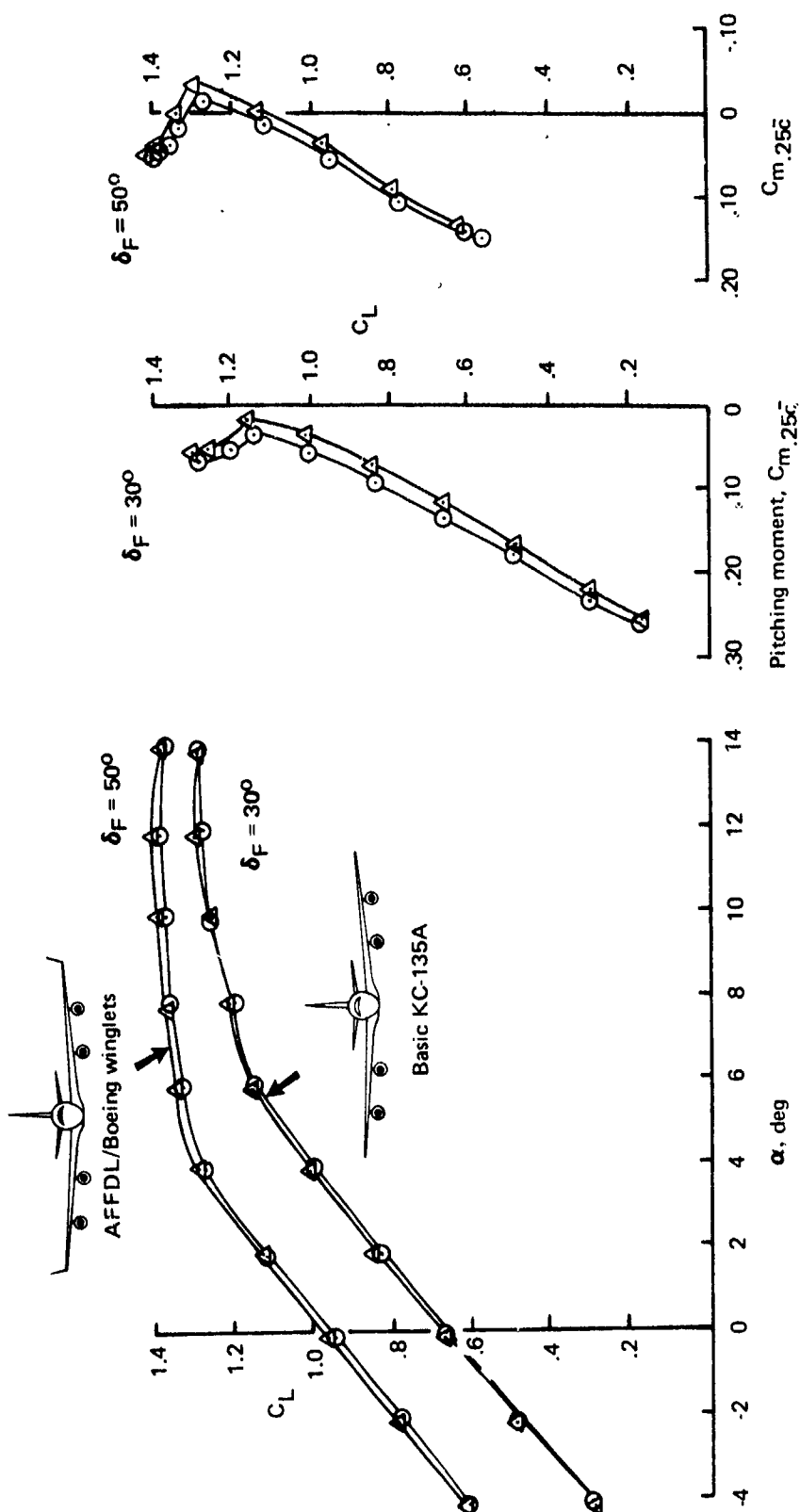
Figure 75. — Low-Speed Lift Curve and Pitching Moment Comparisons of KC-135A With and Without AFFDL/Boeing Winglets
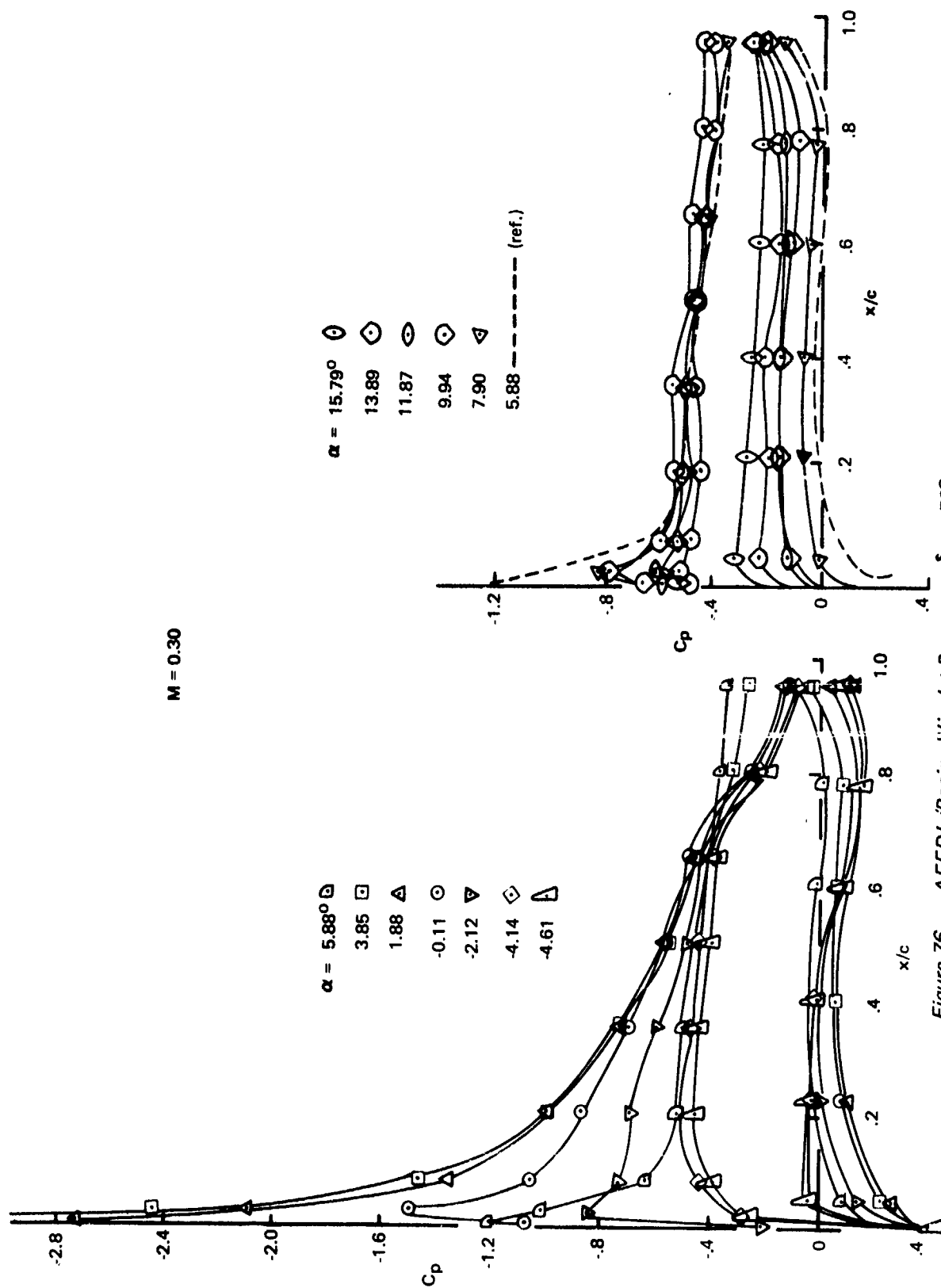
98

M = 0.30

$\alpha = 15.79°$
13.89
11.87
9.94
7.90
5.88 — — — — (ref.)

$\alpha = 5.88°$
3.85
1.88
-0.11
-2.12
-4.14
-4.61

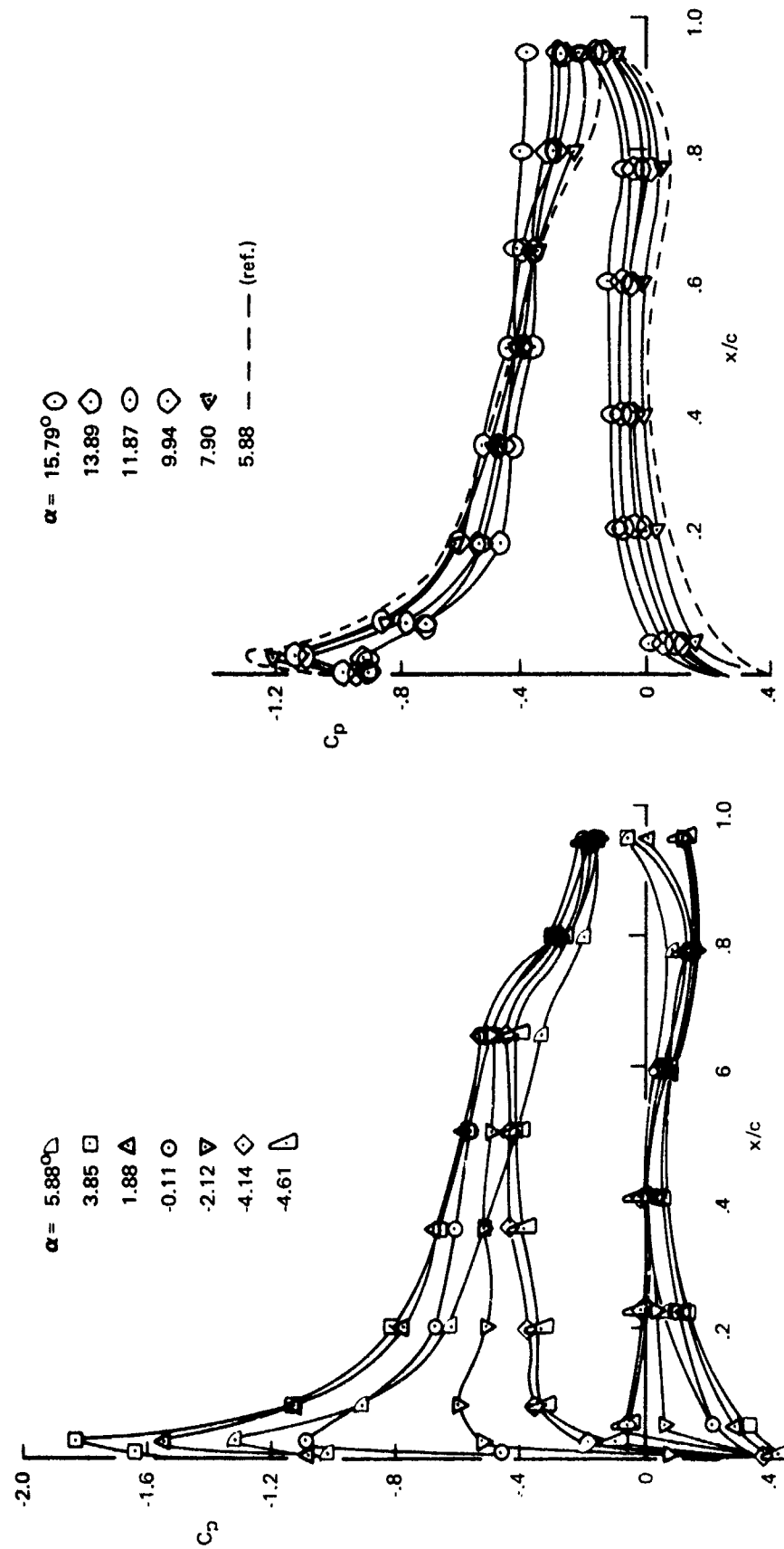Figure 76. — AFFDL/Boeing Winglet Pressures, $\delta_F = 50°$, $\eta_{winglet} = 0.25$

99

Figure 77. – AFFDL/Boeing Winglet Pressures, $\delta_F = 50^o$, $\eta_{winglet} = 0.75$
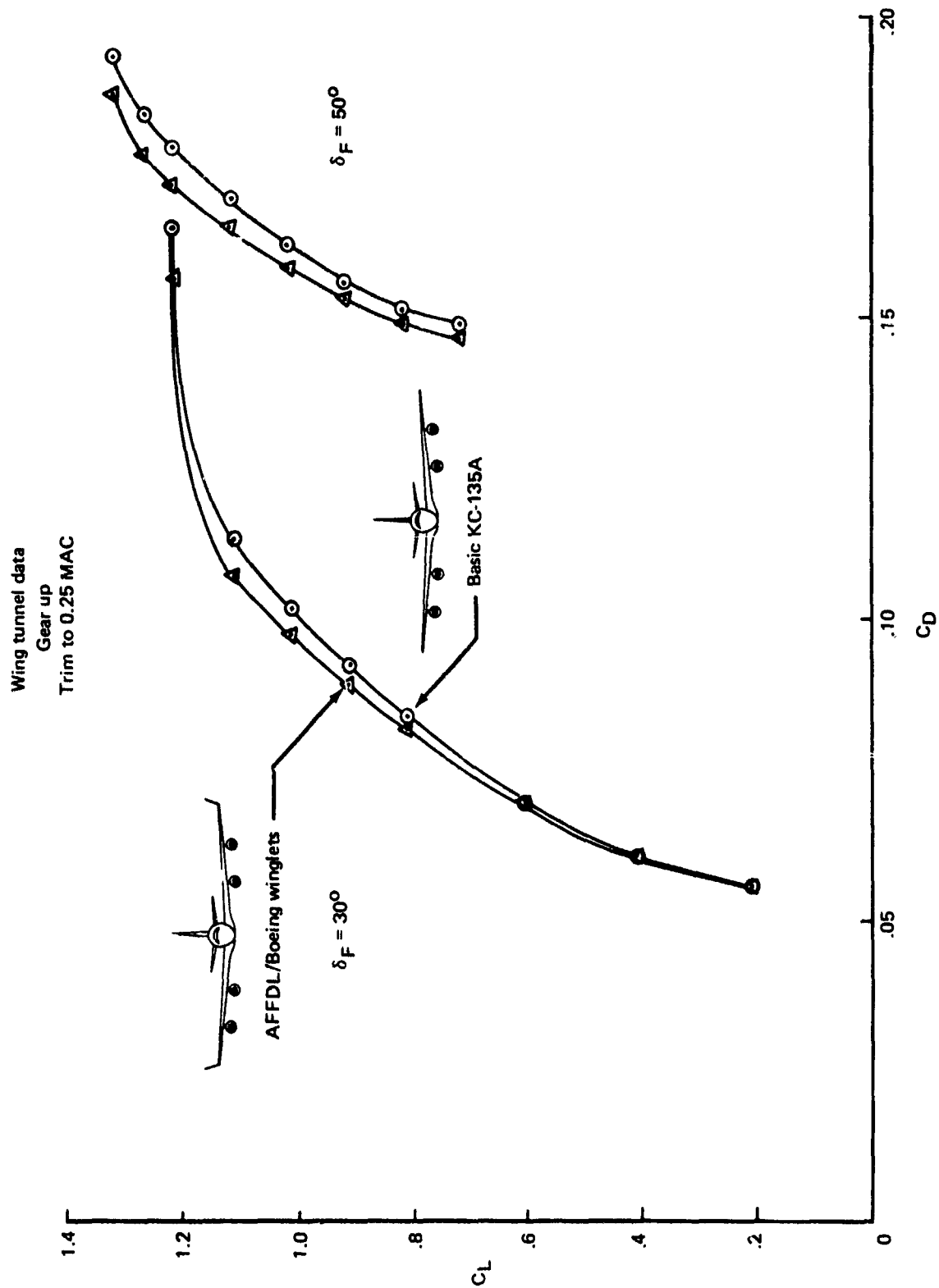
Figure 78. — Low-Speed Trimmed Drag Polar Comparisons of KC-135A With and Without AFFDL/Boeing Winglets
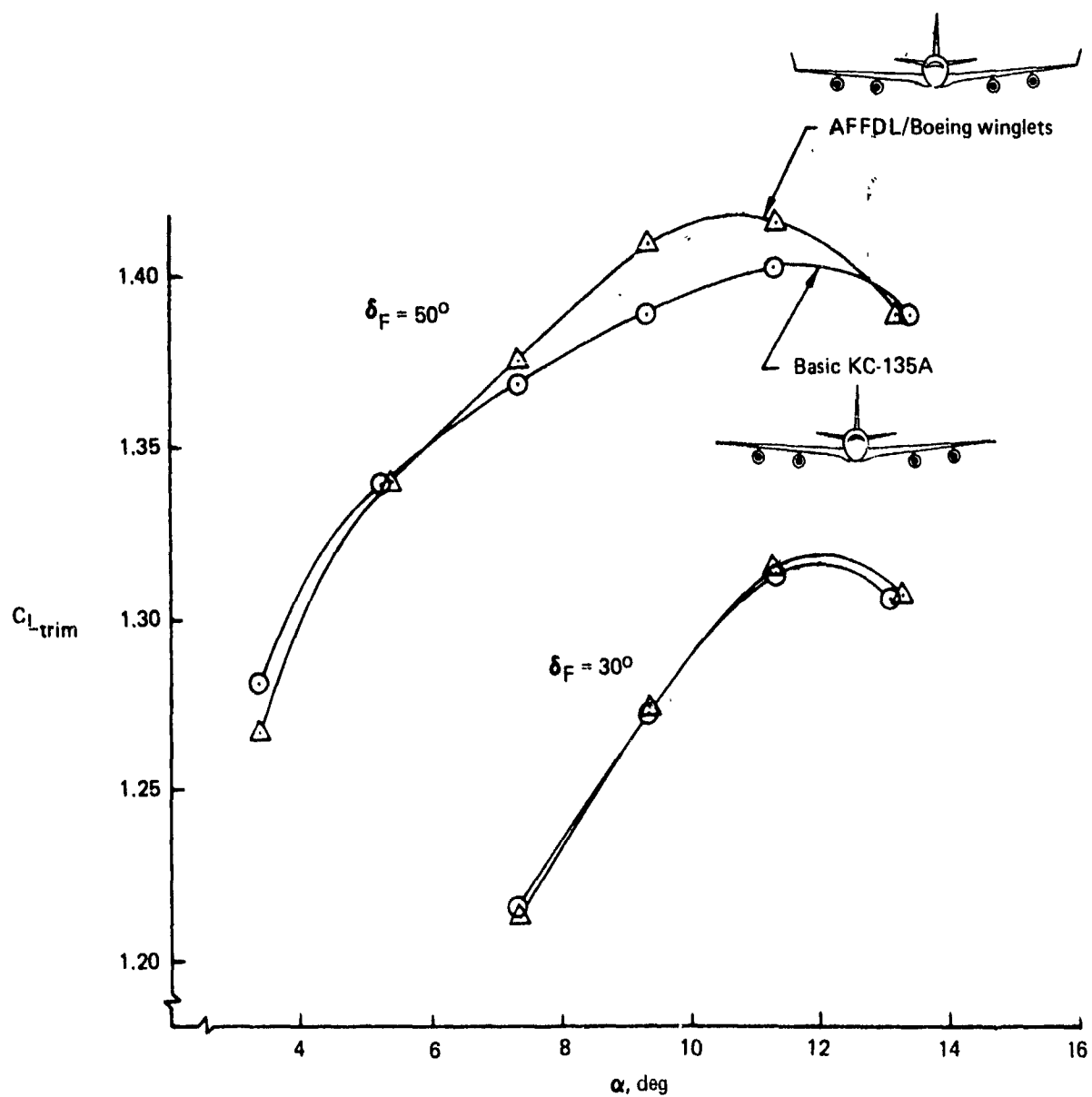
101

Figure 79. — Low-Speed Trimmed Lift Curve Comparisons of KC-135A With and Without
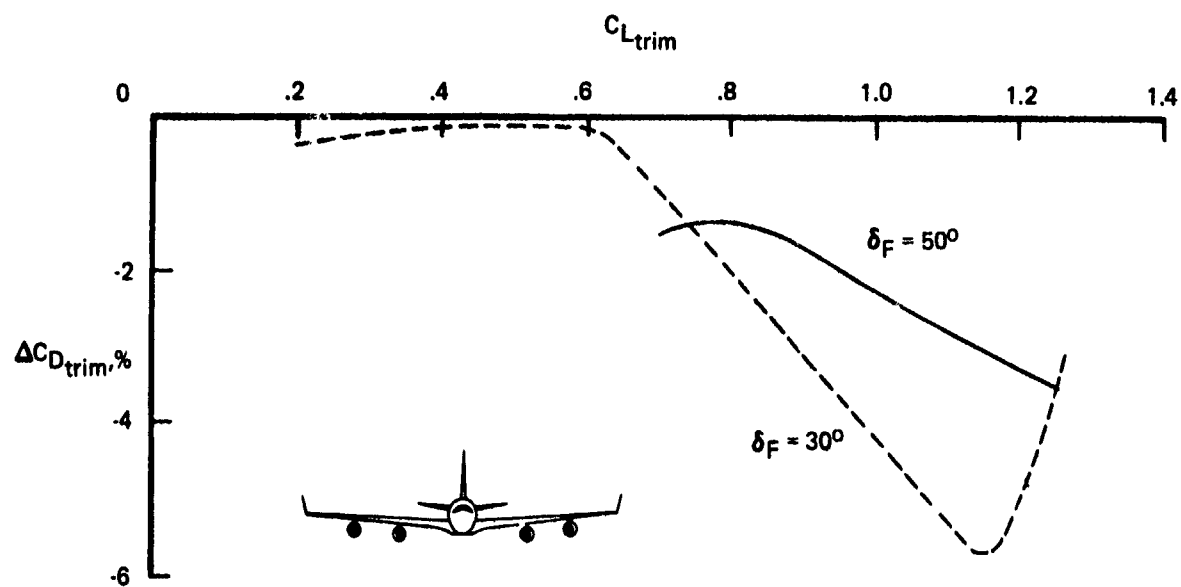AFFDL/Boeing Winglets

Figure 80. — Low-Speed Drag Reduction of KC-135A With AFFDL/Boeing Winglets
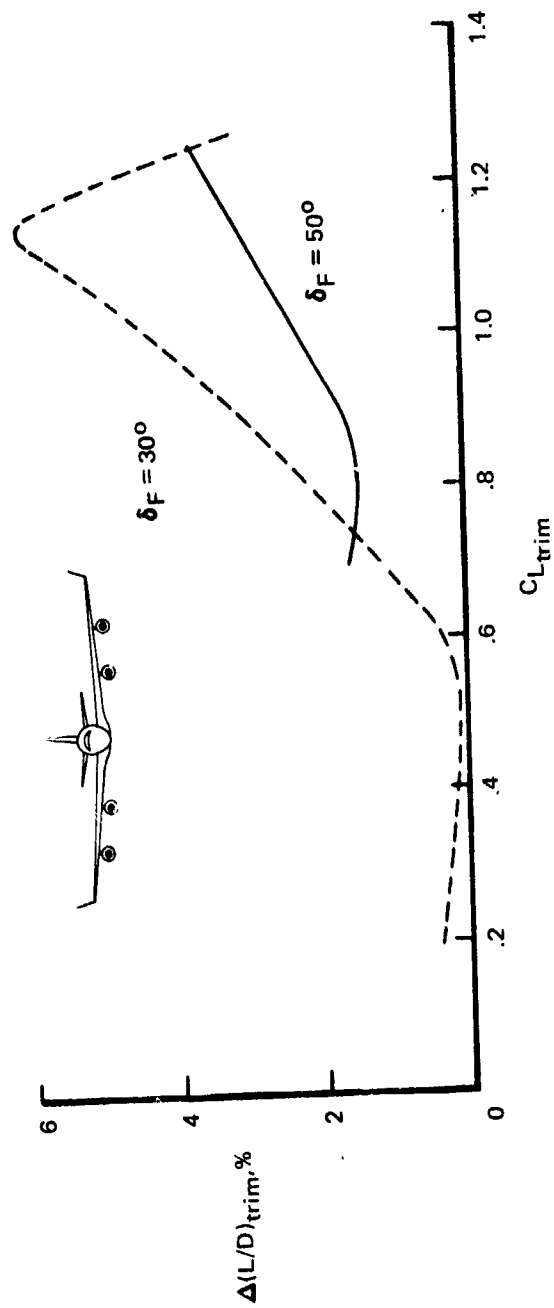
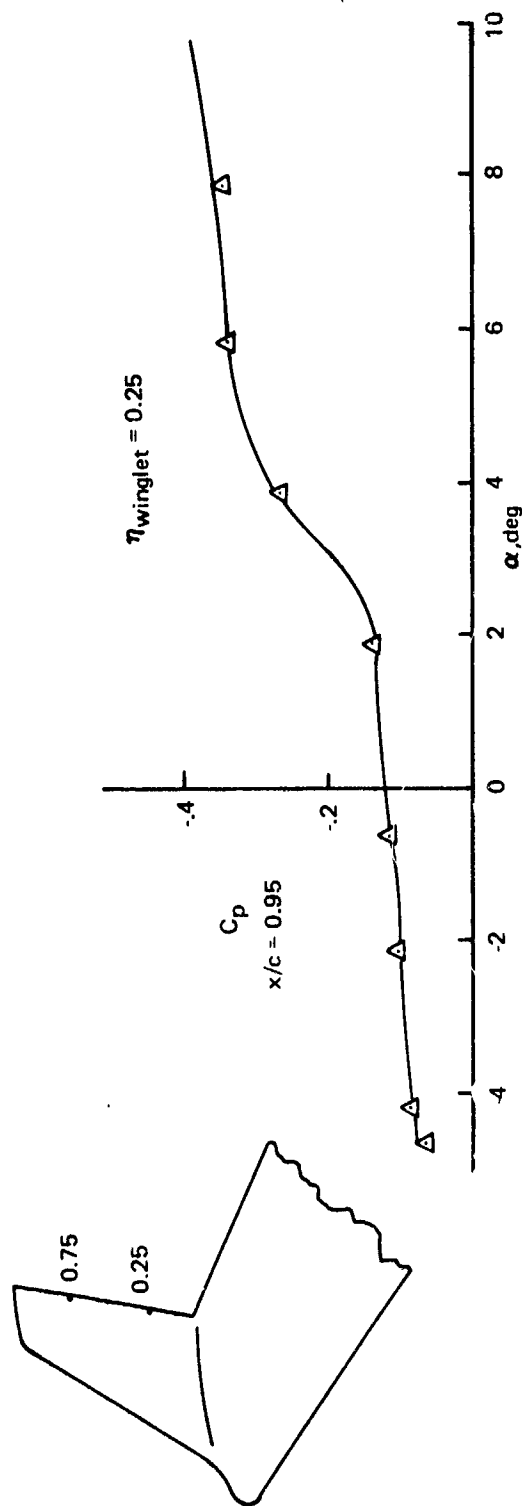Figure 81. — Low-Speed Lift-to-Drag Ratio Increase of KC-135A With AFFDL/Boeing Winglets
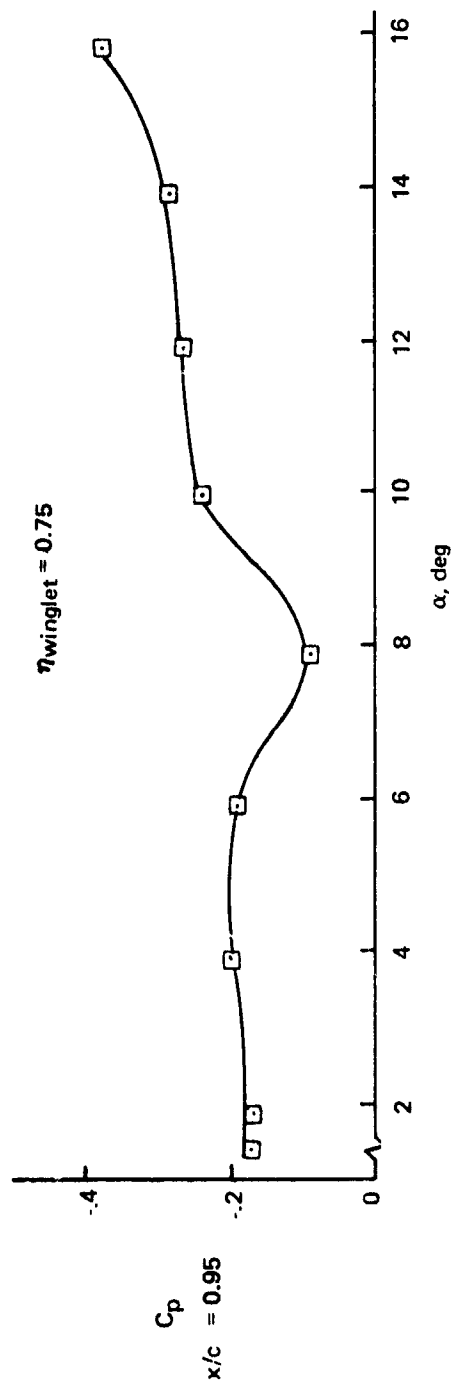
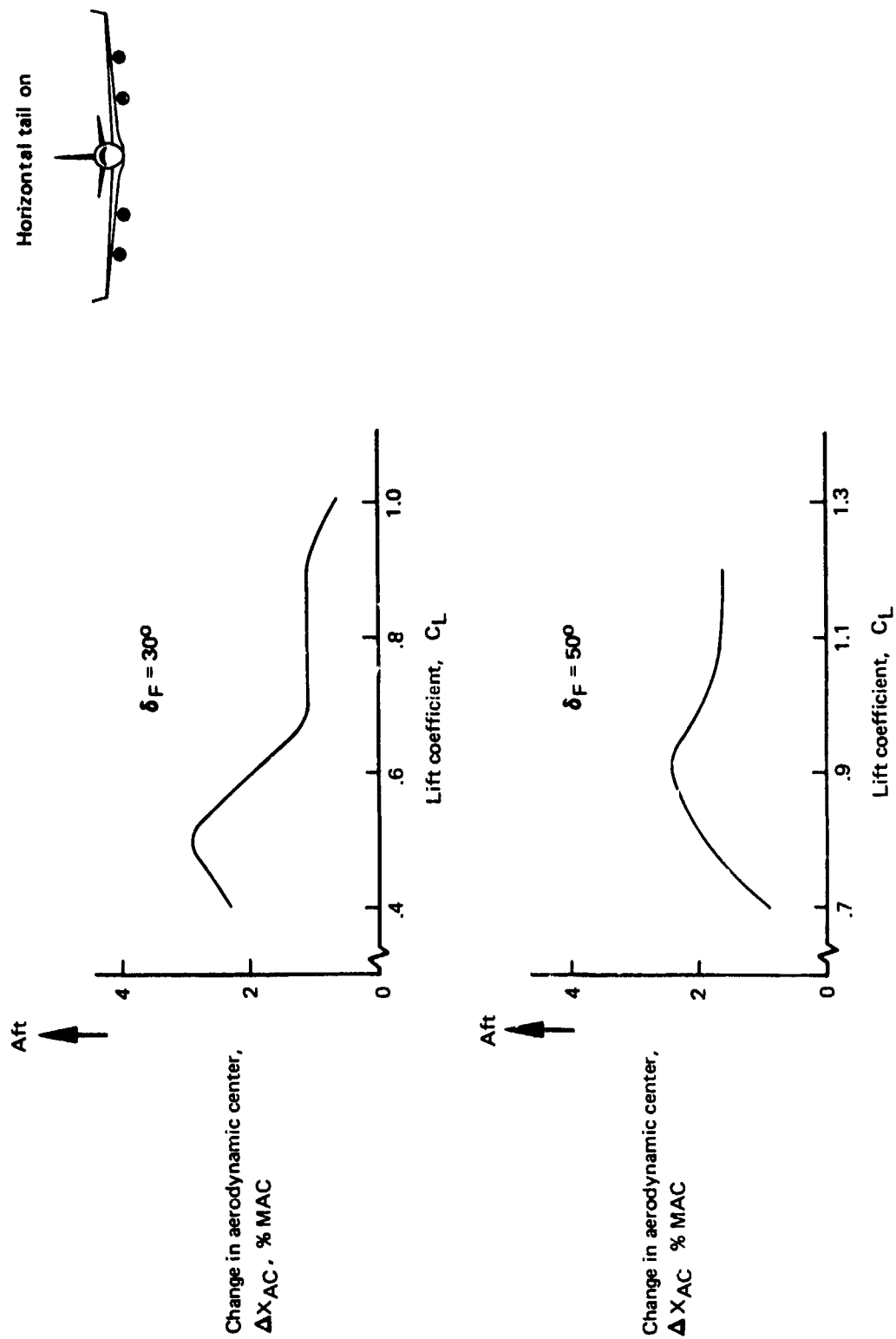Figure 82. — Winglet Trailing-Edge Pressure Separation Analysis

Figure 83. — Effect of AFFDL/Boeing Winglets on KC-135A Aerodynamic Center
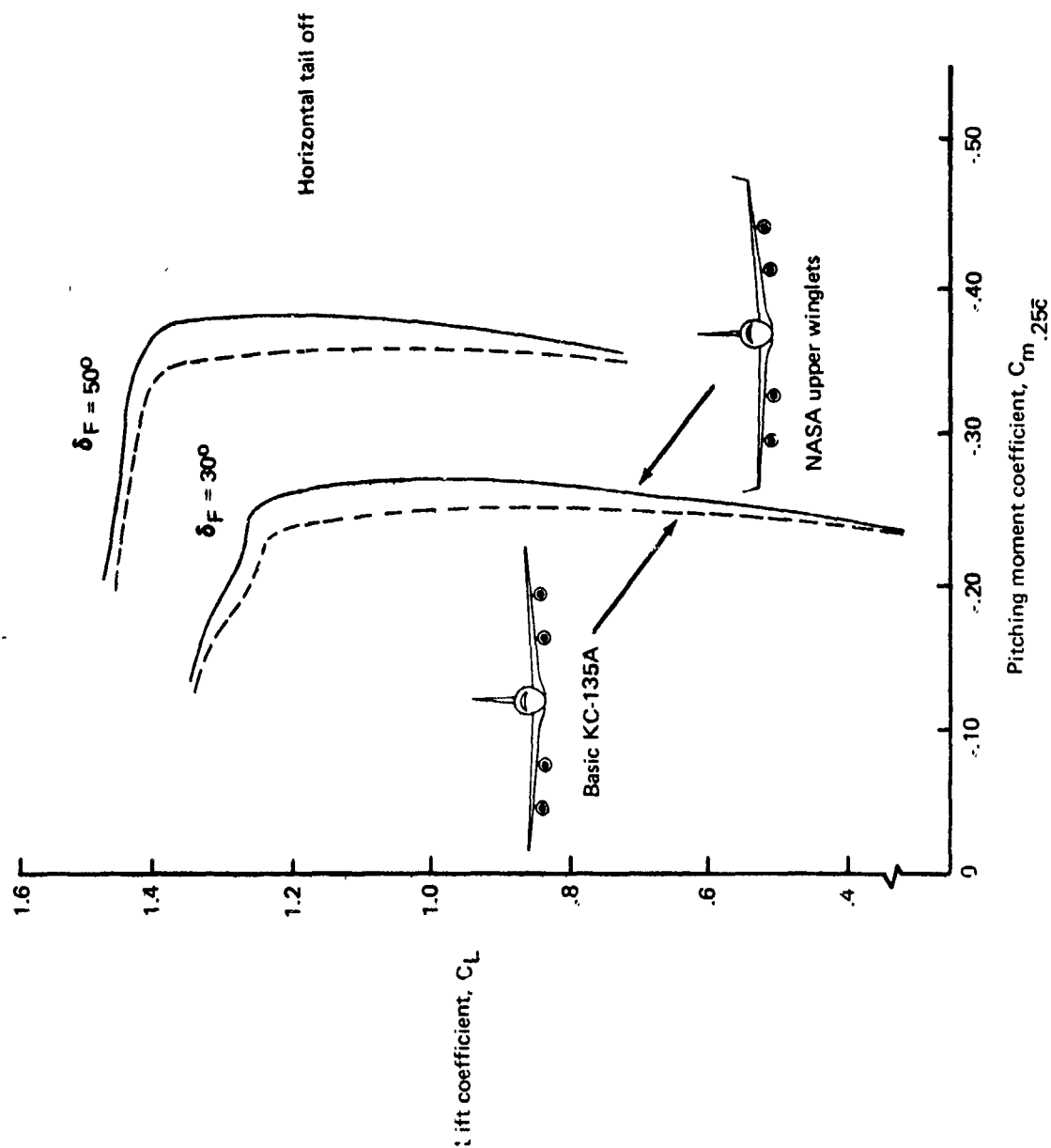
Figure 84. — Effect of NASA Upper Winglets on KC-135A Tail-Off Low-Speed Pitching Moment

107

Figure 85. — Effect of AFFDL/Boeing Winglets on KC-135A Flaps 30° Lateral-Directional Stability
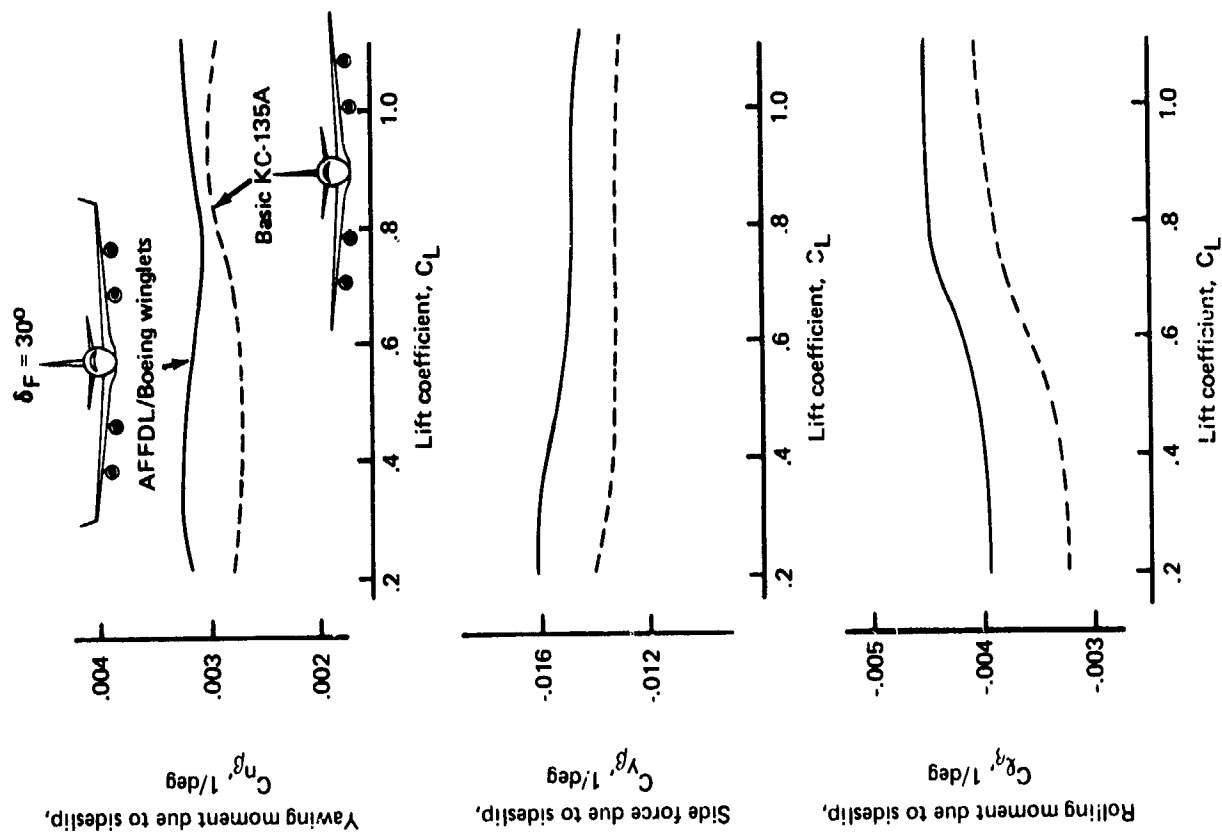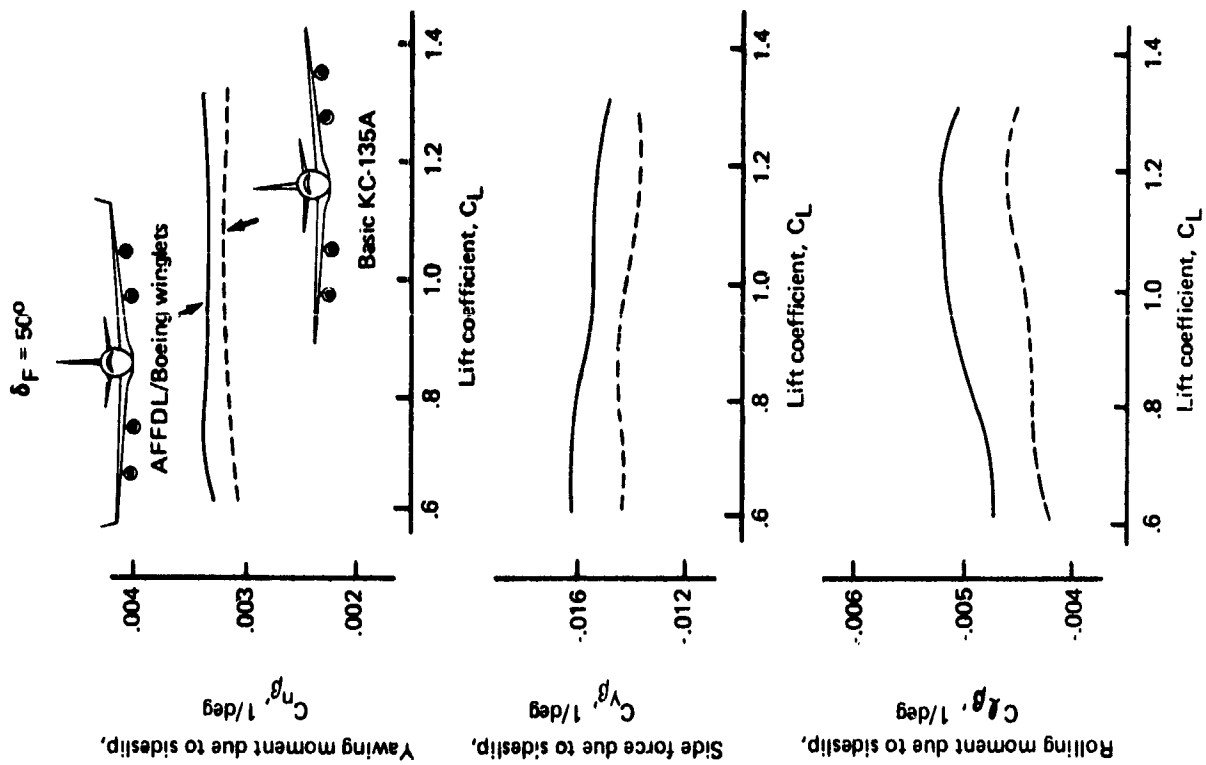
Figure 86. — Effect of AFFDL/Boeing Winglets on KC-135A Flaps 50° Lateral-Directional Stability
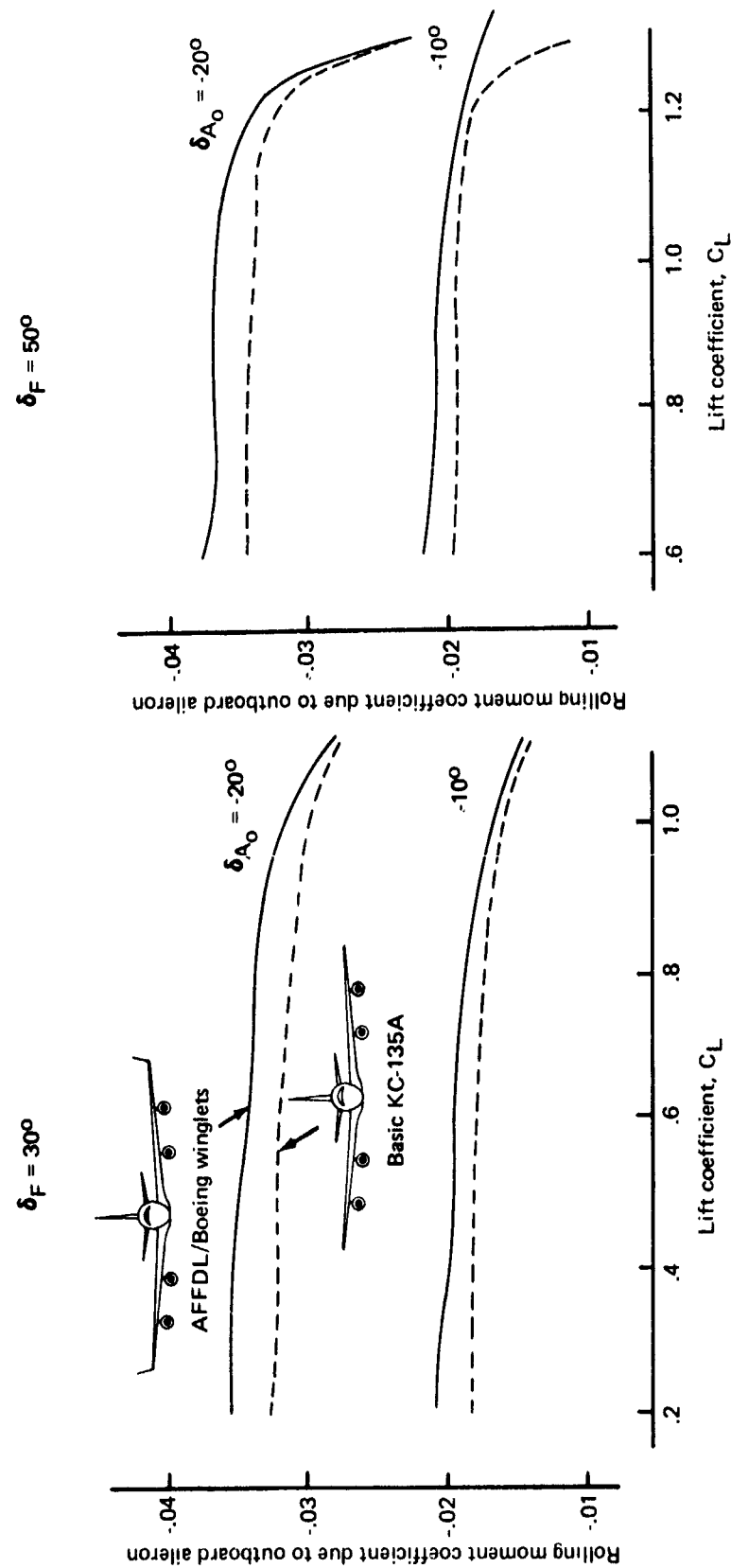
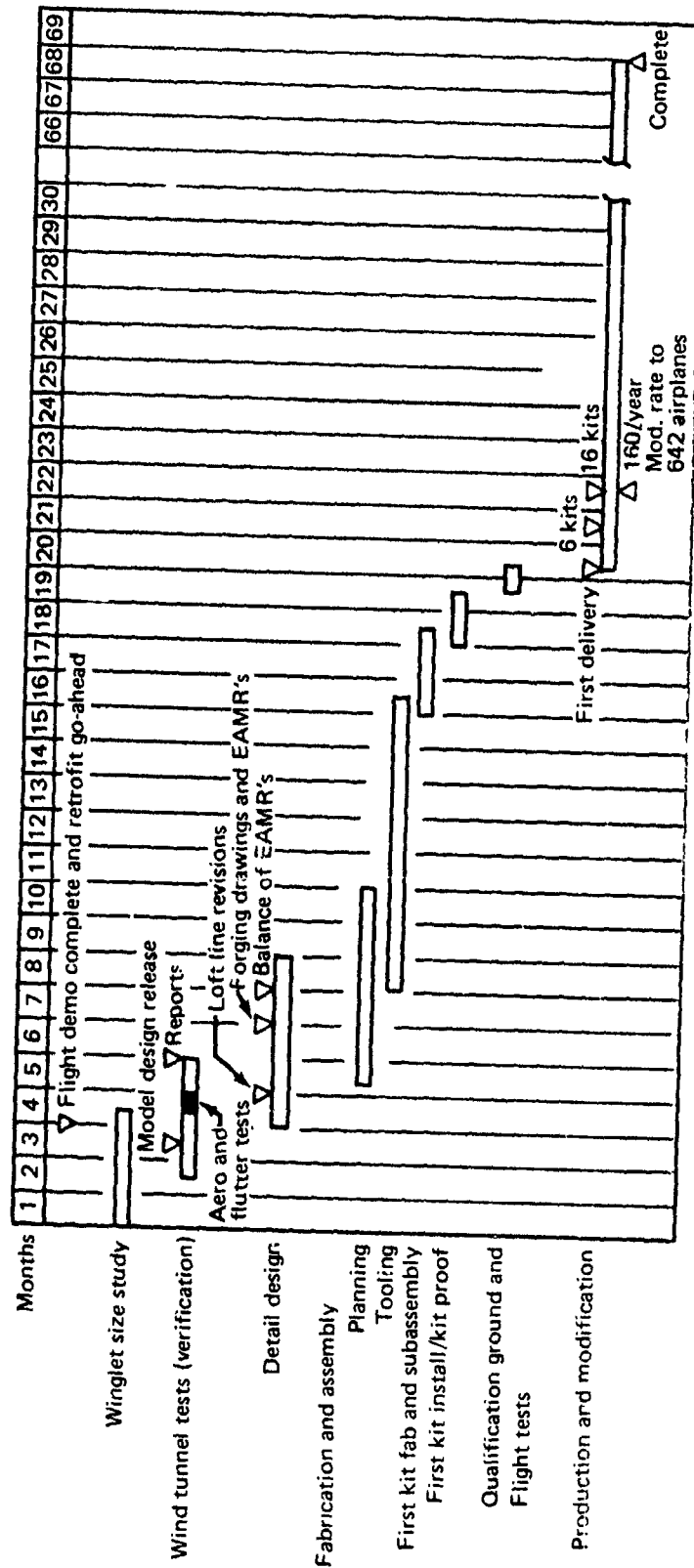*Figure 87. — Effect of AFFDL/Boeing Winglets on KC-135A Low-Speed Outboard Aileron Effectiveness*

110

Figure 88. — Preliminary KC-135A Winglet Retrofit Program Schedule

111
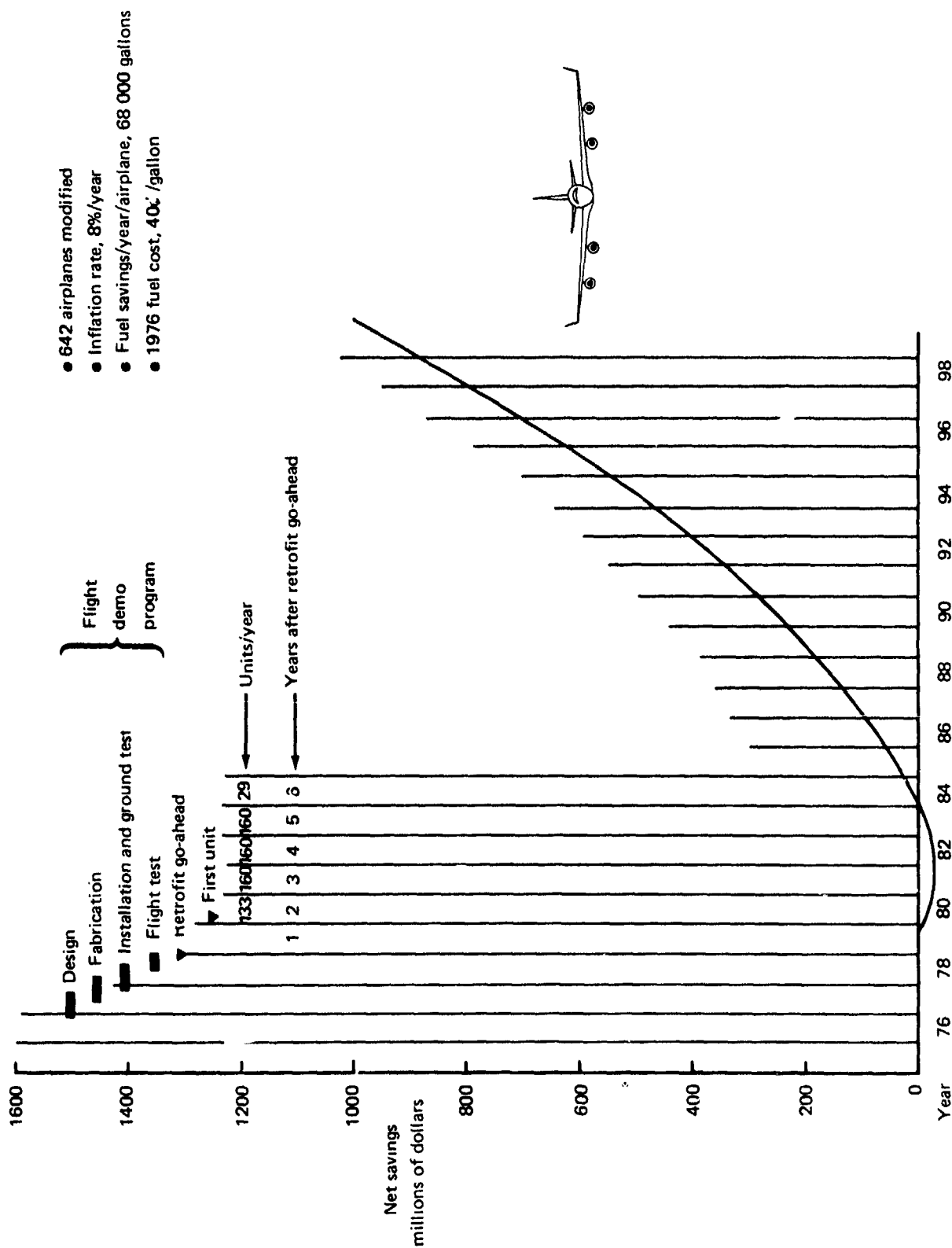
Figure 89. – KC-135A Winglet Cost Benefit Estimate

112

REFERENCES

1. Ishimitsu, K. K.; VanDevender, N.; Dodson, R.; et al.: *Design and Analysis of Winglets for Military Aircraft*. AFFDL-TR-76-6, February 1976.

2. Whitcomb, R. T: *A Design Approach and Selected Wing-Tunnel Results at High Subsonic Speeds for Wing Tip Mounted Winglets*. NASA TN D-8260, July 1976.

3. Ishimitsu, K. K: *Aerodynamic Design and Analysis of Winglets*. AIAA preprint 76-940, AIAA Aircraft Systems and Technology Meeting, Dallas, Texas, September 23-29, 1976.

4. Ramlow, H. D.: *Substantiation Data Report for the KC-135A Flight Manual*. Boeing document D6-5599, December 1964.

5. Dodson, R.: *Design and Analysis of Winglets for Military Aircraft – Preliminary Program Plan To Retrofit Winglets to the KC-135*. Boeing document D3-11136-1, November 1976.

6. Dodson, R.: *Design and Analysis of Winglets for Military Aircraft – Preliminary Program Plan for Winglet Flight Demonstration on the KC-135A Tanker Aircraft*. Boeing document D3-9936-1, November 1975.

APPENDIX
COMPUTER PROGRAMS USED FOR ANALYSIS AND DESIGN OF
WINGLETS

Four computer programs – TEA 372, TEA 242, TEA 230, and TEA 220 – were used for the analysis and design of wing/winglet configurations in three-dimensional flow. The KC-135 winglet designs were completed with TEA 372. TEA 230 calculated the potential flow pressure distributions and span loads of the KC-135A with and without winglets. TEA 242 used the span load from TEA 230 and calculated the induced drag. The chordwise pressure distributions from TEA 230 were used in TEA 200 to calculate the boundary-layer growth and profile drag. TEA 372 is an incompressible, potential flow program in which each lifting surface (wing and winglet) is represented by a multihorseshoe vortex lattice. This lattice is generally placed along the camber line, and there is no simulation of the thickness. A typical lattice for wing/winglet configuration is shown in figure A-1. The dashed outline shows the wing/winglet planforms. The strengths of individual vortex elements are determined by statisfying tangency boundary conditions at specific points on the camber surface. These boundary point locations are shown as small signs in figure A-1. Note also that the presence of the fuselage was not simulated; instead, the wing camber surface was simply extended inboard to the plane of symmetry. Lift, induced drag, and moments for the configuration are obtained by a vector summation of the net force (and force times moment arm) acting on each vortex element.

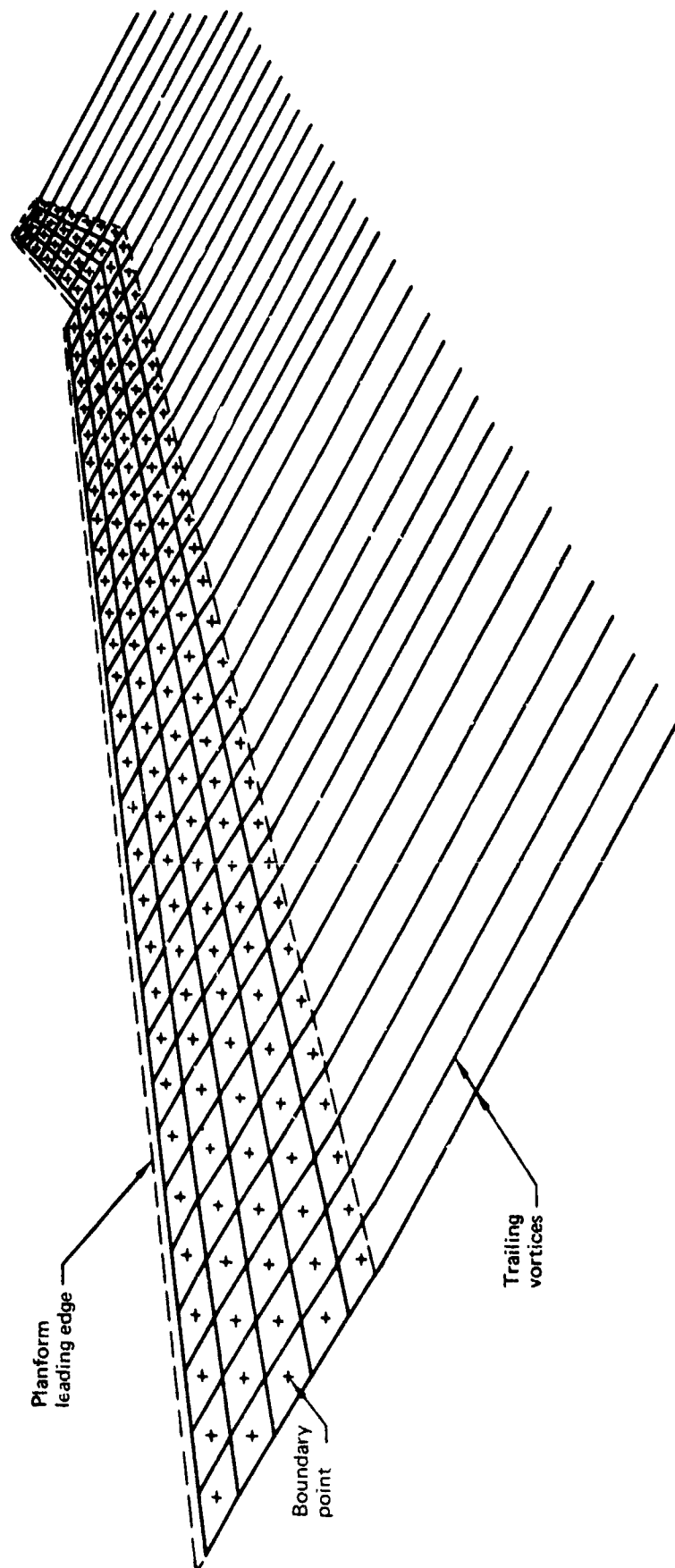Planform
leading edge

Boundary
point

Trailing
vortices

Figure A-1. — Typical Representation of Wing and Winglet in TEA 372 by a Multihorseshoe Vortex Lattice

This program can be used as both an analysis and a design tool. In the design mode, part of the configuration can be held in a fixed position while other parts are allowed to move about some nominal position. The program determines the locations of the movable parts that will give minimum induced drag for the total configuration. In other words, it is an induced drag optimizer.

The optimization capability is especially applicable to the wing-winglet problem. The existing wing geometry must obviously be maintained, but freedom exists to twist and camber the winglet as required to minimize drag. Two types of winglet design (optimization) runs were made during the course of this contract. In the first type, only the section twist was allowed to vary across the winglet to find the point of minimum C_{D_i}. In the second type, both the twist and camber of the winglet sections were allowed to vary. These two design runs give the same minimum C_{D_i}, since C_{D_i} is a function of the spanwise loading and not the manner in which that load is distributed over the chord at a given spanwise station.

The first type of design run was made in cases where the camber line shape was not of any particular interest. The only item of interest was minimum C_{D_i}, and the program would apply whatever twist was necessary to the input sections to obtain the span load distribution for minimum induced drag. This type of run was made throughout the parameter study.

The second type of design run was made in cases where not only was minimum C_{D_i} of interest, but also a specific chordwise loading was desired for good performance in supercritical flow. This type of run was made to design the final winglet once the desired planform and cant angle had been chosen.

The input camber line definition for the winglet is of importance when making an analysis run. In this type of run, all of the input geometry is fixed, and no attempt can be made to optimize C_{D_i}. Throughout the discussions in this report, an "analysis" run means one in which all geometry is fixed. A "design" run means one in which the winglet is allowed to move about some nominal position in order to find the point of minimum C_{D_i}.

The vortex-lattice method of calculating induced drag tends to give answers that are somewhat low (3%) for most near-planar configurations. Induced drag curves plotted later in the report are based on values directly from TEA 372. Even though their absolute magnitudes may be low, increments obtained from these curves should be fairly accurate.

Force and moment coefficients presented from TEA 372 include lift (C_L), induced drag (C_{D_i}), pitching moment ($C_{m.25\bar{c}}$), and rolling moment for half of the configuration (C_{m_X}). The latter two coefficients are both nondimensionalized by wing reference area and mean aerodynamic chord. In this report, C_{m_X} is considered as indicative of wing-root bending moment.

116

TEA 230 is a subsonic potential flow program that can analyze arbitrary configurations with thickness. Source panel and vortex lattices are distributed over the configuration to simulate thickness and lifting effects, respectively. Singularity strengths are determined by solving a set of linear algebraic equations that express exact tangency boundary conditions. Force and moment calculations are made only on source panel singularity surfaces. They are based on the integration of pressures where the pressure is assumed constant over a given panel.

The computer program TEA 242 is an induced drag program, which is used to design and analyze span loadings. The theoretical development of the program uses the concept of the Trefftz plane and a distribution of singularities to model the flow. TEA 242 features a general, nonplanar geometry capability, an optimization option for computing and load distribution for minimum induced drag, and an analysis option to calculate the induced drag produced by arbitrary span loads. For the optimization option, the lift force, bending moment, and pitching moment can be constrained to specific values, and the program will calculate the optimum span load for the minimum induced drag. For the analysis option, the program calculates the lift coefficient, wing bending moment, induced drag efficiency factor, and induced drag.

Computer program TEA 200 calculates the two-dimensional boundary-layer growth on a surface with a known pressure distribution. This program uses the Curle's method to calculate the laminar boundary-layer growth. The transition analysis uses a combination of Schlichting-Ulrich and Granville methods, and the turbulent boundary layer is calculated by the Nash-Hicks method. The momentum thickness, displacement thickness, shape factor, local skin friction, and profile drag are calculated for specified pressure distributions.

117